BEILSTEIN JOURNAL OF ORGANIC CHEMISTRY

Recent advances in materials for organic light emitting diodes

Edited by Eli Zysman-Colman

Generated on 07 November 2026, 03:06

Imprint

Beilstein Journal of Organic Chemistry
www.bjoc.org
ISSN 1860-5397
Email: journals-support@beilstein-institut.de

The *Beilstein Journal of Organic Chemistry* is published by the Beilstein-Institut zur Förderung der Chemischen Wissenschaften.

Beilstein-Institut zur Förderung der Chemischen Wissenschaften
Trakehner Straße 7–9
60487 Frankfurt am Main
Germany
www.beilstein-institut.de

The copyright to this document as a whole, which is published in the *Beilstein Journal of Organic Chemistry*, is held by the Beilstein-Institut zur Förderung der Chemischen Wissenschaften. The copyright to the individual articles in this document is held by the respective authors, subject to a Creative Commons Attribution license.

BEILSTEIN JOURNAL OF ORGANIC CHEMISTRY

Recent advances in materials for organic light emitting diodes

Eli Zysman-Colman

Editorial

Open Access

Address:
Organic Semiconductor Centre, EaStCHEM School of Chemistry, University of St Andrews, North Haugh, St Andrews, Fife, KY16 9ST, UK

Email:
Eli Zysman-Colman - eli.zysman-colman@st-andrews.ac.uk

Keywords:
organic light emitting diodes

Beilstein J. Org. Chem. **2018,** *14,* 1944–1945.
doi:10.3762/bjoc.14.168

Received: 04 June 2018
Accepted: 28 June 2018
Published: 27 July 2018

This article is part of the Thematic Series "Recent advances in materials for organic light emitting diodes".

Guest Editor: E. Zysman-Colman

© 2018 Zysman-Colman; licensee Beilstein-Institut.
License and terms: see end of document.

Organic light emitting diodes (OLEDs) are at the cusp of becoming the dominant technology for the mobile device and display markets. This is largely due to the concerted efforts over the past thirty years to improve the material design, beginning with the first demonstrated viability of this technology in 1987 by Tang and VanSlyke [1]. Emitters in particular have undergone an evolution in design, from fluorescent compounds to phosphorescent organometallic complexes to organic thermally activated delayed fluorescence (TADF) molecules, the latter driving tremendous recent excitement within the field of organic semiconductor research. This thematic issue of the *Beilstein Journal of Organic Chemistry* covers novel phosphorescent and TADF materials design and their inclusion as emitters in OLEDs.

Some highlights in this issue include the work of Thanh-Tuân Bui et al., who provide a welcome perspective on blue TADF materials for OLEDs in the form of a review article [2]. Cristina Cebrián and Matteo Mauro review the advances made in platinum(II) complexes for OLEDs [3]. Rebecca Pittkowski and Thomas Strassner report bright blue-to-blue-green phosphorescent platinum(II) complexes employing sterically bulky diketonate ancillary ligands [4]. In addition, Lin Gan et al. describe a new molecular design approach for orange-emitting TADF molecules employing a fluorenone acceptor [5]. In the full research paper by Feng-Ming Xie et al., they disclose two bipolar, high-energy phenothiazine-5,5-dioxide-based host materials conceived to be used for deep blue OLED devices [6].

The articles in this thematic issue provide a window into the design principles used towards the development of next-generation emitter and host materials for OLEDs. I hope these articles will provide inspiration for further research in this exciting area.

Eli Zysman-Colman

St Andrews, June 2018

Eli Zysman-Colman obtained his Ph.D. from McGill University in 2003. He then completed two postdoctoral fellowships, one in supramolecular chemistry at the Organic Chemistry Institute, University of Zurich and the other in inorganic materials chemistry at Princeton University. After beginning his career in Canada, he moved to the University of St Andrews where he is presently Reader in Optoelectronic Materials and Fellow of the Royal Society of Chemistry. His research program focuses on

the rational design of: (i) luminophores for use in organic light emitting diodes (OLEDs) and light-emitting electrochemical cells (LEECs), two types of electroluminescent devices; (ii) sensing materials employed in electro-chemiluminescence; and (iii) photocatalysts employed in photoredox catalytic reactions.

ORCID® iDs

Eli Zysman-Colman - https://orcid.org/0000-0001-7183-6022

References

1. Tang, C. W.; VanSlyke, S. A. *Appl. Phys. Lett.* **1987,** *51,* 913–915. doi:10.1063/1.98799
2. Bui, T.-T.; Goubard, F.; Ibrahim-Ouali, M.; Gigmes, D.; Dumur, F. *Beilstein J. Org. Chem.* **2018,** *14,* 282–308. doi:10.3762/bjoc.14.18
3. Cebrián, C.; Mauro, M. *Beilstein J. Org. Chem.* **2018,** *14,* 1459–1481. doi:10.3762/bjoc.14.124
4. Pittkowski, R.; Strassner, T. *Beilstein J. Org. Chem.* **2018,** *14,* 664–671. doi:10.3762/bjoc.14.54
5. Gan, L.; Li, X.; Cai, X.; Liu, K.; Li, W.; Su, S.-J. *Beilstein J. Org. Chem.* **2018,** *14,* 672–681. doi:10.3762/bjoc.14.55
6. Xie, F.-M.; Ou, Q.; Zhang, Q.; Zhang, J.-K.; Dai, G.-L.; Zhao, X.; Wie, H.-X. *Beilstein J. Org. Chem.* **2018,** *14,* 869–874. doi:10.3762/bjoc.14.73

License and Terms

This is an Open Access article under the terms of the Creative Commons Attribution License (http://creativecommons.org/licenses/by/4.0). Please note that the reuse, redistribution and reproduction in particular requires that the authors and source are credited.

The license is subject to the *Beilstein Journal of Organic Chemistry* terms and conditions: (https://www.beilstein-journals.org/bjoc)

The definitive version of this article is the electronic one which can be found at: doi:10.3762/bjoc.14.168

BEILSTEIN JOURNAL OF ORGANIC CHEMISTRY

Recent advances on organic blue thermally activated delayed fluorescence (TADF) emitters for organic light-emitting diodes (OLEDs)

Thanh-Tuân Bui[1], Fabrice Goubard[1], Malika Ibrahim-Ouali[2], Didier Gigmes[3] and Frédéric Dumur[*3]

Review

Open Access

Address:
[1]Laboratoire de Physicochimie des Polymères et des Interfaces (LPPI), Université de Cergy-Pontoise, 5 mail Gay Lussac, Neuville sur Oise, 95031 Cergy-Pontoise Cedex, France, [2]Aix Marseille Univ, CNRS, Centrale Marseille, iSm2, Marseille, France and [3]Aix Marseille Univ, CNRS, Institut de Chimie Radicalaire ICR, UMR 7273, F-13397 Marseille, France

Email:
Frédéric Dumur[*] - frederic.dumur@univ-amu.fr

* Corresponding author

Keywords:
blue; electroluminescence; emitter; OLED; TADF

Beilstein J. Org. Chem. **2018,** *14,* 282–308.
doi:10.3762/bjoc.14.18

Received: 13 November 2017
Accepted: 19 January 2018
Published: 30 January 2018

This article is part of the Thematic Series "Recent advances in materials for organic light emitting diodes".

Guest Editor: E. Zysman-Colman

© 2018 Bui et al.; licensee Beilstein-Institut.
License and terms: see end of document.

Abstract

The design of highly emissive and stable blue emitters for organic light emitting diodes (OLEDs) is still a challenge, justifying the intense research activity of the scientific community in this field. Recently, a great deal of interest has been devoted to the elaboration of emitters exhibiting a thermally activated delayed fluorescence (TADF). By a specific molecular design consisting into a minimal overlap between the highest occupied molecular orbital (HOMO) and the lowest unoccupied molecular orbital (LUMO) due to a spatial separation of the electron-donating and the electron-releasing parts, luminescent materials exhibiting small S_1–T_1 energy splitting could be obtained, enabling to thermally upconvert the electrons from the triplet to the singlet excited states by reverse intersystem crossing (RISC). By harvesting both singlet and triplet excitons for light emission, OLEDs competing and sometimes overcoming the performance of phosphorescence-based OLEDs could be fabricated, justifying the interest for this new family of materials massively popularized by Chihaya Adachi since 2012. In this review, we proposed to focus on the recent advances in the molecular design of blue TADF emitters for OLEDs during the last few years.

Introduction

Since the pioneering works of Tang and VanSlyke in 1987 [1], organic light emitting diodes (OLEDs) have known major evolutions of their structures, not only of the device stacking but also of the materials composing the different layers [2]. The interest of both the scientific and industrial communities for organic electroluminescent devices is supported by the fact that

OLEDs have been identified as the key-elements for the fabrication of the next generation display and lighting technology [3]. Notably, lightweight and thin devices can be fabricated onto flexible substrates, favouring the penetration of OLEDs in these two markets. With the aim at reducing the global energy demand on Earth, two parameters govern the power consumption of OLEDs, namely the quantum yield of luminescence of the light emitting material and the device stacking. Indeed, the driving voltage of OLEDs is highly sensitive to the thickness of the different layers, the charge transport ability of the materials but also to their energy levels. By minimizing the energy gaps between adjacent layers and facilitating charge injection from the electrodes, the injection and transportation of holes and electrons can be realized at lower operating voltages. The second parameter concerns the light-emitting ability of the emitter, which is directly related to the nature, and the photoluminescence quantum yield (PLQY) of the emitter. Based on spin statistics, upon electrical excitation, singlet and triplet excitons are formed in a 1:3 ratio [4]. In the case of fluorescent materials, only singlet excitons can be utilized for light emission, limiting the internal quantum efficiency (IQE) of fluorescent OLEDs to 25%. Conversely, phosphorescent materials can both harvest singlet and triplet excitons for emission by intersystem crossing (ISC), enabling to reach a theoretical IQE of 100% for phosphorescent OLEDs [5]. As drawback, triplet emitters are transition-metal complexes mostly based on iridium, platinum and osmium and the scarcity of these metals on Earth, their toxicity and high cost make these materials unsuitable candidates for a mass-production of OLEDs [6]. However, efforts have also been carried out to incorporate emitters comprising less toxic metals, providing mitigate results when tested in devices [7,8]. In 2012, a breakthrough has been obtained by the Adachi group who developed purely organic materials capable to harvest both singlet and triplet excitons for emission [9]. This new family of light emitting materials capable to compete with the well-established triplet emitters and displaying a similar efficiency in devices by developing a new emission mechanism was immediately termed as the third generation of OLEDs emitters that consists of thermally activated delayed fluorescence (TADF) emitters. As specificity, these materials can thermally repopulate the singlet state from the triplet state by reverse intersystem crossing (RISC), leading to an increase of the luminescence intensity. From the OLEDs viewpoint, TADF emitters behave by harvesting both singlet and triplet excitons for radiative transition, excepted that the emission occurs from the singlet state and not from the triplet state (as observed for metal complexes) and that the triplet–triplet annihilation commonly observed with phosphorescent OLEDs [10] can be drastically reduced (see Figure 1). TADF materials can also be metal-free, addressing the fabrication cost and environmental issues. Therefore, TADF emitters retain the high efficiency of the second generation of emitters (triplet emitters), the stability of the first generation of fluorescent materials while eliminating the different problems observed with the two previous generations: triplet–triplet annihilation and low device stability for phosphorescent OLEDs, low IQE for fluorescent OLEDs.

To get full-color displays or white-light OLEDs, the combination of the three primary colors red green blue (RGB) is indispensable. At present, highly emissive and stable blue emitters are actively researched [11-16]. Several points justify the low availability of highly efficient blue materials. First, due to their large bandgaps (ΔE > 3 eV), charge injection from the adjacent

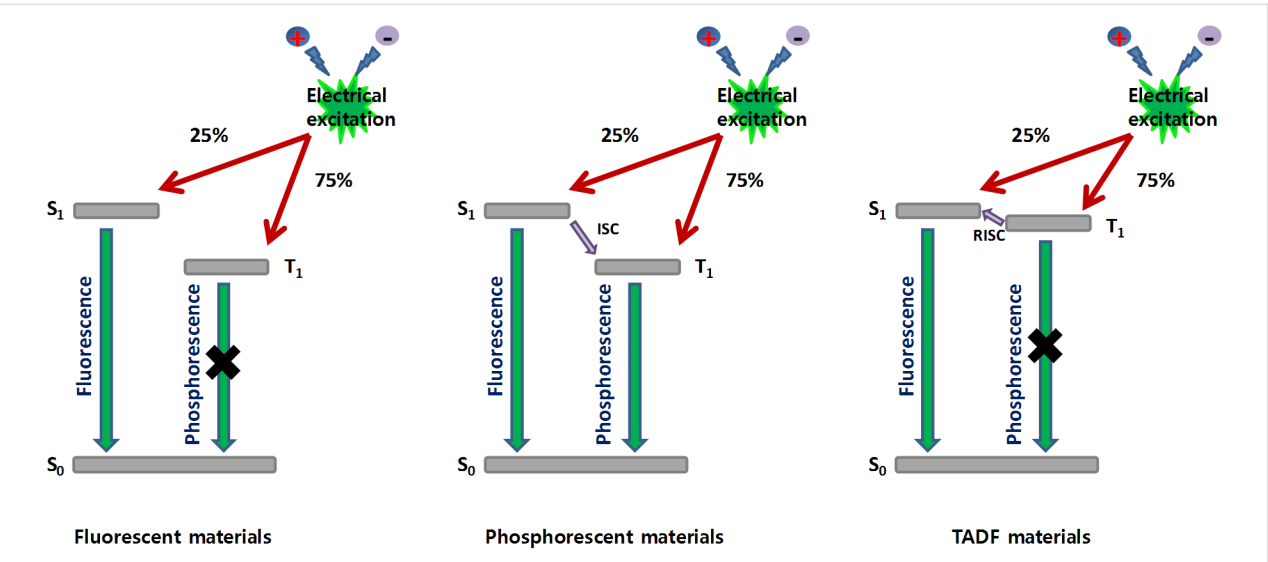


Figure 1: Radiative deactivation pathways existing in fluorescent, phosphorescent and TADF materials.

layers is often difficult, requiring devices to be operated at high voltages [17]. Second, and still related to their wide bandgaps, the probability to transfer an electron from the ground to the excited stable state is considerably reduced, providing materials displaying PLQY greatly reduced compared to that observed for the other colors [18,19]. To end, the propensity of blue emitters to rapidly degradate upon device operation is well established, resulting in a fast and irreversible color shift [20,21]. In this context, TADF blue emitters have been identified as promising candidates to address the color purity, quantum efficiency and long-term device stability issues. Due to the enthusiasm of the scientific community for TADF emitters, this research field evolves extremely rapidly. In this review, a summary of the strategies developed during the last years to design organic blue TADF emitters is presented. It has to be noticed that the values of EQEs reported in the different tables correspond to the maximum EQEs, because many articles do not give sufficient data concerning EQE at the practically relevant luminance of 100 cd/m^2.

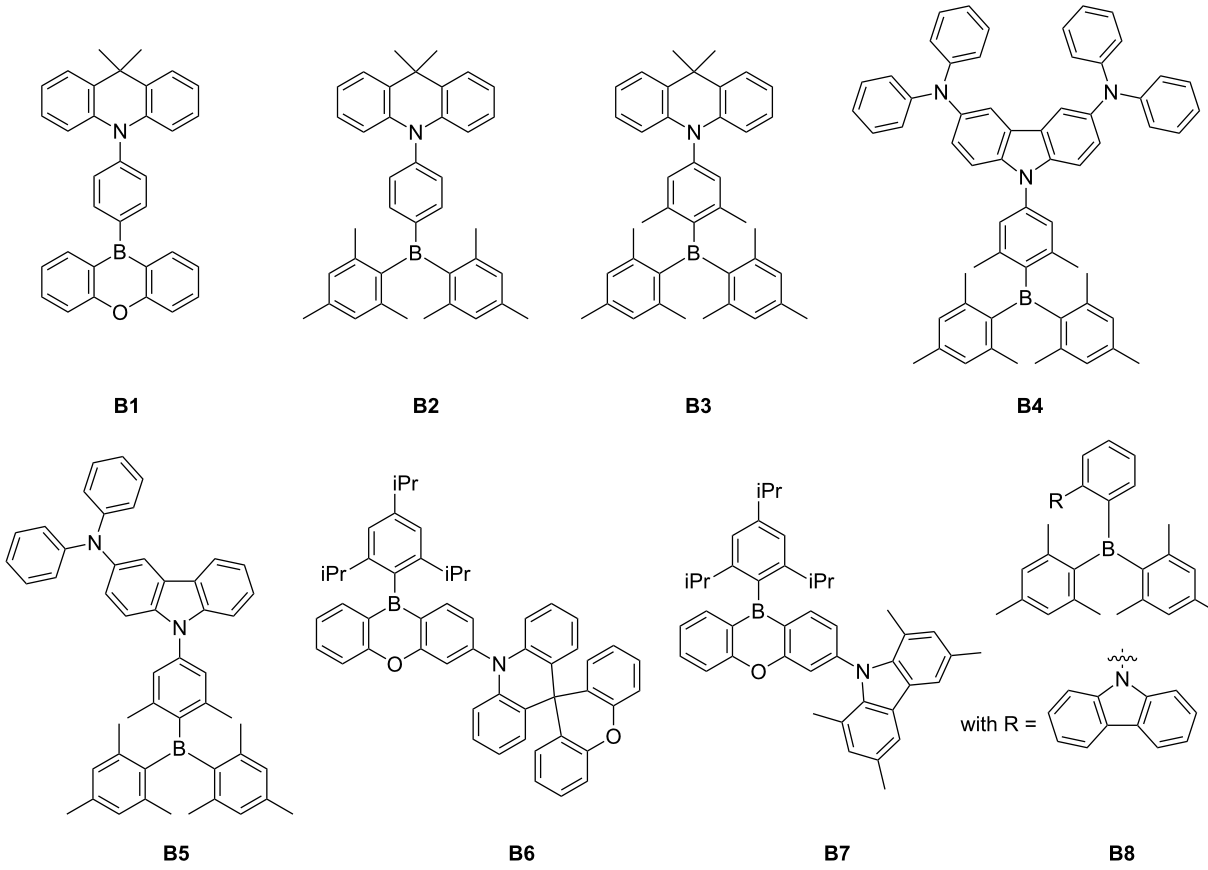
Review

1. Molecular design rules to produce a delayed fluorescence

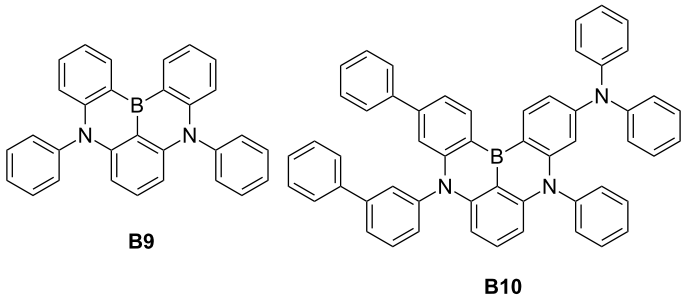
The efficiency of OLEDs is intimately related to the ability of the light-emitting materials to convert a maximum of injected charges into photons. To optimize this, the TADF process is the most promising strategy as it allows converting the generated and lost triplet excitons of the classical fluorescent materials into emissive singlets. By efficiently upconverting the triplet excitons from the triplet (T_1) to the singlet state (S_1), the intrinsic limitation of 25% imposed to fluorescent materials by the 1:3 singlet–triplet ratio can be overcome and an ultimate IQE of 100% can be realized with TADF materials. To promote the endothermic RISC, the energy gap between S_1 and T_1 (ΔE_{ST}) plays a key role and should be as small as possible. From a molecular design viewpoint, ΔE_{ST} can be drastically reduced if the highest occupied molecular orbital (HOMO) and the lowest unoccupied molecular orbital (LUMO) are spatially separated, what can be obtained by a suitable steric hindrance that introduces an internal twist and interrupts the π-conjugation but also by a sufficient distance between the electron-donating and the electron-accepting moieties [22-25]. In the design of TADF materials, it should be mentioned the major importance of the spin–orbit vibronic coupling, in addition to the small ΔE_{ST}. Indeed, a small ΔE_{ST} is not sufficient to ensure for a TADF material an efficient RISC which is a vibronically coupled, spin–orbit coupling process with the involvement of the charge transfer state. To remain efficient, the spin–orbit coupling should still have a significant value, even if the separation of the HOMO and LUMO wavefunctions remain a requirement to minimize ΔE_{ST}. At present, systematic investigations examining the correlation between the spin–orbit coupling and RISC are still scarce [26-29]. Considering that the singlet–triplet energy splitting is one of the key elements for controlling the RISC efficiency, that the dihedral angle between the donor and the acceptor can be difficultly anticipated and that an overlap of both the HOMO/LUMO energy levels could adversely affect the color purity and ΔE_{ST}, it has to be noticed that the photophysical properties and the geometry of molecules that are suspected to be TADF emitters are often investigated by theoretical calculations prior to synthesis, optimizing the chance to get suitable energy levels and the desired ΔE_{ST}. This strategy was notably applied to the design of TADF blue emitters containing triarylboron accepting units. Besides, as we will see in this review, the design of a good TADF material by optimizing its structure by theoretical calculations is not sufficient to ensure the fabrication of highly emissive OLEDs. As observed for phosphorescent emitters, optimization of the device stacking, an appropriate choice of the host as well as the materials in the adjacent layers, an adequate dopant concentration, and the efficient confinement of excitons within the emissive layer are primordial parameters to elaborate high performance OLEDs while maintaining the color purity [30]. Due to the difficulty to address simultaneously these different points, numerous light emitting materials have been revisited several times, providing different electrical and optical device characteristics.

2. Boron-containing TADF emitters

Boron-containing molecules have been extensively investigated in organic electronics [31] as these materials are characterized by a remarkable electron mobility resulting from the presence of a vacant p-orbital on the boron atom [32,33]. Triarylboron compounds are also strong electron acceptors, justifying that numerous groups developed TADF emitters using triarylboron moieties as acceptors. As possible donors, diarylamines have often been proposed (carbazole, triphenylamine, carbazole/triphenylamine hybrids, 9,9-dimethyl-9,10-dihydroacridine), as exemplified in Figure 2 [34-36]. In **B1** and **B2**, isolation of the two parts was obtained by linking the 10*H*-phenoxaborin unit or the dimesitylphenylboron moiety to the 9,9-dimethyl-9,10-dihydroacridine part through a phenylene bridge substituted at the 1,4-positions. By mean of steric repulsions occurring between the hydrogen atoms of the aromatic π-bridge and those of the neighbouring electron-donating and accepting parts, an effective spatial separation of the HOMO and LUMO levels could be obtained, resulting in the rotation of the two end-groups relative to the plane of the central aromatic ring. A dihedral angle of 51.8° was found between the phenylene and the 10*H*-phenoxaborin unit in **B1**, increasing to 88.4° for the dihedral angle between the phenylene and the 9,9-dimethylacridane unit in **B2**. ΔE_{ST} values of 0.013 eV and 0.041 eV were experimentally de-



	B1	B2	B3	B4	B5	B6	B7	B8
reference	[34]	[35]	[37]	[37]	[37]	[38]	[38]	[36]
ΔE_{ST} (eV)	0.013	0.041	0.071	0.058	0.062	0.060	0.012	0.150
decay time delayed component (μs)	2.36	6.71	–	–	–	–	–	–
EQE (%)	15.1	16.0	22.8	21.6	14.0	19.0	20.1	24.1
CIE (x,y) or λ_{EL} (nm)	466	(0.14, 0.24)	(0.22, 0.55)	(0.18, 0.43)	(0.17, 0.30)	(0.14, 0.16)	(0.14 0.30)	(0.14, 0.20)



	B9	B10
reference	39	39
ΔE_{ST} (eV)	0.013	0.041
decay time delayed component (μs)	93.7	65.3
EQE (%)	13.5	20.2
CIE (x,y)	(0.13, 0.09)	(0.12, 0.13)

Figure 2: Boron-containing TADF emitters **B1**–**B10**.

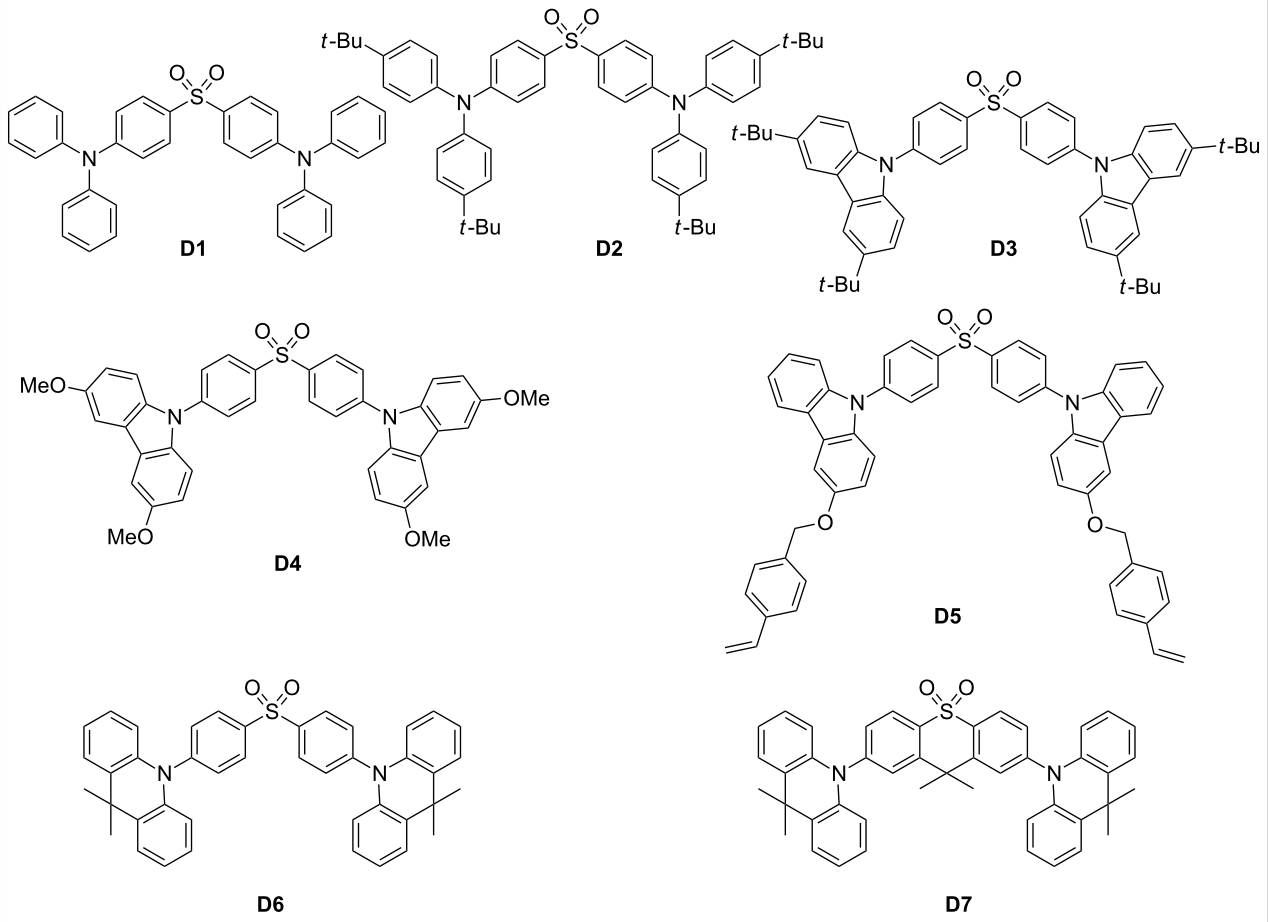
termined for **B1** and **B2**, respectively, calculated from the difference existing between the onset of the fluorescence and the phosphorescence emission. The decay time of the delayed component of luminescence was determined as being 2.36 μs and 6.71 μs for **B1** and **B2**, respectively. When evaluated in multilayered OLEDs, a blue electroluminescence (EL) peaking at 466 nm and 479 nm, an external quantum efficiency (EQE) of 15.1% and 16.0% were obtained for **B1** and **B2**, respectively,

indicating the substantial contribution of the triplet excitons to the luminescence.

Interestingly, compared to **B2**, the introduction of two additional methyl groups in the phenyl part **(B3)** resulted in a clear bathochromic shift of the EL, OLEDs emitting a green light peaking at 502 nm [37]. A blue shift of the emission and sky-blue OLEDs could only be obtained with this acceptor by replacing the electron-donating 9,9-dimethyl-9,10-dihydroacridinyl unit of **B3** by a bis(diphenylamino)carbazole group in **B4** or a diphenylaminocarbazole unit in **B5**. The outstanding EQE of 21.6% could be attained for the sky-blue **B4**-based devices. Still based on the combination of acridan and 10*H*-phenoxaborin units, a complete isolation of the two units could be realized in **B6** by directly functionalizing the 10*H*-phenoxaborin core with a spiro-type acridan group [38]. Using this strategy, pure blue OLEDs exhibiting an EQE of 19.0% and Commission Internationale de l'Eclairage (CIE) coordinates of (0.14, 0.16) were obtained with **B6**. Comparable performances were determined for **B7** (20.1%, (0.14, 0.16)), comprising the sterically demanding tetramethylcarbazole. In these two structures, a large dihedral angle arising from steric repulsions between hydrogen atoms in the *peri*-position of **B6** and from the presence of methyl groups at the 3,6-positions of 1,3,6,8-tetramethylcarbazole in **B7** could be obtained. In fact, the substitution at the 3,6-position of carbazole could maintain a large dihedral angle in **B7** whereas the two methyl groups at the 1,8-positions were introduced for a higher electrochemical stability of the carbazole donor. Finally, by modifying the connectivity between the donor and acceptor in **B8**, a record-high EQE of 24.1% could be realized for pure-blue OLEDs (0.139, 0.150) close to the National Television Standards Committee standard (NTSC) blue values of (0.14, 0.08) [36]. Upon *ortho*-substitution of the dimesitylphenylboron acceptor with a carbazole, a mutual steric hindrance could be exerted between the donor and the acceptor resulting in the large dihedral angle of 72.6°. A S_1–T_1 energy splitting of 0.13 eV could be also experimentally determined for **B8**. Interestingly, the outstanding EL characteristics of **B8**-based devices were assigned to the large contribution of the delayed fluorescence (61%) in the overall luminescence decay of **B8**. A pure blue emission could also be realized by totally blocking the structure, what was done with **B9** and **B10** in which two of the three aromatic rings of triphenylamine were connected to the boron center [39]. By elongating the π-conjugation of the electron-donating group in **B10** compared to **B9**, a more delocalized HOMO level could be generated, resulting in a greater intramolecular charge transfer and an increase of the oscillator strength. As a result, EQE of corresponding OLEDs increased from 13.5% (459 nm, (0.13, 0.09)) for **B9**-based devices to 20.2% (467 nm, (0.12, 0.13)) for **B10**-based devices. If the electron-to-photon conversions are remarkable, none of the OLEDs could reach the brightness of 1000 cd/m^2 owing to a dramatic efficiency roll-off. Precisely, the efficiency roll-off determined for **B9**- and **B10**-based devices was determined as originating from an imbalanced charge transportation and the presence of bimolecular quenching processes occurring at high current density such as triplet–triplet annihilation and exciton–polaron annihilation.

3. Diphenylsulfone-based emitters

Concerning the design of blue TADF emitters, diphenylsulfone is the third most widely studied acceptor in the literature, followed by triarylboron and triazine derivatives. In this field, the contribution of the Adachi's group is remarkable. The first report mentioning a pure blue emission with a diphenylsulfone derivative was reported in 2012 [40]. By a careful control of the π-conjugation length between the donor and the acceptor, **D3**-based OLEDs producing a deep blue emission with CIE coordinates of (0.15, 0.07) were fabricated (see Figure 3). Examination of the phosphorescence spectra of **D1**–**D3** at 77 K revealed their T_1 states to be $^3\pi\pi^*$ states centred on their electron-donating parts. ΔE_{ST} values of 0.54, 0.45 and 0.32 eV were, respectively, determined for **D1**–**D3**. Changes in ΔE_{ST} were explained as follow: By introducing *tert*-butyl groups on the diphenylamine unit, the electron donating ability in **D2** was reinforced compared to **D1**, red-shifting the charge transfer (CT) band and lowering the CT energy as well as ΔE_{ST}. By replacing the diphenylamine unit of **D1** by a *tert*-butyl-substituted carbazole unit in **D3**, the $^3\pi\pi^*$ state was considerably destabilized, raising its energy level and decreasing ΔE_{ST}. Parallel to this, a greater separation of the HOMO and LUMO orbitals was evidenced by theoretical calculations for **D3**, as a result of a larger dihedral angle (49° instead of 32° for **D1** and **D2**), resulting in a smaller energy difference between the singlet and triplet excited states. As expected, the contribution of the slow decay component in the luminescence of **D1**–**D3** decreased with increasing ΔE_{ST}, almost disappearing for **D1**. While using **D1**–**D3** as dopants for multilayer OLEDs, maximum EQEs of OLEDs coincide the order previously determined for the proportion of the delayed component in the total emission of **D1**–**D3** with the EQE (**D1**) < EQE (**D2**) < EQE (**D3**) (2.9%, 5.6% and 9.9% for **D1**–**D3**, respectively). If **D3** displayed the best EQE for the series, a dramatic efficiency roll-off at high current density was observed, as the result of a long TADF lifetime (270 μs). This issue was addressed with **D4** [41]. By replacing the *tert*-butyl groups of **D3** by methoxy groups in **D4**, a significant decrease of ΔE_{ST} was obtained (0.21 eV instead of 0.32 eV for **D3**), reducing the TADF lifetime and efficiency roll-off. More precisely, the higher electron-donating ability and the longer conjugation length of the 3,6-dimethoxycarbazole compared to the 3,6-di-*tert*-butylcarbazole lowered the S_1 state and to a greater extend the T_1 state of **D4**,



	D1	D2	D3	D4	D5	D6	D7
reference	[40]	[40]	[40]	[41]	[42]	[43]	[29]
ΔE_{ST} (eV)	0.54	0.45	0.32	0.21	0.31	0.08	0.15
decay time delayed component (μs)	90	140	270	93	50	7	44
EQE (%)	2.9	5.6	9.9	14.5	2.0	19.5	22.4
CIE (x,y) or λ_{EL} (nm)	421	430	(0.15, 0.07)	(0.16, 0.16)	(0.12, 0.13)	(0.16, 0.20)	(0.16, 0.24)

Figure 3: Diphenylsulfone-based TADF emitters **D1**–**D7**.

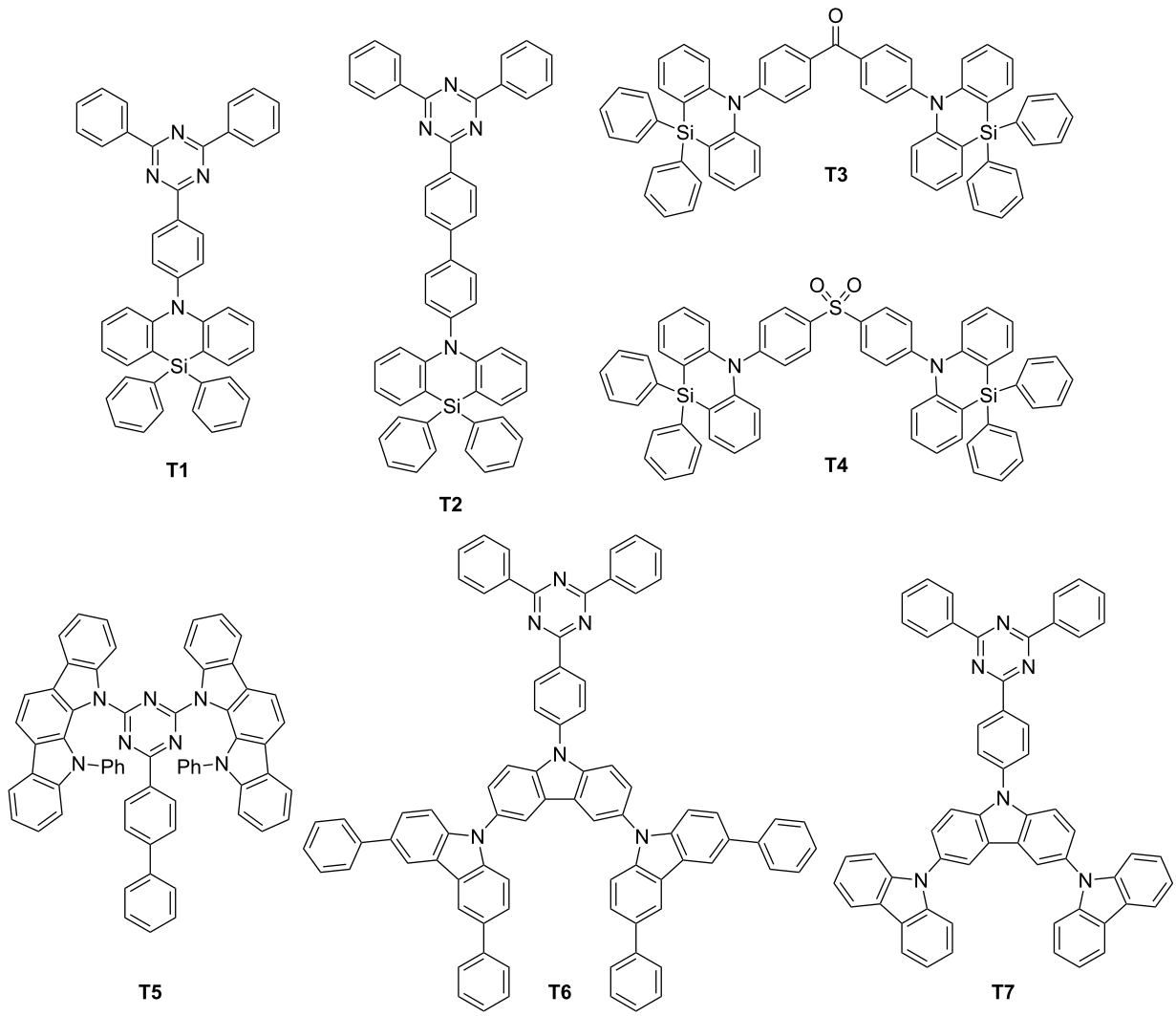
furnishing in turn a molecule with a smaller ΔE_{ST} than **D3**. Jointly, due to the reduction of ΔE_{ST}, a TADF lifetime of 93 μs was determined for **D4**, far from the value measured for **D3** (270 μs). When tested in a similar device structure than that previously used for **D3**, a maximum EQE of 14.5% and a smaller efficiency roll-off was evidenced for **D4**-based devices, attributed to the smaller ΔE_{ST} and the shorter TADF lifetime. Recently, a thermally cross-linkable and solution-processable version of **D4**, i.e., **D5** was reported in the literature [42]. If the strategy is appealing, the final EL performances of **D5**-based OLEDs were far from that obtained with vacuum-processed OLEDs and a maximum EQE of only 2.0% could be reached. Following the basic rule of molecular design consisting in maximizing the dihedral angle to minimize ΔE_{ST}, substitution of diphenylsulfone by 9,9-dimethyl-9,10-dihydroacridine resulting in an almost orthogonality of the two groups in **D6** as a dihedral angle as large as 89° could be determined between 9,9-dimethyl-9,10-dihydroacridine and the connected phenyl ring of the diphenylsulfone unit [43].

A significant reduction of the TADF lifetime (≈7 μs) and a small ΔE_{ST} of 0.08 eV were measured for **D6**, favorable to the fabrication of highly emissive blue OLEDs. Devices fabricated with **D6** furnished a maximum EQE of 19.5% and maintained

the high EQE of 16% at 1000 cd/m^2 with a satisfactory color purity of coordinates (0.16, 0.20). Recently, high-performance TADF based hybrid WOLEDs employing **D6** as the blue emitter were successfully fabricated [44]. Interestingly, WOLEDs showed excellent device characteristics with an EQE of 23.0%, a current and power efficiency of 51.0 cd/A and 51.7 lm/W, respectively. These performances are among the highest values reported to date for hybrid WOLEDs using a TADF material as the blue emitter. Derivative **D6** was also examined in the context of undoped OLEDs [45]. Undoped OLEDs are more attractive than their doped analogues due to an easier fabrication process, a higher reproducibility and reliability. With regards to the highly twisted structure of **D6** and the presence of methyl groups on the 9,9-dimethyl-9,10-dihydroacridine units, this molecule proved to be also nearly insensitive to the concentration, showing an emission maximum for the neat film at 470 nm which is almost similar to that obtained for a 10 wt %-doped mCP film (462 nm where mCP stands for *m-bis*(*N*-carbazolyl)benzene). Parallel to this, the fluorescence and TADF lifetime were almost the same for both the doped and undoped film, making **D6** a candidate applicable for the design of undoped OLEDs. Trilayered undoped OLEDs fabricated with **D6** displayed a sky-blue emission peaking at 480 nm, with an EQE of 19.5% at a luminance of 100 cd/m^2, slightly red-shifted compared to the emission observed for doped OLEDs. Clearly, the specific design of **D6** and its highly twisted structure efficiently weakened the π–π-stacking interactions, providing a general design rule for the elaboration of TADF emitters insensitive to the concentration. Belonging to the same family of structure than **D6**, **D7** that derives from the 9,9-dimethylthioxanthene-*S,S*-dioxide structure provided a better color purity (465 nm, (0.16, 0.24) for **D7** instead of 480 nm for **D6**) and a higher EQE (22.4% for **D7** instead of 19.5% for **D6**) than **D6** by optimizing the architecture of the doped EML [29]. By selecting the host of appropriate polarity, the combination of **D7** with the correct host could minimize the RISC barrier, optimize the RICS rate and thus maximize the TADF efficiency. While combining the blue TADF emitter **D7** with a green and an orange TADF emitter, all-TADF white OLEDs with 16% EQE could be fabricated [30].

4. Triazine–pyrimidine based emitters

Among possible electron acceptors, another structure has been extensively regarded as an adequate electron acceptor for the design of blue TADF emitters and this structure is the triazine unit. When combined with the azasiline donor, OLEDs displaying the unprecedented EQE of 22.3% were obtained [46]. As specificity, azasiline is a 6-membered heterocycle comprising a silicon atom introduced instead of a carbon atom to enlarge the HOMO–LUMO gap and lower the HOMO level. Due to the sp^3 hybridization of the silicon atom, two phenyl rings can be introduced on the silicon-bridged structure providing bulkiness and rigidity to the donor. Intermolecular interactions are thus efficiently prevented and the conformation disorder drastically reduced. When used as electron donor in **T1**, a ΔE_{ST} of 0.14 eV was determined experimentally, with a TADF lifetime of 25.4 μs and a 13:87 ratio between the prompt and delayed fluorescence. OLEDs fabricated with **T1** and a mCP:TSPO1 cohost (with TSPO1 = diphenyl-4-(triphenylsilyl)-phenylphosphine oxide) furnished a blue emission peaking at 463 nm, with CIE coordinates of (0.149, 0.197) and a low efficiency roll-off. Another key and general design rule for obtaining a small ΔE_{ST} consists in the physical separation of the donor and the acceptor by elongating the spacer that couples the two partners. Following this recommendation, an additional phenyl ring was introduced between the donor and the acceptor in **T2**, providing the extended version of **T1** (see Figure 4) [47]. As expected, the phenyl ring increased the separation of the HOMO and LUMO orbitals, such that ΔE_{ST} decreased. A value as low as 0.04 eV was experimentally determined for **T2**. In doped devices, **T2** demonstrated an EL efficiency of 4.7% with a deep blue emission (0.151, 0.087) approaching the NTSC blue standard (0.14, 0.08). However, a comparison with the previous EL performance evidenced that EQEs obtained with **T2** are 5 times lower than that obtained with **T1**, despites the more favorable S_1–T_1 energy splitting. This problem is commonly observed if the isolation of the electron-donating and electron-accepting parts is obtained upon extension of the distance between the two moieties. Indeed, as a consequence of this strategy, a weaker intramolecular charge transfer takes place and a reduction of the oscillator strength in the D–A diad is observed, resulting in a drastic reduction of the PLQY and thus of the external quantum efficiency. In the same study, authors examined the case of two TADF emitters based on a donor–acceptor–donor (D–A–D) structure, i.e., **T3** and **T4**, where azasiline was used as the donor and diphenylsulfone or benzophenone as the acceptors. Here again, the higher twisted molecular structure of **T4** was beneficial in terms of ΔE_{ST}, color purity and EL performances. Thus, the higher internal torsion of **T4** furnished OLEDs with a deeper blue emission (0.154, 0.107) than devices fabricated with **T3** (0.174, 0.310). Even if the EQE of **T4**-based devices was lower than that of **T3**-based devices (2.3% for **T4**-based OLEDs instead of 11.4% for **T3**-based devices), it is attributable to the higher color purity of **T4**-based devices and not to differences of ΔE_{ST} (0.07 eV and 0.06 eV for **T3** and **T4**, respectively). Azasiline is a promising electron donor but examples of blue TADF emitters are still scarce. The opposite situation is found for carbazole, which has long been considered as an excellent donor and a large variety of blue TADF emitters have been designed on the basis of this scaffold. At least 19 examples of blue TADF emitters can be cited, the molecules differing by the



	T1	T2	T3	T4	T5	T6	T7	T7
reference	[46]	[47]	[47]	[47]	[48]	[48]	[48]	[49]
ΔE_{ST} (eV)	0.14	0.04	0.06	0.07	0.09	0.09	0.28	0.35
decay time delayed component (μs)	25.4	–	–	–	–	–	–	–
EQE (%)	22.3	4.7	11.4	2.3	7.7	20.6	16.8	12.2
CIE (x,y)	(0.15, 0.20)	(0.15, 0.09)	(0.17, 0.31)	(0.15, 0.11)	(0.26, 0.43)	(0.19, 0.35)	(0.17 0.27)	(0.18, 0.32)

Figure 4: Triazine-based TADF emitters **T1**–**T3, T5**–**T7 and** azasiline derivatives **T3** and **T4**.

strategy used to connect the donor(s) to triazine. However, contrarily to azasiline that possesses a six-membered central ring, carbazole only possesses a five-membered central ring, inducing a deviation of the two adjacent aromatic rings. As a result, carbazole is not capable to induce the same encumbrance as that of azasiline by inducing smaller steric effects and the substitution of the 1,8-positions is often required to maintain a large dihedral angle.

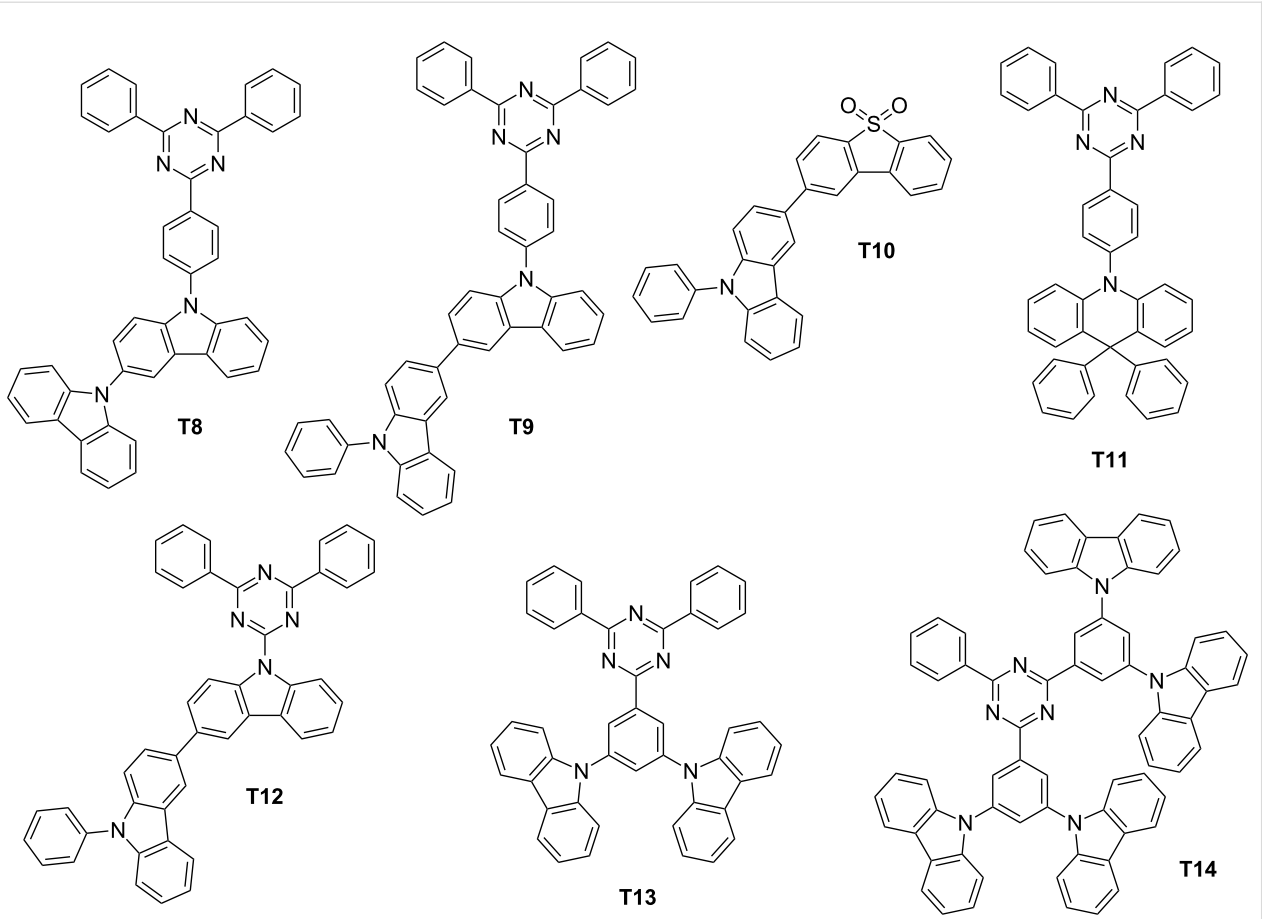
As interesting design rules, Adachi determined that the extension of the electronic delocalization of both the HOMO and LUMO energy levels could greatly increase the rate of the radiative decay by inducing a large oscillator strength while lowering ΔE_{ST}, even for emitters for which only a small overlap between the two wavefunctions is observed [48]. These findings constitute a second guideline for the molecular design of TADF emitters that can address the distance and the reduction

of the oscillator strength issue previously mentioned. To establish this, a series of molecules **T5**–**T8** with varying length of the π-conjugated system for the donating part was investigated. Thus, for **T5** and **T6**, a similar ΔE_{ST} value of 0.09–0.12 eV was experimentally determined for the two emitters. However, significant differences were determined for their PLQYs and values of 0.1 and 0.7 were measured for **T5** and **T6**, respectively. By theoretical calculations, the oscillator strength of **T6** was found to be 13.6 times greater than that of **T5**, supporting the enhanced luminescence of **T6** by the higher delocalization of its HOMO level. This trend was confirmed by keeping the acceptor constant in **T6**–**T8**. An increase of ΔE_{ST} while reducing the possible electronic delocalization over the electron-donating part was clearly evidenced going from **T6** to **T8**. In OLEDs, EL performances followed the same trend, with the highest EQE obtained with **T6** (EQE = 20.6%) and the lowest one with **T8** (EQE = 14.6%). A lower color purity was obtained for **T6**-based devices (λ_{EL} = 487 nm) compared to **T7** and **T8** (λ_{EL} = 478 and 477 nm, respectively) [22]. A worse result was obtained for **T5** that produced a blue-green EL at 506 nm. Recently, an extensive work was devoted to examine the degradation mechanisms in blue TADF OLEDs and **T7** was revisited in this context [49]. The synergy of an electro-oxidation process together with a photo-oxidation was determined as playing a critical role in the degradation of blue TADF emitters. In fact, a parallel can be easily done with the treatment of wastewater, where pollutants are removed from water by combining a photochemical and an electrochemical process [50]. During this study, the localization of the triplet spin density was found determinant for the stability of blue TADF emitters. To evidence this, four emitters (**T7**, **T9**–**T11**) exhibiting the same S_1 and T_1 energy levels, the same TADF lifetimes but differing by the distribution of the triplet spin densities were examined (see Figure 4 and Figure 5). Notably, for **T9**, the triplet spin density was found to be mainly localized on the bicarbazole donor, whereas for **T7** and **T10**, the triplet spin density is localized on their acceptor fragment. To end, the triplet spin density of **T11** is delocalized over the entire structure. While examining the device lifetime, **T9**-based devices had the longest device lifetime (32 hours), far from **T10**-, **T7**- and **T11**-based OLEDs (1.4 h, 2.8 h and 0.9 h, respectively), demonstrating the higher stability of the emitters with a triplet spin density centered onto the donor unit. In another study, an analogue of **T9**, i.e., **T12**, differing by the removal of a phenyl ring between the carbazole and the triazine units proved once again the crucial role of the oscillator strength in the photophysical properties [51]. Notably, major differences in the separation of their HOMO and LUMO energy levels were determined by theoretical calculations. An overlap of the two electronic wavefunctions was detected for **T9** whereas the two orbitals are strongly localized in the case of **T12**. Resulting from this marked localization in **T12**, a smaller variation of the electronic density upon excitation is expected, reducing the oscillator strength and the PLQY. When tested in devices, only a green-blue emission was obtained with **T12** (see Figure 5) [52]. The Influence of the oscillator strength on OLEDs characteristics could also be evidenced while comparing **T13** and **T14** [53]. Molecular orbital calculations performed on **T13** and **T14** showed the two molecules to exhibit a similar electronic distribution, what was confirmed by UV–visible and photoluminescence (PL) spectroscopy. Only a slight red shift of the absorption was detected for **T14** as the result of the strengthened donating ability of the dicarbazolylphenyl moieties. Similarly, almost identical ΔE_{ST} were determined with values of 0.25 and 0.27 eV for **T13** and **T14**, respectively). As it could be anticipated, **T14** furnished slightly better EL performances (18.9%) compared to that measured for **T13** (17.8%), due to its more extended donating part but also owing to its higher PLQY. Conversely, the color purity was higher for **T13**-based devices (λ_{EL} = 459 nm) instead of 467 nm for **T14**-based devices. However, a remarkable device stability was demonstrated for **T14**-based OLEDs, 80% of the initial luminance being retained after 52 hours. This value was reduced to only 5 hours for **T13**-based OLEDs. A comparison established with an iridium complex, i.e., tris[1-(2,4-diisopropyldibenzo[*b*,*d*]furan-3-yl)-2-phenyl-1*H*-imidazole]iridium(III) ($Ir(dbi)_3$) evidenced the relevance of the TADF approach, as a device lifetime of only 18 hours was found while operating OLEDs in the same conditions. The spatial separation of the electron-donating part from the electron-accepting moiety by elongating the spacer has already been discussed and the drawbacks evoked.

Minimization of the electron density overlap can also be realized by means of an *ortho*-phenyl linkage, enabling to maintain the donor in proximity of the acceptor.

In this situation, one aromatic ring of the donor and/or the acceptor is substituted at the 1,2-positions, generating a highly-twisted structure. Five blue TADF emitters **T15**–**T19** were designed on this basis (see Figure 6). By increasing the number of carbazoles in **T16** compared to **T15**, a decrease of ΔE_{ST} was logically observed (0.06 eV for **T15** and 0.03 eV for **T16**) [54]. A large torsion angle of 66° and 67° were, respectively, determined by theoretical calculations for **T15** and **T16**, favorable to the separation of the two orbitals. In devices, a remarkable enhancement of the EL performances was realized by increasing the number of carbazole units. Thus, a maximum EQE of 12.2% was realized with **T15**, whereas an EQE of 16.5% was determined for **T16**-based devices.

This enhancement can also be attributable to an increase of the oscillator strength from **T15** to **T16**, the number of donors

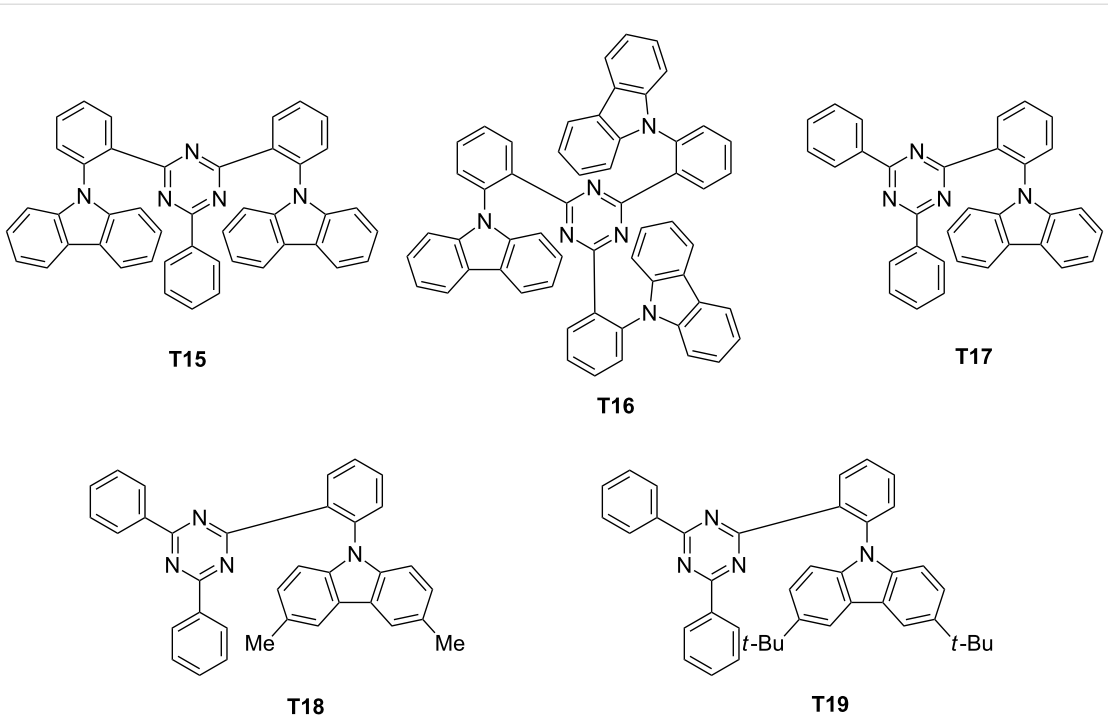


	T8	T9	T10	T11	T12	T13	T14
reference	[48]	[49]	[49]	[49]	[51]	[53]	[53]
ΔE_{ST} (eV)	0.32	0.31	0.38	0.28	–	–	–
decay time delayed component (μs)	–	–	–	–	–	3.1	2.8
EQE (%)	14.6	20.5	11.8	18.2	–	17.8	18.9
CIE (x,y)	(0.18, 0.28)	(0.18, 0.34)	(0.21, 0.39)	(0.19, 0.36)	–	(0.15, 0.16)	(0.16, 0.22)

Figure 5: Triazine-based TADF emitters **T8**, **T9**, **T11**–**T14** and carbazole derivative **T10**.

being increased. The low efficiency roll-off of **T16**-based devices was assigned to the specific design of the emitter, with the triazine acceptor being totally surrounded by carbazoles. As a result, triplet–triplet annihilation by the Dexter mechanism could be efficiently prevented, enabling to maintain high efficiencies at high current density. Although the number of carbazole units increased, no modification of the EL position was detected, the emission peaking at 467 and 468 nm for **T15**- and **T16**-based devices. In the same spirit, other authors examined the possible impact of the substitution pattern of the carbazole unit on the photophysical properties.

While maintaining the same number of carbazole units on the emitter and by varying the substitution pattern of the carbazole core, only a weak influence on the EL characteristics was evidenced [55]. In fact, performances only varied by their differences of PLQYs (16.7%, 50.5% and 43.0% for **T17**, **T18** and **T19**, respectively), the three molecules exhibiting similar photophysical properties (ΔE_{ST}, emission wavelength and decay times of the delayed emission). Recently, a potential alternative to the *ortho*-substitution of the triazine acceptor by carbazole moieties was examined, consisting in introducing methyl groups in the proper position of the triazine or the carbazole moieties

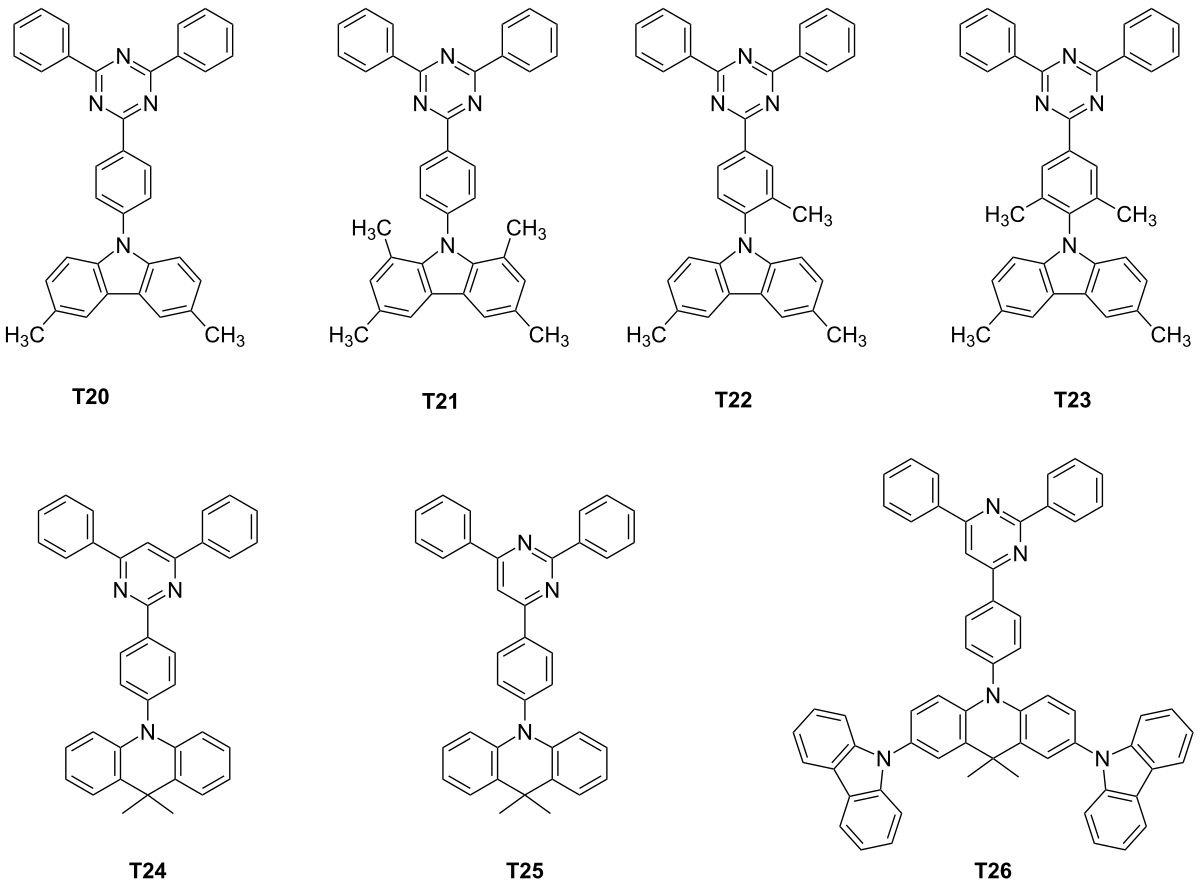


	T15	T16	T17	T18	T19
reference	[54]	[54]	[55]	[55]	[55]
ΔE_{ST} (eV)	0.06	0.03	–	–	–
decay time delayed component (μs)	5.4	5.0	3.9	3.9	3.9
EQE (%)	12.2	14.9	9.3	14.7	12.3
CIE (x,y)	(0.15, 0.21)	(0.15, 0.22)	(0.15, 0.22)	(0.17, 0.34)	(0.17, 0.31)

Figure 6: Triazine-based TADF emitters **T15**–**T19**.

[56]. By changing the methyl group positions, optical properties of **T20–T23** were not significantly modified, contrarily to their ΔE_{ST} (see Figure 7). In fact, the authors evidenced the introduction of methyl groups at the 1,8-positions of carbazole to be harmful for producing a deep-blue emission whereas the substitution of the central phenyl ring by methyl groups could provide the same molecular twist than the 1,8-substitution of carbazole while maintaining a large optical bandgap. In fact, dihedral angles of 49.9, 86.8, 71.4 and 82.4° were determined by density functional theory (DFT) calculations between the donor plane and the acceptor plane for **T20**–**T23**, respectively. Due to its lesser twisted structure and based on the design rule previously evoked (orthogonality between the donor and the acceptor is researched to isolate the two groups), **T20** showed the higher ΔE_{ST} of the series. Theoretical calculations clearly evidenced for **T20** the HOMO level to extend to the neighbouring phenylene bridge, adversely affecting ΔE_{ST}. Conversely, the large dihedral angle of **T21**–**T23** contributed to spatially separate the HOMO from the LUMO orbitals. By electrochemistry, an appreciable reduction of the oxidation potential was detected (+0.87 V) for **T21** which is substituted at the 1,8-positions of the donor whereas **T20**, **T22** and **T23** exhibited the same oxidation potentials (+0.97 V). By PL, T_1 states of **T20**, **T22** and **T23** proved to be ^{3}LE states whereas a ^{3}CT state was found for **T21**.

To evidence this, examination of the phosphorescence spectra of **T20–T23** in a frozen toluene matrix at 77 K revealed for **T20**, **T22** and **T23** to exhibit well-resolved vibrational structures, demonstrating their T_1 states to be ^{3}LE states. Conversely, only a broad spectrum was obtained for **T21**, and its triplet state was assigned to a ^{3}CT state. Precisely, by its large dihedral angle, **T21** differs from **T20**, **T22** and **T23** by the order of its orbitals, ^{3}LE and ^{3}CT being inverted in this case. Analysis of the transient PL decay curves showed **T20** to exhibit a negligible delayed fluorescence as a result of large ΔE_{ST}. On the

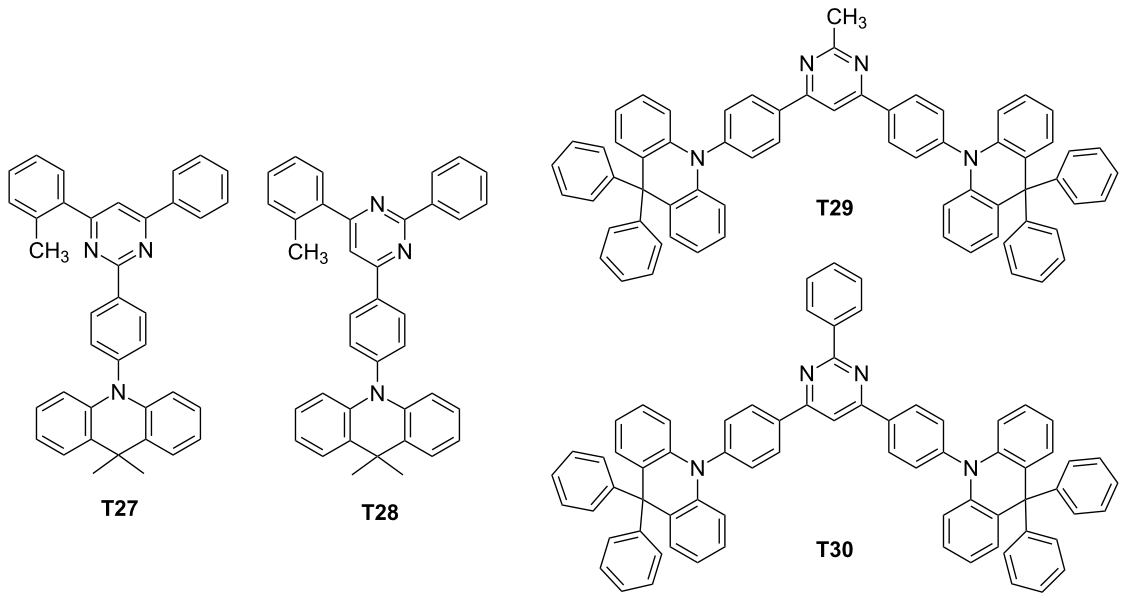


	T20	T21	T22	T23	T24	T25	T26
reference	[56]	[56]	[56]	[56]	[57]	[57]	[57]
ΔE_{ST} (eV)	0.43	0.07	0.17	0.15	0.25	0.17	0.12
decay time delayed component (μs)	–	3.5	13.0	10.3	178	87	55
EQE (%)	7.2	22.0	19.2	18.3	11.8	18.6	22.8
CIE (x,y)	–	–	(0.15, 0.10)	(0.15, 0.10)	(0.16, 0.21)	(0.18, 0.33)	(0.21, 0.38)

Figure 7: Triazine- and pyrimidine-based TADF emitters **T20**–**T26**.

opposite, prompt and delayed fluorescence components were clearly evidenced for **T21**–**T23**. Lifetimes of the delayed components for **T21**–**T23** were 3.5, 13.0 and 10.3 μs, respectively. Due to the inability of **T20** to upconvert its electrons from the triplet to the singlet state, **T20**-based device could only reach an EQE of 7.2%. On the opposite, maximum EQEs of 22.0, 19.2 and 18.3% were obtained for **T21**–**T23**-based devices, with CIE coordinates of (0.148, 0.098) and (0.150, 0.097) for **T22**- and **T23**-based devices, respectively. As anticipated, a lower color purity was obtained for **T21**-based devices resulting from its lower oxidation potential. Recently, a significant enhancement of blue OLED performances was obtained by replacing the triazine acceptor by a 2,4,6-triphenylpyrimidine unit in donor-acceptor-based TADF emitters [57]. Considering that the electron acceptor is not symmetrical anymore, positions of the nitrogen atoms will significantly influence the distribution of the electronic cloud and potentially the overlap with the HOMO level. Examination of the electronic properties of **T24** revealed the HOMO and the LUMO levels are located on both the donor and acceptor part, respectively, without any contribution of the phenyl linker. Another situation was found for **T25** and **T26** since the LUMO predominantly extends on both the acceptor and the phenyl ring which is between the donor and the 4,6-diphenylpyrimidine fragment. Due to the smaller overlap of the

two wavefunctions, a weaker intramolecular charge transfer was attended, enabling to provide an emission in the blue or sky-blue region. Optical properties were evaluated in solution confirming this trend, with an emission at 455, 476, and 496 nm for **T24**–**T26**, respectively. Major differences could be found in the contribution of the delayed component in the luminescence decay. Following the trend determined for the intramolecular charge transfer, a regular increase of the prompt component in the overall decay of the three emitters was found, evidencing the up-conversion of the triplet excitons to the singlet ones. The best EQE was obtained for **T26**-based devices (22.8%) consistent with the higher delocalization of its electron-donating part, its smaller ΔE_{ST} and the higher contribution of the delayed component in the overall luminescence decay. A regular decrease of the EQE was observed for **T25**-based devices (18.6%) and **T24**-based devices (11.8%), confirming the absence of delayed fluorescence for the last emitter and the reduction of the strength of ICT interactions. Interestingly, the EQE reported for **T26**-based devices is among the best so far reported for blue OLEDs. Attesting the interest of the community for this new acceptor, other authors developed quasi-simultaneously a structure–performance relationship with **T24**, **T25** and **T27**–**T28** (see Figure 8) [58]. The choice of pyrimidine as the electron acceptor was notably justified by authors due to the easier synthesis of the central core and a versatile peripheral substitution. Additionally, compared to triazine, the LUMO level of pyrimidine is slightly destabilized, facilitating the access to wide bandgap materials. In this work, a more intriguing behaviour was found even for **T24** and **T25** that have just been discussed above since mechanochromic properties were evidenced for the four emitters. Based on photophysical investigations, the presence of two different packing modes in the solid state were proven. When tested in OLEDs, no clear conclusions could be deduced as results of opposite trends were detected. Thus, if the EQE of **T24**-based OLEDs was lower than that determined for **T27**-based OLEDs (7.2% and 11.8%, respectively), the opposite trend was found with **T25** and **T28** (12.6% and 11.8%, respectively). Only the influence of the symmetrical or the unsymmetrical substitution of the pyrimidine acceptor by the donor was evidenced, following the conclusions of previous authors.



	T27	T28	T29	T30
reference	[58]	[58]	[59]	[59]
ΔE_{ST} (eV)	0.13	0.13	0.26	0.24
decay time delayed component (μs)	–	–	–	–
EQE (%)	11.8	11.8	19.0	20.8
CIE (x,y)	(0.17, 0.21)	(0.18, 0.30)	(0.16, 0.21)	(0.16, 0.24)

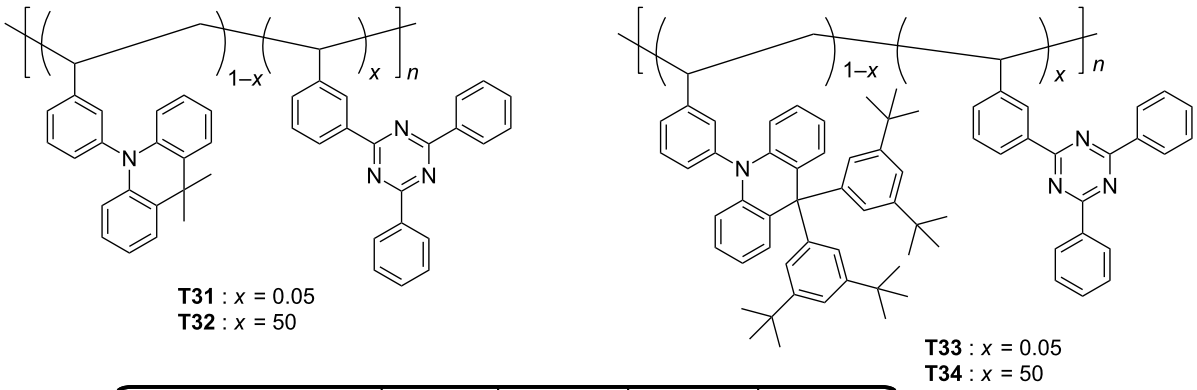
Figure 8: Pyrimidine-based TADF emitters **T27**–**T30**.

Finally, two D–A–D triads comprising the 9,9-diphenyl-9,10-dihydroacridine donor were reported in 2016 [59]. Here again, existence of relatively large dihedral angles of 82–87° between the donor unit and the nearby phenylene linker for **T29** and **T30** was confirmed by quantum chemical calculations. Resulting from the almost perfect orthogonality, a good confinement of the electronic density of the two orbitals was obtained with a HOMO level predominantly located on the donor and a distribution of the LUMO over the central pyrimidine acceptor core and the adjacent phenylene linkers small ΔE_{ST} were determined (0.16 and 0.15 eV for **T29** and **T30**, respectively), indicative of reduced electronic correlations between frontier orbitals and accounting for their high performance. Indeed, EQEs of 19.0 and 20.8%, an EL at 468 and 472 nm were, respectively, determined for **T29** and **T30**. However, the efficiency roll-off was quite severe and this drawback was assigned to the relatively long exciton lifetimes of **T29** and **T30** in doped films (330 and 210 μs, respectively). Recently, an original strategy to combine the electron-donating 9,9-dimethyl-10-phenylacridan with the electron-accepting 2,4,6-triphenyl-1,3,5-triazine was reported under the form of random copolymers derived from a polystyrene (**T31**–**T34**, see Figure 9) [60]. Contrarily to the classical TADF materials in which the electron donor is connected to the acceptor, interactions between the two moieties occur by mean of a through-space charge transfer (TSCT). Polystyrenes of different compositions **T31**–**T34** were examined, varying by the acceptor content (5 or 50 wt % of acceptor) and the donor units, i.e., 9,9-dimethyl-10-phenylacridan or 9,9-bis(3,5-di-*tert*-butylphenyl)-10-phenylacridan. Precisely, effect of the steric hindrance on TADF properties of the polymers was investigated by introducing a steric hindrance on the electron donor. Use of polystyrene to generate EL materials is counterintuitive due to its inherent insulating character, but EL polymers substituted with iridium complexes have previously been studied in the literature, evidencing the pertinence of the strategy [61].

In this case, charge transport properties are provided by the substituents attached to the polymer chain. As main finding of this work, the detrimental effect of the steric hindrance was demonstrated, no TSCT effects and no TADF features were detected for **T33** and **T34**. Conversely, for the less hindered polymers, a delayed fluorescence could be evidenced for the two polymers **T31** and **T32**, with a ratio for the prompt/delayed component of 13/87, respectively. ΔE_{ST} values of 0.019 (**T31**) and 0.021 eV (**T32**) were also determined by examining the fluorescence and phosphorescence spectra. Interestingly, the bluest EL emission (472 nm) was obtained for the polymer only containing 5 wt % of acceptor **T31**, with an EQE peaking at 12.1% for these solution-processed OLEDs, what is remarkable. Conversely, a less blue emission was obtained for **T32**, the emission peaking in the blue-green region (497 nm).

5. Phenoxaphosphine oxide and phenoxathiin dioxide derivatives

Recently, phenoxaphosphine oxide and phenoxathiin dioxide have gained interest as electron acceptors since the first report mentioning their use as acceptors was published by Lee et al. in



	T31	T32	T33	T34
reference	[60]	[60]	[60]	[60]
ΔE_{ST} (eV)	0.019	0.021	–	–
decay time delayed component (μs)	1.17	1.28	–	–
EQE (%)	3.1	12.1	0.21	0.33
CIE (x,y)	(0.22, 0.43)	(0.18, 0.27)	(0.23, 0.24)	(0.21, 0.20)

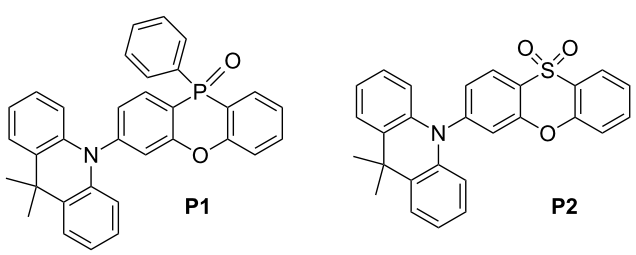
Figure 9: Triazine-based TADF polymers **T31**–**T32**.

2016 [62]. Prior to this work, phenoxaphosphine oxide derivatives were mostly studied for the design of flame-retardants [63] or as chiral molecules for fullerene recognition [64-66]. Similarly, the scope of applications of phenoxathiin dioxide ranged from antimicrobial activity [67] to the use as inhibitor for *Hepatitis C* virus infection [68]. Here, in the context of OLEDs, Lee et al. reported two blue TADF emitters, **P1** and **P2** (see Figure 10), containing a phenoxaphosphine oxide or a phenoxathiin dioxide acceptor covalently linked to a dimethylacridan donor.

Theoretical calculations predicted the two molecules to adopt in their optimized molecular geometries a highly twisted conformation, what is a requirement for a spatial separation of the HOMO and LUMO energy levels. As attended, the LUMOs of **P1** and **P2** are localized on the acceptor moieties whereas their HOMOs are mostly distributed on the donor. Separation of the frontier orbitals lead to ΔE_{ST} values of 0.02 (**P1**) and 0.10 eV (**P2**), which are in perfect accordance with the experimental data: ΔE_{ST} = 0.03 and 0.06 eV for **P1** and **P2**, respectively. Interestingly, theoretical calculations also showed the higher electron-accepting ability of the phenoxathiin dioxide moiety compared to that of the phenoxaphosphine oxide group owing to the stronger electron-withdrawing properties of the sulfone group, with a theoretical LUMO level at −1.52 and −1.24 eV for **P2** and **P1,** respectively. In multilayered devices, remarkable CIE coordinates could be realized with **P1**- and **P2**-based OLEDs ((0.15, 0.14) with **P1** and (0.16, 0.26) with **P2**), combined with high EQEs (12.3% and 20.5%, respectively). Additionally, for **P2**-based devices, the efficiency roll-off could be remarkably suppressed and an EQE as high as 13% could be maintained at the luminance of 1000 cd·m^{-2}.

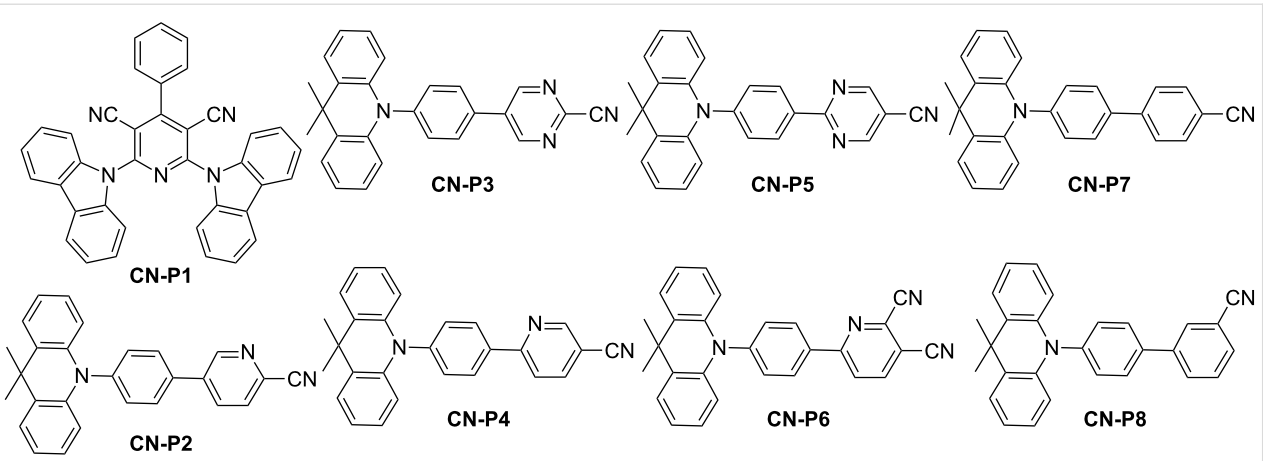
6. CN-Substituted pyridine and pyrimidine derivatives

In 2015, Liu et al. constructed a novel blue TADF emitter **CN-P1** comprising a carbazole donating moiety connected to a pyridine-3,5-dicarbonitrile accepting group (see Figure 11) [69]. The choice of pyridine-3,5-dicarbonitrile as acceptor was notably motivated by the outstanding charge-transport ability and the remarkable electrochemical stability of this group [70,71]. Thus, **CN-P1** had a small singlet−triplet splitting (ΔE_{ST} = 0.04 eV), fairish PLQY in doped films (49.7%), and a delayed decay lifetime of 46.6 μs, which suggests that it could be a promising candidate as emitter. EL performance of **CN-P1** was investigated in OLEDs with different **CN-P1** doping concentrations in *m*CP as the emitting layers. The highest EQE (21.2%) of devices was obtained at 13 wt % doping conditions. It was found that the maximum EQEs are enlarged along with the increase of doping concentration, which can be mainly attributed to the more efficient exciton utilization with a higher emitter concentration. However, EQEs decreased with the further concentration increase of **CN-P1** due to the strong interaction and aggregation between **CN-P1** molecules at high doping concentration in the emitting layer. Authors obtained EL spectra red-shifting from sky-blue (λ_{max} = 475 nm, CIE = (0.18, 0.26)) to greenish-blue (λ_{max} = 510 nm, CIE = (0.24, 0.40)) emissions by varying the doping concentration from 5 to 50 wt %. Such red shift is clearly caused by the interaction between **CN-P1** molecules at high dopant concentrations. Parallel to this, **CN-P1** molecules can also increase the polarity of the EML, thus introducing a solvatochromaticity-like shift comparable to that observed in solutions while varying the solvents polarity. The optimized device exhibited a maximum current efficiency of 47.7 cd·A^{-1}, and a maximum power efficiency of 42.8 lm·W^{-1} without any light outcoupling structures, indicating that nearly 100% of excitons are harvested for light emission. Such high performance should not only be attributed to the fairish PLQY and the efficient RISC process from T_1 to S_1 of **CN-P1** emitter, but also owed to the reasonable high T_1, good charge mobility, and well-matched PL spectrum of the mCP host with the **CN-P1** absorption spectrum. Still based on pyridine derivatives, Pan et al. prepared a series of twisted D–π–A type emitters based on the dimethylacridan and different CN-substituted acceptors (pyridine, pyrimidine, and benzene, see Figure 11) [72]. Theoretical calculations showed the different emitters to adopt a nearly orthogonal conformation between the donor and the central aromatic ring, interrupting the



	P1	P2
reference	[62]	[62]
ΔE_{ST} (eV)	0.03	0.06
decay time delayed component (μs)	3.8	2.7
EQE (%)	12.3	20.5
CIE (x,y)	(0.15, 0.14)	(0.16, 0.26)

Figure 10: Phenoxaphosphine oxide and phenoxathiin dioxide-based TADF emitters **P1** and **P2**.



	CN-P1	CN-P2	CN-P3	CN-P4	CN-P5	CN-P6	CN-P7	CN-P8
reference	[69]	[72]	[72]	[72]	[72]	[72]	[72]	[72]
ΔE_{ST} (eV)	0.04	0.19	0.09	0.18	0.04	0.032	0.439	0.403
decay time delayed component (μs)	46.6	19.3	11.6	14.5	5.2	1.9	0.03	0.01
EQE (%)	21.2	23.9	31.3	23.1	30.6	29.2	5.7	1.6
CIE (x,y)	(0.20, 0.35)	(0.24, 0.49)	(0.32, 0.59)	(0.28, 0.54)	(0.34, 0.57)	(0.43, 0.55)	(0.17, 0.18)	(0.16, 0.06)

Figure 11: CN-Substituted pyridine and pyrimidine derivatives **CN-P1**–**CN-P8**.

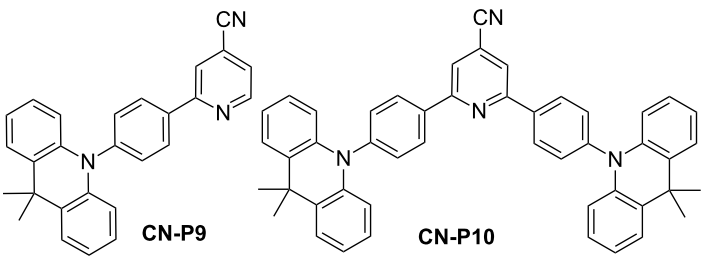
π-conjugation and localizing the HOMO level on the acridan moiety and the LUMO level on the central accepting group. The calculations also predicted a more planar phenyl–pyrimidine/phenyl–pyridine conformation (i.e., a smaller dihedral angle) in **CN-P5**/**CN-P4** and a more twisted phenyl–pyrimidine/phenyl–pyridine conformation (i.e., a larger dihedral angle) in **CN-P3**/**CN-P2**. All the DFT-optimized data were in perfect accordance with single crystal X-ray diffraction analyses. The results showed that the molecular conformations (twist angles in D-spacer-A diads) could be easily tuned by controlling the orientation of the nitrogen atom(s) in the heteroaromatic rings relative to the donor plane. In fact, two main groups of molecules were identified. Thus, **CN-P3**, **CN-P5** and **CN-P6** are characterized by a relatively small ΔE_{ST} of 0.032–0.090 eV, show the most pronounced contribution of the delayed component in PL with emission quantum yields for the delayed component of luminescence in the 38–44% range.

These molecules also exhibit high reverse intersystem crossing rates ($k_{RISC} > 15 \times 10^4$ s^{-1}). Conversely, **CN-P2** and **CN-P4** show larger ΔE_{ST} (0.180 − 0.190 eV) than **CN-P3**, **CN-P5** and **CN-P6** and lower TADF contributions in PL with smaller quantum yields for the delayed component of luminescence (19–23%). Smaller RISC were also determined (k_{RISC} of $< 8 \times 10^4$ s^{-1}). Finally, TADF contribution on the total luminescence of **CN-P7** and **CN-P8** was the weakest of the series (≤1%) as a result of their extremely large ΔE_{ST} (>400 meV). Due to the weak contribution of the TADF process, these emitters could be nearly assimilated to conventional fluorescent emitters. All light-emitting materials show lifetimes for the prompt decay component of luminescence in the 6.5–27 ns range whereas the lifetimes for the delayed decay component varied from 1.9 to 19 μs. All compounds were tested in OLED and all devices exhibited a relatively low turn-on voltage (≈2.5 V) and a low operation voltage (≈3.5–4 V for a brightness of 100 $cd \cdot m^{-2}$). Devices using high-PLQY emitters (PLQY = 90–100%) exhibited rather high EQEs of up to 23.1–31.3%, while **CN-P7** and **CN-P8** having the lower PLQYs gave inferior EQEs of 5.7% and 1.6%, respectively. Noticeably, emitters showing the most pronounced TADF characteristics (i.e., **CN-P6**, **CN-P3**, and **CN-P5**) furnished the remarkable EL efficiencies of 29.2% (96.3 $cd \cdot A^{-1}$, 105.5 $lm \cdot W^{-1}$), 31.3% (104.5 $cd \cdot A^{-1}$, 117.2 $lm \cdot W^{-1}$), and 30.6% (103.7 $cd \cdot A^{-1}$, 116.3 $lm \cdot W^{-1}$), respectively. On the opposite, **CN-P2** and **CN-P4** showing the less pronounced TADF characteristics exhibited similarly high PLQYs (90–92%) but lower EQEs (23–24%). Finally, **CN-P8,** in which the TADF contribution is almost inexistent, furnished the low EQE of 5.7% (this is also the material exhibiting the lowest PLQY (36%)), yet such an EQE is still significantly higher than it can be expected from a conventional non-TADF fluorescent emitter of similar PLQY (i.e., EQE can be estimated to be ≈2.5–3% at most), suggesting

therefore the contribution from the delayed fluorescence in the overall EL process. Although **CN-P6**, **CN-P5**, and **CN-P3** could reach high maximum EQEs, different efficiency roll-off behaviours could be evidenced with the following order: **CN-P6** < **CN-P5** < **CN-P3**. Such a trend for the efficiency roll-off correlate well with the order of their delayed fluorescence lifetimes and their RISC decay rate values in the host film: **CN-P6** < **CN-P5** < **CN-P3** for the delayed fluorescence lifetimes and **CN-P6** > **CN-P5** > **CN-P3** for k_{RISC}. Such correlation is also observed for **CN-P4** and **CN-P2** devices. It has been rationalized that a small delayed fluorescence lifetime (and thus effective RISC) is beneficial for faster triplet-to-singlet conversion, for reducing the triplet exciton population at higher brightness/current, and thus for reducing associated quenching mechanisms (e.g., triplet–triplet annihilation, etc.). This year, Sasabe et al. reported high efficiency blue OLEDs using isonicotinonitrile-based fluorescent emitters comprising 9,10-dihydro-9,9-dimethylacridine(s) as donor unit(s) [73]. The chemical structures of the two emitters **CN-P9** and **CN-P10** is given in Figure 12. While evaluating the optical and photophysical properties of the different materials, all compounds showed reasonably high PLQYs (71–79%) in the host films, with a sky-blue emission located at 489 and 495 nm for **CN-P9** and **CN-P10**, respectively. Delayed luminescence lifetimes of 453.7 µs and 116.9 µs, sufficiently small ΔE_{ST} of 0.30 eV and 0.28 eV to allow a RISC were also determined for **CN-P9** and **CN-P10**, respectively. Performances of the two sky-blue emitters **CN-P9** and **CN-P10** were then evaluated in OLEDs. **CN-P9**-based devices showed a sky-blue emission with CIE chromaticity coordinates of (0.19, 0.36), a low turn-on voltage of 3.1 V and an EQE of 15%. In contrast, **CN-P10**-based devices showed still a sky-blue emission with CIE coordinates of (0.22, 0.45), a low turn-on voltage of 2.9 V but an EQE peaking at 22%, resulting from its smaller ΔE_{ST}. Considering the EQE values overcoming the 5% EQE limit for fluorescent materials, contribution of a TADF process in the overall emission of these two emitters was clearly demonstrated.

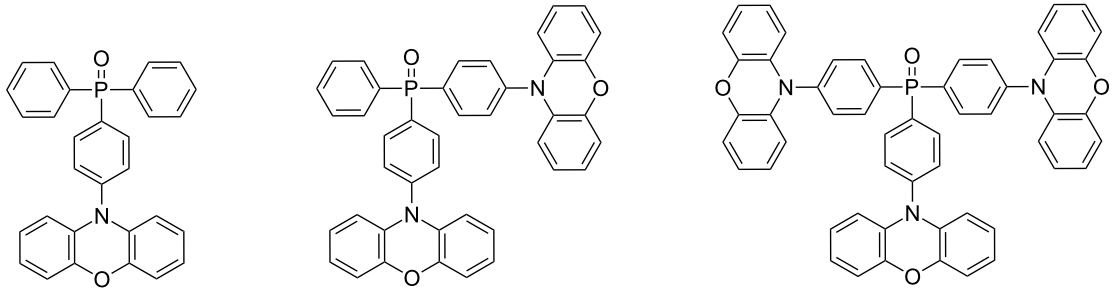
7. Phosphine oxide derivatives

Blue thermally activated delayed fluorescence (TADF) dyes are basically combinations of strong acceptors and weak donors. In their recent work, Duan et al. employed a weak acceptor group to construct a series of weak acceptor−strong donor (WASD)-type emitters with a phenoxazine donor [74]. The molecular structures of these fluorescent compounds, namely 4-(10*H*-phenoxazin-10-yl)phenyl)diphenylphosphine oxide (**PO-1**), bis(4-(10*H*-phenoxazin-10-yl)phenyl)phenylphosphine oxide (**PO-2**), and tris(4-(10*H*-phenoxazin-10-yl)phosphine oxide (**PO-3**) are given in Figure 13. Similar absorption spectra were measured in dilute solutions for all compounds, with three characteristic bands detected around 370, 320, and 240 nm. The first one was assigned to a n→π* transition from the phenoxazine group to the triphenylphosphine oxide group whereas the second and the third peak was attributed to π→π* transitions of the phenoxazine and the phenyl moities, respectively. A relation of proportionality was demonstrated in the intensities of the band, directly related to the number of phenoxazine groups per molecule. Almost identical PL spectra were determined for these molecules, proving the insulating character of the phosphine oxide group and the pertinence of the WASD strategy to preserve the emission color. Consistent with TD-DFT results, ΔE_{ST} decreased from 0.26 to 0.19 and finally 0.11 eV for **PO-1**, **PO-2** and **PO-3**, respectively. Relatively high PLQYs were also determined (45%, 57%, and 65%, for **PO-1**, **PO-2** and **PO-3**, respectively). PLQY of **PO-3**-based films were determined as 67%, higher than the values determined for **PO-2**- and **PO-1**-doped films. The prompt fluorescence lifetimes of **PO-1**, **PO-2**, and **PO-3** are gradually increasing from 8 to 13 to 20 ns. In contrast, the respective order of the delayed fluorescent lifetimes is reversed, at 95, 31, and 17 µs, accompanied by a gradual increase of the quantum yields of 36%, 45%, and 51%, respectively. **PO-1**-based OLED achieved EL emissions with peaks at 448 nm and CIE coordinates of (0.16, 0.12), corresponding to a deep-blue light. **PO-2**-based devices displayed a blue emission peaking at 460 nm and CIE coordinates of (0.16, 0.20).



	CN-P9	CN-P10
reference	[73]	[73]
ΔE_{ST} (eV)	0.30	0.28
decay time delayed component (µs)	454	117
EQE (%)	15.2	21.6
CIE (x,y)	(0.19, 0.36)	(0.22, 0.45)

Figure 12: CN-Substituted pyridine derivatives **CN-P9** and **CN-P10**.



PO-1 PO-2 PO-3

	PO-1	PO-2	PO-3
reference	[74]	[74]	[74]
ΔE_{ST} (eV)	0.26	0.19	0.11
decay time delayed component (μs)	95	31	17
EQE (%)	6.3	10.6	15.3
CIE (x,y)	(0.16, 0.12)	(0.16, 0.20)	(0.17, 0.20)

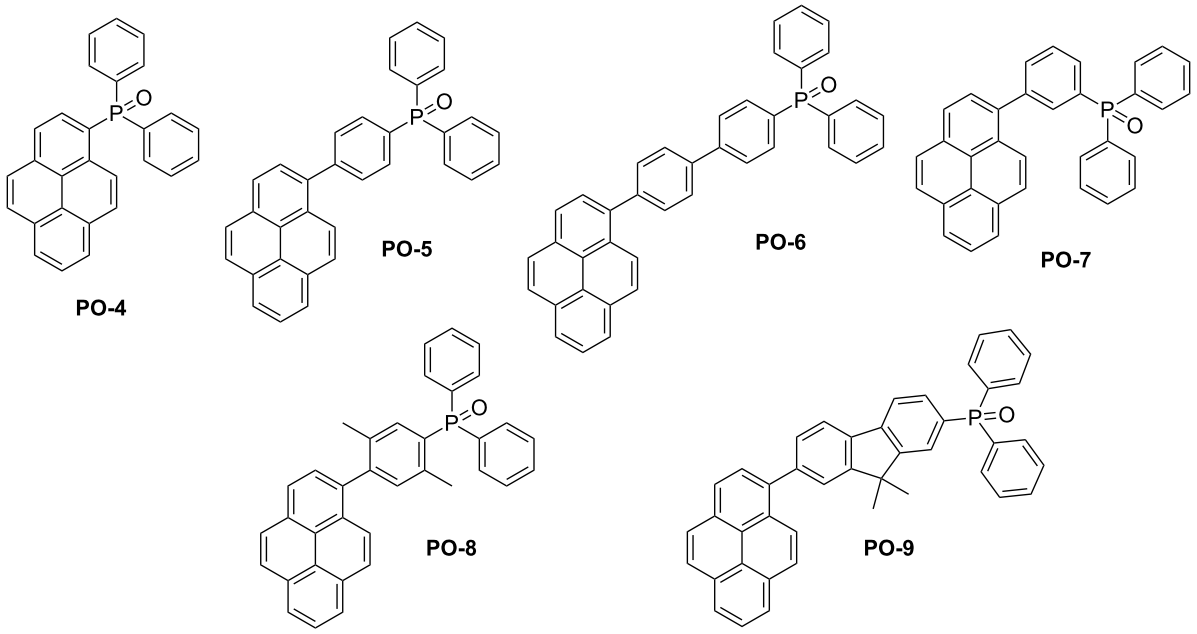
Figure 13: Phosphine oxide-based TADF blue emitters **PO-1**–**PO-3**.

OLEDs fabricated with **PO-3** produced a pure-blue EL emission peaking at 464 nm, an EQE up to 15.3%, a low efficiency roll-off and CIE coordinates of (0.17, 0.20). With aim at simplifying the device fabrication, other authors tried to develop emitters **PO-4**–**PO-9** specifically designed for the fabrication of non-doped OLEDs (see Figure 14) [75]. To reach this goal, the electron-transport diphenylphosphine oxide group was attached to pyrene moieties, providing molecules with good film-forming abilities. High performance of OLEDs was assigned to the judicious combination of an enhanced charge transport ability due to the presence of the diphenylphosphine oxide group, the formation of pyrene excimers in the solid state and the assistance of the TADF property. More precisely, a contribution of a TADF process to the overall EL emission of OLEDs is suggested by the presence within the emissive layer of both pyrene and pyrene excimers, resulting in the presence of close-lying singlet and triplet states for the two forms. Besides, if a blue emission of the pyrene excimer assisted by TADF is suggested by the authors, no clear evidence of TADF is provided.

To support the presence of a TADF effect in the devices, the authors tentatively assigned the existence of the delayed component of fluorescence by the presence of close-lying singlet and triplet states in both pyrene derivatives and excimers, favorable to a reverse intersystem crossing giving rise to a delayed fluorescence. Multilayered OLEDs fabricated with **PO-4**–**PO-9** showed interesting efficiencies, with EQEs ranging from 7.2 to 9.1%. The contribution of the diphenylphosphine oxide group to the electron mobilities of these emitters was clearly evidenced by fabricating OLEDs using **PO-4**–**PO-9** as electron-carriers. By comparing with a reference electron-transport material, i.e., Alq_3, a two-fold enhancement of EQEs could be determined while using these materials as electron-transport layers, evidencing their higher electron mobilities compared to that of tris(8-hydroxyquinoline)aluminum Alq_3. Best OLEDs were obtained with **PO-8**, EQE peaking at 9.1%.

8. Benzonitrile derivatives

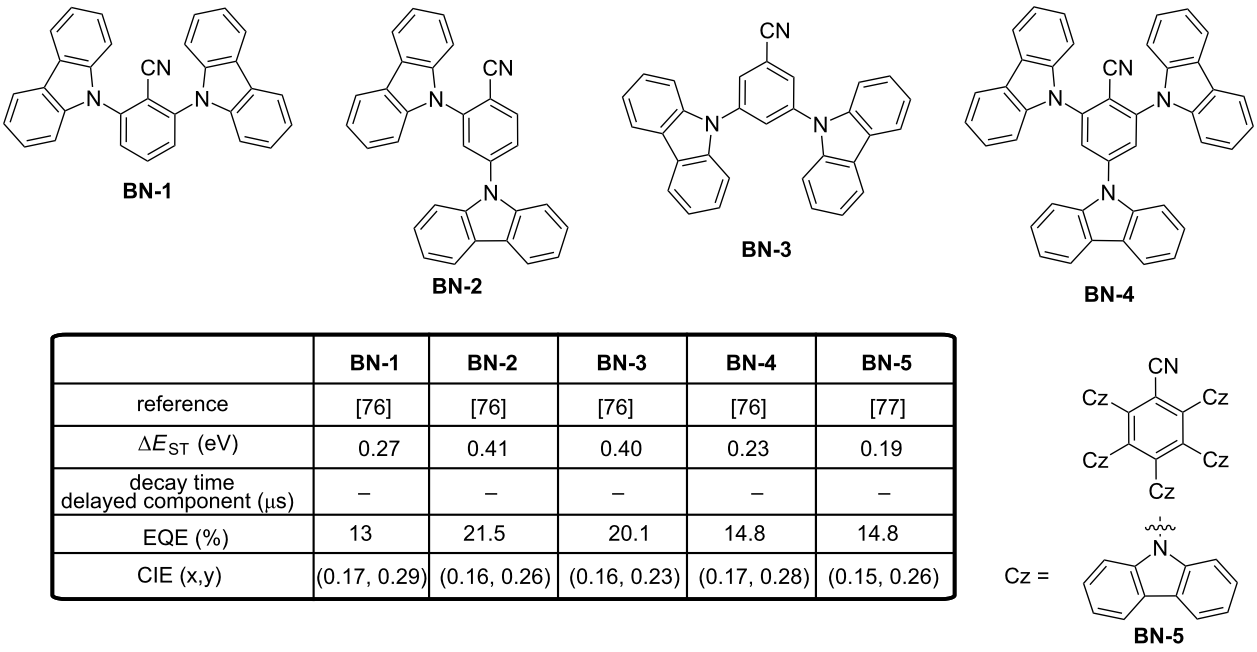
In the search for new acceptors, benzonitrile was identified as a promising candidate capable to contribute to the design of deep blue TADF emitters. Precisely, the cyano moiety is a group limiting the size of electron acceptor moiety by its compacity while remaining one of the strongest electron-accepting groups at disposal for chemists. By combining benzonitrile with two or three carbazole units, and due to the planarity of the two structures (carbazole, benzonitrile), a sufficient steric hindrance could be induced to provide the highly twisted structures **BN-1**–**BN-4** (see Figure 15) [76]. The four carbazolyl benzonitrile derivatives **BN-1**–**BN-4** were easily prepared in a one-step approach through aromatic nucleophilic substitution. Encouraging results were obtained with the four emitters while using high-triplet-energy hosts with favorable carrier injection/transporting abilities.



	PO-4	PO-5	PO-6	PO-7	PO-8	PO-9
reference	[75]	[75]	[75]	[75]	[75]	[75]
ΔE_{ST} (eV)	–	–	–	–	–	–
decay time delayed component (μs)	9	–	–	–	–	–
EQE (%)	7.4	7.2	7.9	8.0	9.1	8.1
CIE (x,y)	(0.18, 0.27)	(0.15, 0.38)	(0.19, 0.26)	(0.17, 0.23)	(0.16, 0.17)	(0.18, 0.24)

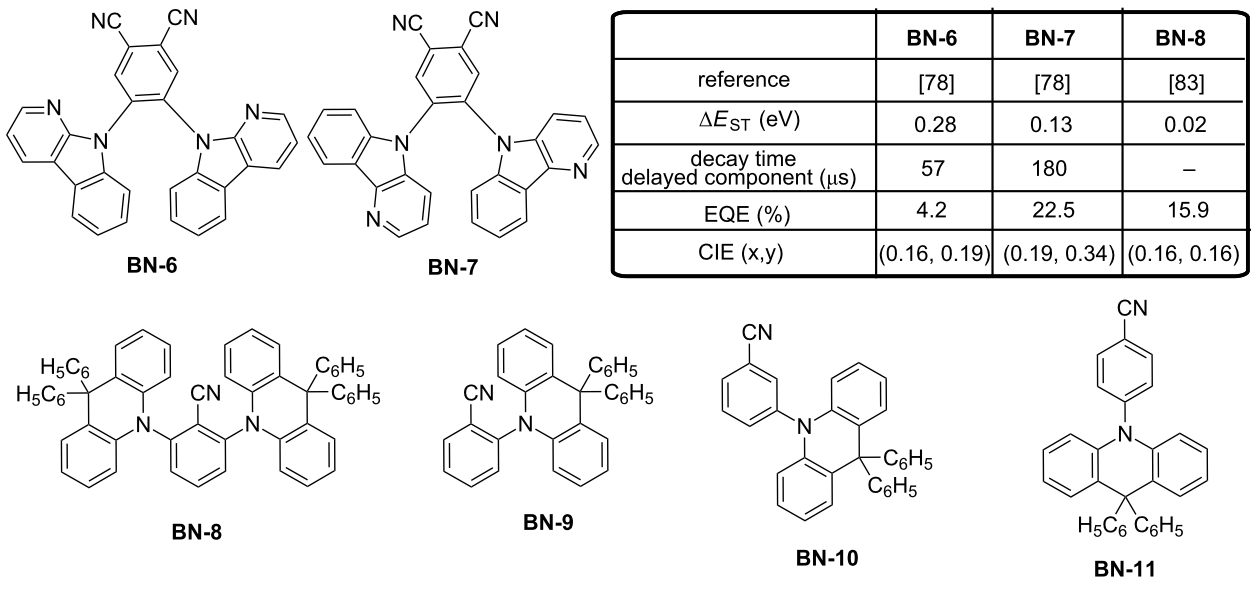
Figure 14: Phosphine oxide-based TADF blue emitters **PO-4**–**PO-9**.

The best performance was obtained with **BN-2**, endowing blue-emitting devices with a maximum EQE of 21.5%, which is among the highest values reported for blue TADF devices with an emission peak located at 470 nm. Another possibility could be to increase the number of carbazole units around the benzonitrile moiety. A benzonitrile derivative substituted by five carbazoles (**BN-5**) was synthesized and characterized by the Adachi team [77]. The OLEDs displayed a light-blue emission and a maximum EQE of 14.8%. Still based on this approach, the group of Hyuk Kwon went even further by introducing a nitrogen atom in the donor, furnishing the carbazole-derived α- and δ-carboline where the nitrogen heteroatom is introduced at the α- and δ-position respective to the central nitrogen atom (**BN-6** and **BN-7**, respectively, see Figure 16) [78]. Incorporation of carbolines in these two structures is justified by the fact that this group has recently been identified as an electron-transport material exhibiting a high triplet energy [79-82]. Even if the introduction of heteroatoms in aromatic compounds can increase the molecular relaxation, the bandgap and the triplet energies will simultaneously increase, consequently diminishing ΔE_{ST}. Effectiveness of the strategy was clearly evidenced by the blue emission produced by OLEDs containing **BN-2** as the emitter (CIE coordinates of (0.19, 034), EL at 486 nm) and the high EQE of 22.5% attested of the TADF characteristics of the emitter. In contrast, **BN-1**-based devices demonstrated a low EQE of 4.2% resulting from its low PLQY (37% contrarily to 93% for **BN-2**) and the poor contribution of the delayed component to the overall emission (7% contrarily to 45% for **BN-2**). As a positive point, the EL spectrum of **BN-1**-based devices was blue shifted at 473 nm. Therefore, undeniably, it can be concluded that the effect of the heteroatom position in the carboline donor moiety is essential. Notably, for the two materials, the HOMO and LUMO energy levels of **BN-1** and **BN-2** are isolated from each other, but a partial overlap exists in **BN-1** due to the weaker donating ability of the α-carboline moiety. Jointly, theoretical calculations evidenced a larger bond length change between the ground and excited states for **BN-1** (0.048 Å vs 0.041 Å for **BN-2** between the carboline and the phenyl group). As a result of this, the higher molecular relaxation in **BN-1** is expected to favour the non-



	BN-1	BN-2	BN-3	BN-4	BN-5
reference	[76]	[76]	[76]	[76]	[77]
ΔE_{ST} (eV)	0.27	0.41	0.40	0.23	0.19
decay time delayed component (μs)	–	–	–	–	–
EQE (%)	13	21.5	20.1	14.8	14.8
CIE (x,y)	(0.17, 0.29)	(0.16, 0.26)	(0.16, 0.23)	(0.17, 0.28)	(0.15, 0.26)

Figure 15: Benzonitrile-based emitters **BN-1**–**BN-5**.



	BN-6	BN-7	BN-8
reference	[78]	[78]	[83]
ΔE_{ST} (eV)	0.28	0.13	0.02
decay time delayed component (μs)	57	180	–
EQE (%)	4.2	22.5	15.9
CIE (x,y)	(0.16, 0.19)	(0.19, 0.34)	(0.16, 0.16)

Figure 16: Benzonitrile-based emitters **BN-6**–**BN-11**.

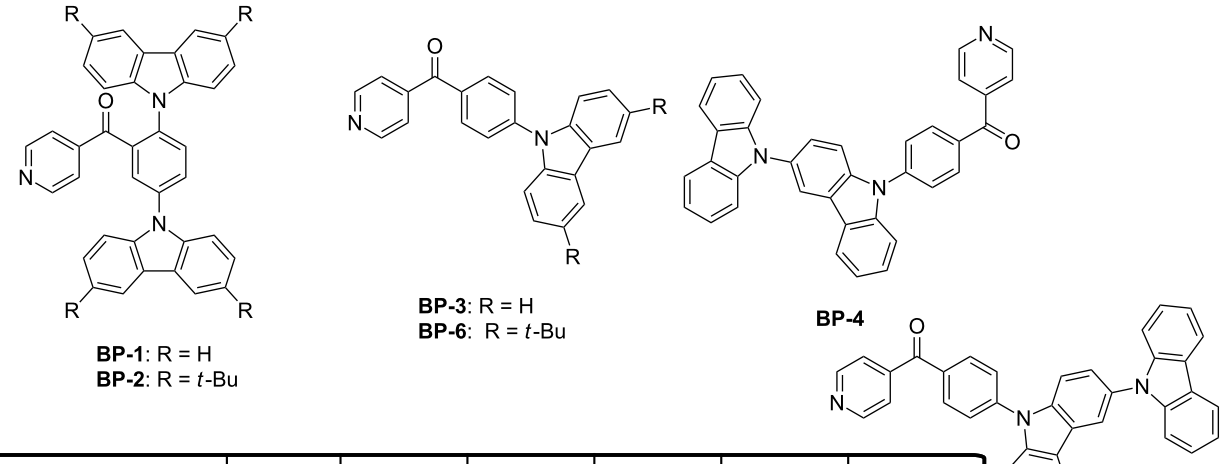
radiative processes, adversely affecting the EL performance. Another study revealed the importance of the donor moiety position compared to benzonitrile for high EL efficiency. In an effort to maximize the TADF process, Adachi developed a series of four highly twisted molecules **BN-8**–**BN11** consisting of the combination of 9,9-diphenylacridane donor unit(s) connected to a benzonitrile central core (see Figure 16) [83]. As first conclusions extracted from the theoretical calculations, the predicted ΔE_{ST} values were similar for all molecules (0.03 eV), suggesting that the substitution position has no effect on the up-conversion properties. Parallel to this, examination of the PL spectra of **BN-8**–**BN-11** showed the PL maximum to be located

at 454 and 441 nm for **BN-8** and **BN-9**, respectively, whereas the emission was detected at 433 and 428 nm for the *meta*-substituted **BN-10** and *para*-substituted **BN-11**, respectively.

It was thus concluded that the π-conjugation was maximized upon *ortho*-substitution and the introduction of two donor units on **BN-8** optimized the delayed emission intensity so that **BN-8** was the only one to be tested in devices. OLEDs fabricated using **BN-8** as an emitter showed a blue emission at 463 nm (with CIE coordinates of (0.16, 0.16)) that coincides the PL emission maximum together with the high EQE of 15.9%. However, examination of the chemical stability of an encapsulated film of **BN-8** evidenced the emission intensity of the film to decrease in less than 5 min upon photoexcitation. Theoretical calculations pointed out the *ortho*-substitution to enhance the TADF efficiency because of the optimized steric hindrance but also to decrease the bond dissociation energy as a value of only 0.94 eV for the C–N bond was determined, much lower than the singlet and triplet energies of the molecules (2.75 eV and 2.73 eV, respectively).

9. Benzoylpyridine and di(pyridinyl)methanone–carbazole derivatives

Emitters displaying efficient RISC and high PLQY are promising candidates for OLEDs and molecules comprising phenyl(pyridin-4-yl)methanone as the acceptor moiety are one of those. As first approach, the two carbazole donors were introduced at the *ortho*- and *meta*-positions of the phenyl ring of the acceptor (see Figure 17, **BP-1** and **BP-2**) [84]. Very small ΔE_{ST} of 0.03 and 0.04 eV and very high PL efficiencies of 88.0 and 91.4% were, respectively, determined for **BP-1** and **BP-2** in codoped films. These values are higher than that determined in solution for the two molecules (4.4 to 14.2% depending of the solvent for **BP-1**, 2.8 to 34.0% depending of the solvent for **BP-2**), demonstrating the suppression of the collisional and the intramolecular rotational quenching in thin films. However, the substitution pattern of carbazole drastically modified the emission wavelengths and a red-shift of approximately 20 nm was observed upon introduction of *tert*-butyl substituents on **BP-2**. Conversely, a higher electrochemical stability was determined for **BP-2** upon repeating CV scans, the two reactive C_3 and C_6 sites in *para*-position relative to the nitrogen atom of the carbazole being blocked by the *tert*-butyl groups. In multilayered devices, the bluer emitter **BP-1** provided efficiencies comparable to those obtained with iridium-based phosphorescent OLEDs at similar EL wavelength [85,86]. Notably, sky-blue **BP-1**-based OLEDs reached a maximum efficiency of 24% for the light peaking at 488 nm. The same year (2016), the same authors changed their strategy and combined all electron donors together, replacing the former D–A–D triads by D–A diads [87]. To tune the electron donating ability, carbazoles were introduced at the outer position of a carbazole unit, at the 3 and 3,6-conjugated positions of the first carbazole, resulting in donors composed in total of one to three carbazole groups.

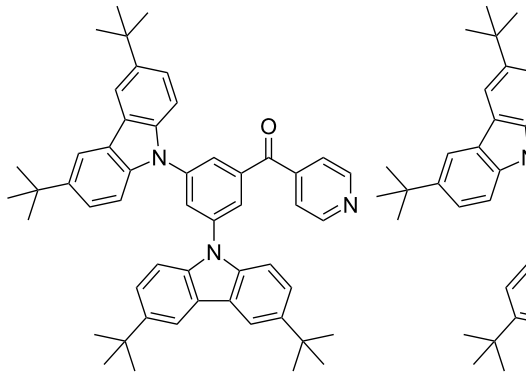


	BP-1	BP-2	BP-3	BP-4	BP-5	BP-6
reference	[83]	[83]	[87]	[87]	[87]	[87]
ΔE_{ST} (eV)	0.03	0.04	0.29	0.07	0.05	0.13
decay time delayed component (μs)	0.6	1	–	–	0.65	–
EQE (%)	24.0	27.2	4.2	11.0	23.9	9.4
CIE (x,y)	(0.17, 0.36)	(0.30, 0.64)	(0.16, 0.13)	(0.18, 0.28)	(0.19, 0.32)	(0.17, 0.27)

Figure 17: Benzoylpyridine-carbazole hybrid emitters **BP-1**–**BP-6**.

Comparison established with this series of emitters evidenced a clear decrease of ΔE_{ST} upon expending the size of the donating part and the number of carbazole units per donor. Thus, ΔE_{ST} decreased from 0.29 eV for **BP-3** to 0.07 eV for **BP-4** and 0.05 eV for **BP-5**, consistent with a higher spatial HOMO and LUMO separation and a more extended molecular HOMO orbital distribution.

Unfortunately, despites these favorable features, a significant red-shift of the emission was evidenced for **BP-4** and **BP-5** as a result of a dual emission, one corresponding to a carbazole-centered π–π* transition at high energy and an additional but unexpected intramolecular charge transfer only observed for **BP-4** and **BP-5** at lower energy. A clear shift of the emission maximum was notably evidenced in toluene, the maximum emission wavelength shifting from 440 nm for **BP-3** to 480 nm for **BP-4** and 482 nm for **BP-5**. Therefore, only blue devices could be fabricated with the mono-substituted emitter **BP-3** and a comparison was established with **BP-6** differing from **BP-3** by the substitution pattern of the unique carbazole. Once again, a red-shift of the emission was observed upon incorporation of *tert*-butyl groups on carbazole, the emission in toluene being detected at 467 nm. Evaluation of the potential of **BP-3** and **BP-6** as new developed emitters for OLEDs confirmed the trend observed by PL and **BP-3** furnished a more blue OLED than **BP-6**, with an external efficiency peaking at 9.4%. By optimizing the device structure [88], the same authors could drastically increase the EQE of **BP-3**-based devices up to 18.4%, even if a non-negligible red-shift of the emission wavelength could be observed: 474 nm, (0.16, 0.25) for this study [88] contrarily to the previous emission detected at 452 nm, (0.13, 0.16) [87]. Inspired by the structure of **BP-2**, the same authors developed a series of three fluorescent molecules by varying the position of the nitrogen atom of the pyridine moieties **BP-7**–**BP-9** [89]. All molecules are characterized by high PLQYs in thin films, ranging from 92 to 97%, and small ΔE_{ST} varying from 0.01 eV for **BP-7** to 0.05 eV for **BP-8** and 0.02 for **BP-9**. Despites these appealing photophysical characteristics, positions of EL peaks appeared at 490, 476 and 490 nm for **BP-7**–**BP-9**-based devices, respectively, therefore in the blue-green region. While comparing with the standard triplet emitter Firpic, a clear enhancement of the EL performance was observed, EQE of Firpic-based OLEDs peaking at 18.7% whereas EQEs of 2.1, 24.6 and 28.0% could be, respectively, realized with the three TADF emitters **BP-7**–**BP-9** (see Figure 18). Here again, the ability of TADF emitters to outperform the standard



	BP-7	BP-8	BP-9	BP-10
reference	[89]	[89]	[89]	[90]
ΔE_{ST} (eV)	0.01	0.05	0.02	0.02
decay time delayed component (μs)	18.0	7.3	6.9	0.27
EQE (%)	28.1	24.6	28.0	31.9
CIE (x,y) or λ_{EL} (nm)	(0.17, 0.37)	(0.15, 0.28)	(0.16, 0.37)	464

Figure 18: Benzoylpyridine-carbazole hybrid emitters **BP-7**–**BP-10**.

phosphorescent emitters was demonstrated. Finally, the key to produce a pure blue emission with pyridine-based emitters seems to have been found with the di(pyridinyl)methanone electron-accepting core that could furnish a superior pure blue emission compared to emitters based on the benzoylpyridine core [90]. By introducing two pyridines in bis(6-(3,6-di-*tert*-butyl-9*H*-carbazol-9-yl)pyridin-3-yl)methanone (**BP-10**), a nearly planar molecule could be obtained, favouring the horizontal molecular orientation of the molecule within the co-doped emissive layer. By this specific arrangement in the EML, a perfect stacking of the molecules parallel to the substrate was determined, providing an isotropic orientation of the transition dipole moment. Finally, OLEDs fabricated with **BP-10** with a classical device structure furnished a record-breaking EQE of almost 32% with a relatively low dopant concentration (7 wt %) and an emission located at 464 nm.

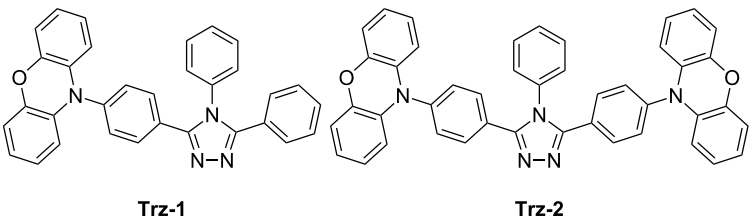
10. Triazole derivatives

3,4,5-Triphenyl-4*H*-1,2,4-triazole is a good electron acceptor but also a remarkable electron-transport material used for the design of numerous OLED materials ranging from charge-transport materials to light-emitting materials [91-93]. Logically, combination of 3,4,5-triphenyl-4*H*-1,2,4-triazole with the electron-donor phenoxazine could provide emitters with TADF properties if conveniently associated and such assemblies were reported for the first time in 2013 (see Figure 19) [94]. Comparison of the diad **Trz-1** and the triad **Trz-2** evidenced in the absence of oxygen the triad **Trz-2** to be more luminescent than the diad **Trz-1** (29.8 and 43.1% for **Trz-1** and **Trz-2**, respectively). This trend was confirmed with the design of another series of diad/triads comprising an oxadiazole as the central electron acceptor. This characteristic is opposite to the trend classically reported in the literature where the molecules with a large oscillator strength show a high PLQY [95]. In the present case, the opposite situation was found as the more luminescent materials **Trz-2** showed the smaller oscillator strength, evidencing that the order of the PLQYs was not only controlled by the oscillator strength, but also by a competition with vibronic couplings responsible from nonradiative deactivation pathways. The fabrication of OLEDs with the most luminescent **Trz-2** furnished sky-blue OLEDs reflecting its PL spectrum in thin doped films (λ_{EL} = 456 nm, EQE = 6.4%).

11. Triphenylamine derivatives

Triphenylamine is a remarkable electron-donating group that found applications in numerous research fields ranging from OLEDs to organic photovoltaics [96]. In the context of TADF blue emitters, an original strategy to tune the emission wavelength consisted in solely changing the sulfur atom valence state of the thioxanthone core, enabling the emission color to shift from blue to yellow [97]. Even if several connecting modes for the triphenylamine moieties onto the thioxanthone core was envisioned, a blue PL was only detected for **TPA-1** by introducing the two triphenylamine groups at the *para*-positions of the carbonyl group in 9*H*-thioxanthen-9-one (see Figure 20). Because of this specific substitution, a minimal HOMO/LUMO overlap was evidenced by theoretical calculations. Despites the symmetrical substitution of **TPA-1** and the reduction of the oscillator strength in the triad, the PLQY remained high, reaching 35% regardless doped or neat films under air conditions. In a standard device stacking, highly efficient emission could be realized as a maximum EQE value of 23.7% was obtained for OLEDs comprising an emissive layer with a doping concentration of 1 wt % and CIE coordinates of (0.139, 0.280).

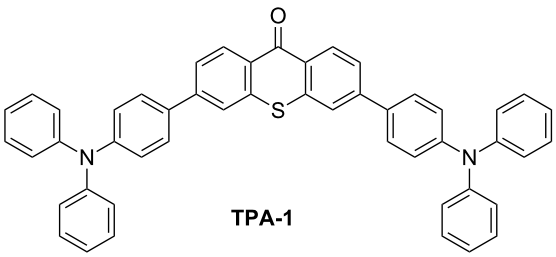
In 2017, more blue OLEDs were obtained by using malononitrile as the electron acceptor [98]. The molecular orientation of the emitting material is essential to optimize the EL characteristics and an increase of the external efficiency by up to 46% can be achieved if the molecules are perfectly aligned horizontally by giving rise to light-outcoupling effects [99-101]. In this work, **TPA-2** and **TPA-3** share a similar ΔE_{ST} and similar PL characteristics but major differences were found upon fabrication of OLEDs with these two materials. Notably, the current efficiency of OLEDs elaborated with **TPA-3** as dopant was approximately 9 times higher than that determined for **TPA-2**-based OLEDs (12.6 and 1.4 cd/A, respectively). To explain these differences, the perfect horizontal orientation of **TPA-3** in



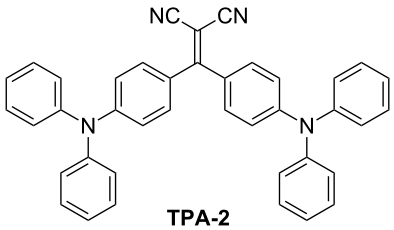
Trz-1 **Trz-2**

	Trz-1	Trz-2
reference	[94]	[94]
ΔE_{ST} (eV)	–	0.23
decay time delayed component (μs)	0.016	28.88
EQE (%)	–	6.4
CIE (x,y)	–	(0.16, 0.15)

Figure 19: Triazole-based emitters **Trz-1** and **Trz-2**.



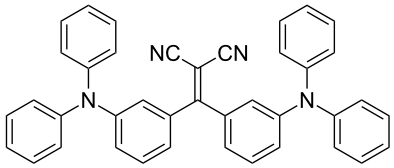
TPA-1



TPA-2

	TPA-1	TPA-2	TPA-3
reference	[97]	[98]	[98]
ΔE_{ST} (eV)	0.38	0.114	0.098
decay time delayed component (μs)	–	10	10
EQE (%) or CE (cd/A)	23.7 %	1.38 cd/A	12.62 cd/A
CIE (x,y)	(0.14, 0.28)	(0.17, 0.17)	(0.16, 0.20)

CE: current efficiency



TPA-3

Figure 20: Triarylamine-based emitters **TPA-1**–**TPA-3**.

doped films contrarily to the weak crystallinity and random orientation of **TPA-2** resulted in an improvement of the light extraction for **TPA-3**-based devices, justifying the enhanced performance.

Conclusion

To conclude, a wide range of strategies are currently developed to produce a blue TADF emission. Among the different findings that can constitute a guideline for the molecular design for blue TADF emitters, it can be cited: 1) The interruption of the π-conjugation by introducing an orthogonality between the donor and the acceptor to minimize the coupling between the two parts, 2) the fact to maintain the donor close to the acceptor to prevent a complete isolation of the donor and the acceptor, 3) the extension of the π-conjugated system of the donor and/or acceptor to maximize the oscillator strength and thus to increase the PLQY, 4) a minimization of ΔE_{ST} to optimize the rate constant of the reverse intersystem crossing, 5) the elaboration of light emitting materials with lifetimes of the delayed component of luminescence as short as possible to address the excited states annihilation issue, 6) a careful selection of the connectivity introduced between the electron donor/acceptor moieties as exemplified by the difference of the EL performance for materials differing by the substitution (*ortho*-, *meta*- and *para*-position of aromatic rings). The different results and observations reported in this review have clearly evidenced that a great deal of efforts has still to be done to produce a deep blue EL, as evidenced in Figure 21. At present, the bluest emitters reported in the literature, i.e., emitters with CIE *x*-coordinate below 0.16 and CIE *y*-coordinate below 0.10 only four are known: **D3** (0.15, 0.07) [29], reported in 2012, **T22** and **T23** (0.15, 0.10) [45], reported in 2017, and finally **CN-P8** (0.16, 0.06) [59], reported in 2016. **D3**, **T22** and **T23** are all based on carbazole, but carbazole is certainly not the best candidate for the design of highly stable deep blue emitter because of the photo-assisted electrochemical degradation processes it can initiate.

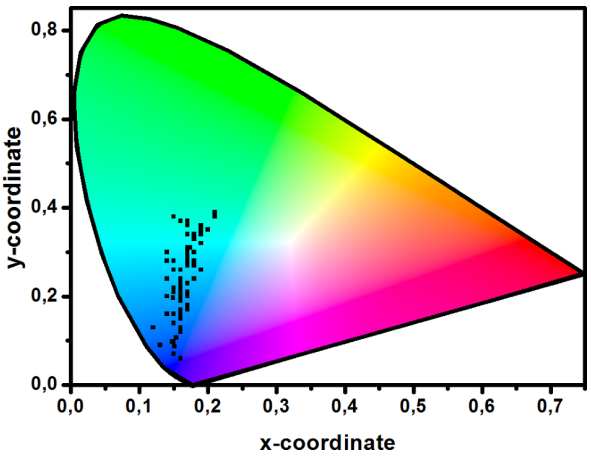


Figure 21: Distribution of the CIE coordinates of ca. 90 blue TADF emitters listed in this review.

Since 2016, a great deal of efforts has been done to investigate new structures issued from communities other than Organic Electronics and electron donors such as phenoxaphosphine oxide or phenoxathiin dioxide and electron acceptors such as α- and δ-carbolines that have historically been used for the design

of biologically active molecules are now commonly used during the elaboration of light emitting materials. Blue and stable emitters that will be developed in the future will certainly comprise such unprecedented moieties. Recently, another aspect of crucial importance to increase the EL performance concerns the molecular alignment of the emitter molecules in OLEDs as this can have an important effect on the outcoupling efficiency; this point warrants more systematic investigations in the future.

ORCID® iDs

Thanh-Tuân Bui - https://orcid.org/0000-0002-5367-2738
Frédéric Dumur - https://orcid.org/0000-0003-4872-094X

References

1. Tang, C. W.; VanSlyke, S. A. *Appl. Phys. Lett.* **1987,** *51,* 913–915. doi:10.1063/1.98799
2. Gaspar, D. J.; Polikarpov, E. *OLED Fundamentals: Materials, Devices, and Processing of Organic Light-Emitting Diodes;* CRC Press/Taylor and Francis Group: Boca Raton, FL, United States (US), 2015.
3. Fröbel, M.; Schwab, T.; Kliem, M.; Hofmann, S.; Leo, K.; Gather, M. C. *Light: Sci. Appl.* **2015,** *4,* e247. doi:10.1038/lsa.2015.20
4. Baldo, M. A.; O'Brien, D. F.; Thompson, M. E.; Forrest, S. R. *Phys. Rev. B: Condens. Matter Mater. Phys.* **1999,** *60,* 14422–14428. doi:10.1103/PhysRevB.60.14422
5. Baldo, M. A.; O'Brien, D. F.; You, Y.; Shoustikov, A.; Sibley, S.; Thompson, M. E.; Forrest, S. R. *Nature* **1998,** *395,* 151–154. doi:10.1038/25954
6. Dumur, F.; Bertin, D.; Gigmes, D. *Int. J. Nanotechnol.* **2012,** *9,* 377–395. doi:10.1504/IJNT.2012.045343
7. Dumur, F. *Synth. Met.* **2014,** *195,* 241–251. doi:10.1016/j.synthmet.2014.06.018
8. Dumur, F. *Org. Electron.* **2015,** *21,* 27–39. doi:10.1016/j.orgel.2015.02.026
9. Uoyama, H.; Goushi, K.; Shizu, K.; Nomura, H.; Adachi, C. *Nature* **2012,** *492,* 234–238. doi:10.1038/nature11687
10. Tao, Y.; Yang, C.; Qin, J. *Chem. Soc. Rev.* **2011,** *40,* 2943–2970. doi:10.1039/c0cs00160k
11. Godumala, M.; Choi, S.; Cho, M. J.; Choi, D. H. *J. Mater. Chem. C* **2016,** *4,* 11355–11381. doi:10.1039/C6TC04377A
12. Wong, M. Y.; Zysman-Colman, E. *Adv. Mater.* **2017,** *29,* 1605444. doi:10.1002/adma.201605444
13. Li, Y.; Liu, J.-Y.; Zhao, Y.-D.; Cao, Y.-C. *Mater. Today* **2017,** *20,* 258–266. doi:10.1016/j.mattod.2016.12.003
14. Yang, Z.; Mao, Z.; Xie, Z.; Zhang, Y.; Liu, S.; Zhao, J.; Xu, J.; Chi, Z.; Aldred, M. P. *Chem. Soc. Rev.* **2017,** *46,* 915–1016. doi:10.1039/C6CS00368K
15. Im, Y.; Kim, M.; Cho, Y. J.; Seo, J.-A.; Yook, K. S.; Lee, J. Y. *Chem. Mater.* **2017,** *29,* 1946–1963. doi:10.1021/acs.chemmater.6b05324
16. Im, Y.; Byun, S. Y.; Kim, J. H.; Lee, D. R.; Oh, C. S.; Yook, K. S.; Lee, J. Y. *Adv. Funct. Mater.* **2017,** *27,* 1603007. doi:10.1002/adfm.201603007
17. Zhu, M.; Yang, C. *Chem. Soc. Rev.* **2013,** *42,* 4963–4976. doi:10.1039/c3cs35440g
18. Fu, H.; Cheng, Y.-M.; Chou, P.-T.; Chi, Y. *Mater. Today* **2011,** *14,* 472–479. doi:10.1016/S1369-7021(11)70211-5
19. Chen, W.-C.; Lee, C.-S.; Tong, Q.-X. *J. Mater. Chem. C* **2015,** *3,* 10957–10963. doi:10.1039/C5TC02420J
20. Winter, S.; Reineke, S.; Walzer, K.; Leo, K. *Proc. SPIE* **2008,** *6999,* 69992N. doi:10.1117/12.782784
21. Scholz, S.; Kondakov, D.; Lüssem, B.; Leo, K. *Chem. Rev.* **2015,** *115,* 8449–8503. doi:10.1021/cr400704v
22. Endo, A.; Sato, K.; Yoshimura, K.; Kai, T.; Kawada, A.; Miyazaki, H.; Adachi, C. *Appl. Phys. Lett.* **2011,** *98,* 083302. doi:10.1063/1.3558906
23. Busmann, H.-G.; Staerk, H.; Weller, A. *J. Chem. Phys.* **1989,** *91,* 4098–4105. doi:10.1063/1.457624
24. Berberan-Santos, M. N.; Garcia, J. M. M. *J. Am. Chem. Soc.* **1996,** *118,* 9391–9394. doi:10.1021/ja961782s
25. Turro, N. J.; Ramamurthy, V.; Scaiano, J. C. *Principles of Molecular Photochemistry: An Introduction;* Chapter 2; University Science Books: Sausalito, 2008.
26. Etherington, M. K.; Franchello, F.; Gibson, J.; Northey, T.; Santos, J.; Ward, J. S.; Higginbotham, H. F.; Data, P.; Kurowska, A.; Lays Dos Santos, P.; Graves, D. R.; Batsanov, A. S.; Dias, F. B.; Bryce, M. R.; Penfold, T. J.; Monkman, A. P. *Nat. Commun.* **2017,** *8,* No. 14987. doi:10.1038/ncomms14987
27. Samanta, P. K.; Kim, D.; Coropceanu, V.; Brédas, J.-L. *J. Am. Chem. Soc.* **2017,** *139,* 4042–4051. doi:10.1021/jacs.6b12124
28. Gibson, J.; Monkman, A. P.; Penfold, T. J. *ChemPhysChem* **2016,** *17,* 2956–2961. doi:10.1002/cphc.201600662
29. dos Santos, P. L.; Ward, J. S.; Bryce, M. R.; Monkman, A. P. *J. Phys. Chem. Lett.* **2016,** *7,* 3341–3346. doi:10.1021/acs.jpclett.6b01542
30. de Sa Pereira, D.; dos Santos, P. L.; Ward, J. S.; Data, P.; Okazaki, M.; Takeda, Y.; Minakata, S.; Bryce, M. R.; Monkman, A. P. *Sci. Rep.* **2017,** *7,* No. 6234. doi:10.1038/s41598-017-06568-3
31. Turkoglu, G.; Cinar, M. E.; Ozturk, T. *Molecules* **2017,** *22,* No. 1522. doi:10.3390/molecules22091522
32. Kinoshita, M.; Kita, H.; Shirota, Y. *Adv. Funct. Mater.* **2002,** *12,* 780–786. doi:10.1002/adfm.200290007
33. Nagai, A.; Kobayashi, S.; Nagata, Y.; Kokado, K.; Taka, H.; Kita, H.; Suzuri, Y.; Chujo, Y. *J. Mater. Chem.* **2010,** *20,* 5196–5201. doi:10.1039/b924729g
34. Kitamoto, Y.; Namikawa, T.; Ikemizu, D.; Miyata, Y.; Suzuki, T.; Kita, H.; Sato, T.; Oi, S. *J. Mater. Chem. C* **2015,** *3,* 9122–9130. doi:10.1039/C5TC01380A
35. Kitamoto, Y.; Namikawa, T.; Suzuki, T.; Miyata, Y.; Kita, H.; Sato, T.; Oi, S. *Org. Electron.* **2016,** *34,* 208–217. doi:10.1016/j.orgel.2016.04.030
36. Lee, Y. H.; Park, S.; Oh, J.; Shin, J. W.; Jung, J.; Yoo, S.; Lee, M. H. *ACS Appl. Mater. Interfaces* **2017,** *9,* 24035–24042. doi:10.1021/acsami.7b05615
37. Suzuki, K.; Kubo, S.; Shizu, K.; Fukushima, T.; Wakamiya, A.; Murata, Y.; Adachi, C.; Kaji, H. *Angew. Chem., Int. Ed.* **2015,** *54,* 15231–15235. doi:10.1002/anie.201508270
38. Numata, M.; Yasuda, T.; Adachi, C. *Chem. Commun.* **2015,** *51,* 9443–9446. doi:10.1039/C5CC00307E
39. Hatakeyama, T.; Shiren, K.; Nakajima, K.; Nomura, S.; Nakatsuka, S.; Kinoshita, K.; Ni, J.; Ono, Y.; Ikuta, T. *Adv. Mater.* **2016,** *28,* 2777–2781. doi:10.1002/adma.201505491
40. Zhang, Q.; Li, J.; Shizu, K.; Huang, S.; Hirata, S.; Miyazaki, H.; Adachi, C. *J. Am. Chem. Soc.* **2012,** *134,* 14706–14709. doi:10.1021/ja306538w
41. Wu, S.; Aonuma, M.; Zhang, Q.; Huang, S.; Nakagawa, T.; Kuwabara, K.; Adachi, C. *J. Mater. Chem. C* **2014,** *2,* 421–424. doi:10.1039/C3TC31936A

42. Sun, K.; Xie, X.; Liu, Y.; Jiang, W.; Ban, X.; Huang, B.; Sun, Y. *J. Mater. Chem. C* **2016,** *4,* 8973–8979. doi:10.1039/C6TC02634F
43. Zhang, Q.; Li, B.; Huang, S.; Nomura, H.; Tanaka, H.; Adachi, C. *Nat. Photonics* **2014,** *8,* 326–332. doi:10.1038/nphoton.2014.12
44. Wu, Z.; Luo, J.; Sun, N.; Zhu, L.; Sun, H.; Yu, L.; Yang, D.; Qiao, X.; Chen, J.; Yang, C.; Ma, D. *Adv. Funct. Mater.* **2016,** *26,* 3306–3313. doi:10.1002/adfm.201505602
45. Zhang, Q.; Tsang, D.; Kuwabara, H.; Hatae, Y.; Li, B.; Takahashi, T.; Lee, S. Y.; Yasuda, T.; Adachi, C. *Adv. Mater.* **2015,** *27,* 2096–2100. doi:10.1002/adma.201405474
46. Sun, J. W.; Baek, J. Y.; Kim, K.-H.; Moon, C.-K.; Lee, J.-H.; Kwon, S.-K.; Kim, Y.-H.; Kim, J.-J. *Chem. Mater.* **2015,** *27,* 6675–6681. doi:10.1021/acs.chemmater.5b02515
47. Sun, J. W.; Baek, J. Y.; Kim, K.-H.; Huh, J.-S.; Kwon, S.-K.; Kim, Y.-H.; Kim, J.-J. *J. Mater. Chem. C* **2017,** *5,* 1027–1032. doi:10.1039/C6TC04653C
48. Hirata, S.; Sakai, Y.; Masui, K.; Tanaka, H.; Lee, S. Y.; Nomura, H.; Nakamura, N.; Yasumatsu, M.; Nakanotani, H.; Zhang, Q.; Shizu, K.; Miyazaki, H.; Adachi, C. *Nat. Mater.* **2015,** *14,* 330–336. doi:10.1038/nmat4154
49. Cui, L.-S.; Deng, Y.-L.; Tsang, D. P.-K.; Jiang, Z.-Q.; Zhang, Q.; Liao, L.-S.; Adachi, C. *Adv. Mater.* **2016,** *28,* 7620–7625. doi:10.1002/adma.201602127
50. Yang, J.; Chen, C.; Ji, H.; Ma, W.; Zhao, J. *J. Phys. Chem. B* **2005,** *109,* 21900–21907. doi:10.1021/jp0540914
51. Shizu, K.; Noda, H.; Tanaka, H.; Taneda, M.; Uejima, M.; Sato, T.; Tanaka, K.; Kaji, H.; Adachi, C. *J. Phys. Chem. C* **2015,** *119,* 26283–26289. doi:10.1021/acs.jpcc.5b07798
52. Serevičius, T.; Nakagawa, T.; Kuo, M.-C.; Cheng, S.-H.; Wong, K.-T.; Chang, C.-H.; Kwong, R. C.; Xia, S.; Adachi, C. *Phys. Chem. Chem. Phys.* **2013,** *15,* 15850–15855. doi:10.1039/c3cp52255e
53. Kim, M.; Jeon, S. K.; Hwang, S.-H.; Lee, J. Y. *Adv. Mater.* **2015,** *27,* 2515–2520. doi:10.1002/adma.201500267
54. Cha, J.-R.; Lee, C. W.; Gong, M.-S. *Dyes Pigm.* **2017,** *140,* 399–406. doi:10.1016/j.dyepig.2017.01.053
55. Cha, J.-R.; Lee, C. W.; Lee, J. Y.; Gong, M.-S. *Dyes Pigm.* **2016,** *134,* 562–568. doi:10.1016/j.dyepig.2016.08.023
56. Cui, L.-S.; Nomura, H.; Geng, Y.; Kim, J. U.; Nakanotani, H.; Adachi, C. *Angew. Chem., Int. Ed.* **2017,** *56,* 1571–1575. doi:10.1002/anie.201609459
57. Nakao, K.; Sasabe, H.; Komatsu, R.; Hayasaka, Y.; Ohsawa, T.; Kido, J. *Adv. Opt. Mater.* **2017,** *5,* 1600843. doi:10.1002/adom.201600843
58. Ganesan, P.; Ranganathan, R.; Chi, Y.; Liu, X.-K.; Lee, C.-S.; Liu, S.-H.; Lee, G.-H.; Lin, T.-C.; Chen, Y.-T.; Chou, P.-T. *Chem. – Eur. J.* **2017,** *23,* 2858–2866. doi:10.1002/chem.201604883
59. Park, I. S.; Lee, J.; Yasuda, T. *J. Mater. Chem. C* **2016,** *4,* 7911–7916. doi:10.1039/C6TC02027E
60. Shao, S.; Hu, J.; Wang, X.; Wang, L.; Jing, X.; Wang, F. *J. Am. Chem. Soc.* **2017,** *139,* 17739–17742. doi:10.1021/jacs.7b10257
61. Dumur, F.; Guillaneuf, Y.; Guerlin, A.; Wantz, G.; Bertin, D.; Miomandre, F.; Clavier, G.; Gigmes, D.; Mayer, C. R. *Macromol. Chem. Phys.* **2011,** *212,* 1616–1628. doi:10.1002/macp.201100167
62. Lee, S. Y.; Adachi, C.; Yasuda, T. *Adv. Mater.* **2016,** *28,* 4626–4631. doi:10.1002/adma.201506391
63. Zhang, Y.; Ni, Y.-P.; He, M.-X.; Wang, X.-L.; Chen, L.; Wang, Y.-Z. *Polymer* **2015,** *60,* 50–61. doi:10.1016/j.polymer.2015.01.030
64. Yamamura, M.; Saito, T.; Nabeshima, T. *J. Am. Chem. Soc.* **2014,** *136,* 14299–14306. doi:10.1021/ja507913u
65. Yamamura, M.; Sukegawa, K.; Nabeshima, T. *Chem. Commun.* **2015,** *51,* 12080–12083. doi:10.1039/C5CC04194E
66. Yamamura, M.; Hasegawa, T.; Nabeshima, T. *Org. Lett.* **2016,** *18,* 816–819. doi:10.1021/acs.orglett.6b00105
67. Al-Hiari, Y. M.; Sweileh, B. A. *Asian J. Chem.* **2006,** *18,* 2285–2298.
68. Yu, W.; Coburn, C. A.; Yang, D.-Y.; Meinke, P. T.; Wong, M.; Rosenblum, S. B.; Chen, K. X.; Njoroge, G. F.; Chen, L.; Dwyer, M. P.; Jiang, Y.; Nair, A. G.; Selyutin, O.; Tong, L.; Zeng, Q.; Zhong, B.; Ji, T.; Hu, B.; Agrawal, S.; Xia, E.; Zhai, Y.; Liu, R.; Kong, R.; Ingravallo, P.; Asante-Appiah, E.; Nomeir, A.; Fells, J.; Kozlowski, J. A. *Bioorg. Med. Chem. Lett.* **2016,** *26,* 3158–3162. doi:10.1016/j.bmcl.2016.04.084
69. Liu, W.; Zheng, C.-J.; Wang, K.; Chen, Z.; Chen, D.-Y.; Li, F.; Ou, X.-M.; Dong, Y.-P.; Zhang, X.-H. *ACS Appl. Mater. Interfaces* **2015,** *7,* 18930–18936. doi:10.1021/acsami.5b05648
70. Li, N.; Wang, P.; Lai, S.-L.; Liu, W.; Lee, C.-S.; Lee, S.-T.; Liu, Z. *Adv. Mater.* **2010,** *22,* 527–530. doi:10.1002/adma.200902430
71. You, J.; Lai, S.-L.; Liu, W.; Ng, T.-W.; Wang, P.; Lee, C.-S. *J. Mater. Chem.* **2012,** *22,* 8922–8929. doi:10.1039/c2jm00078d
72. Pan, K.-C.; Li, S.-W.; Ho, Y.-Y.; Shiu, Y.-J.; Tsai, W.-L.; Jiao, M.; Lee, W.-K.; Wu, C.-C.; Chung, C.-L.; Chatterjee, T.; Li, Y.-S.; Wong, K.-T.; Hu, H.-C.; Chen, C.-C.; Lee, M.-T. *Adv. Funct. Mater.* **2016,** *26,* 7560–7571. doi:10.1002/adfm.201602501
73. Sasabe, H.; Onuma, N.; Nagai, Y.; Ito, T.; Kido, J. *Chem. – Asian J.* **2017,** *12,* 648–654. doi:10.1002/asia.201601641
74. Duan, C.; Li, J.; Han, C.; Ding, D.; Yang, H.; Wei, Y.; Xu, H. *Chem. Mater.* **2016,** *28,* 5667–5679. doi:10.1021/acs.chemmater.6b01691
75. Mallesham, G.; Swetha, C.; Niveditha, S.; Mohanty, M. E.; Babu, N. J.; Kumar, A.; Bhanuprakash, K.; Rao, V. J. *J. Mater. Chem. C* **2015,** *3,* 1208–1224. doi:10.1039/C4TC01753F
76. Zhang, D.; Cai, M.; Bin, Z.; Zhang, Y.; Zhang, D.; Duan, L. *Chem. Sci.* **2016,** *7,* 3355–3363. doi:10.1039/C5SC04755B
77. Tanimoto, S.; Suzuki, T.; Nakanotani, H.; Adachi, C. *Chem. Lett.* **2016,** *45,* 770–772. doi:10.1246/cl.160290
78. Kim, G. H.; Lampande, R.; Im, J. B.; Lee, J. M.; Lee, J. Y.; Kwon, J. H. *Mater. Horiz.* **2017,** *4,* 619–624. doi:10.1039/C6MH00579A
79. Sasabe, H.; Toyota, N.; Nakanishi, H.; Ishizaka, T.; Pu, Y.-J.; Kido, J. *Adv. Mater.* **2012,** *24,* 3212–3217. doi:10.1002/adma.201200848
80. Cui, L.-S; Liu, Y.; Yuan, X.-D.; Li, Q.; Jiang, Z.-Q.; Liao, L.-S. *J. Mater. Chem. C* **2013,** *1,* 8177–8185. doi:10.1039/c3tc31675k
81. Mazetyte, D.; Krucaite, G.; Grazulevicius, J. V.; Chiang, C. I.; Yang, F. C.; Jou, J. H.; Grigalevicius, S. *Opt. Mater.* **2013,** *35,* 604–608. doi:10.1016/j.optmat.2012.10.054
82. Byeon, S. Y.; Jeon, S. K.; Hwang, S.-H.; Lee, J. Y. *Dyes Pigm.* **2015,** *120,* 258–264. doi:10.1016/j.dyepig.2015.04.024
83. Noda, H.; Kabe, R.; Adachi, C. *Chem. Lett.* **2016,** *45,* 1463–1466. doi:10.1246/cl.160814
84. Rajamalli, P.; Senthilkumar, N.; Gandeepan, P.; Huang, P.-Y.; Huang, M.-J.; Ren-Wu, C.-Z.; Yang, C.-Y.; Chiu, M.-J.; Chu, L.-K.; Lin, H.-W.; Cheng, C.-H. *J. Am. Chem. Soc.* **2016,** *138,* 628–634. doi:10.1021/jacs.5b10950
85. Shih, C.-H.; Rajamalli, P.; Wu, C.-A.; Chiu, M.-J.; Chu, L.-K.; Cheng, C.-H. *J. Mater. Chem. C* **2015,** *3,* 1491–1496. doi:10.1039/C4TC02348J
86. Chou, H.-H.; Cheng, C.-H. *Adv. Mater.* **2010,** *22,* 2468–2471. doi:10.1002/adma.201000061

87. Rajamalli, P.; Senthilkumar, N.; Gandeepan, P.; Ren-Wu, C.-C.; Lin, H.-W.; Cheng, C.-H. *ACS Appl. Mater. Interfaces* **2016,** *8,* 27026–27034. doi:10.1021/acsami.6b10678
88. Rajamalli, P.; Senthilkumar, N.; Gandeepan, P.; Ren-Wu, C.-Z.; Lin, H.-W.; Cheng, C.-H. *J. Mater. Chem. C* **2016,** *4,* 900–904. doi:10.1039/C5TC03943F
89. Rajamalli, P.; Thangaraji, V.; Senthilkumar, N.; Ren-Wu, C.-C.; Lin, H.-W.; Cheng, C.-H. *J. Mater. Chem. C* **2017,** *5,* 2919–2926. doi:10.1039/C7TC00457E
90. Rajamalli, P.; Senthilkumar, S.; Huang, P.-Y.; Ren-Wu, C.-C.; Lin, H.-W.; Cheng, C.-H. *J. Am. Chem. Soc.* **2017,** *139,* 10948–10951. doi:10.1021/jacs.7b03848
91. Adachi, C.; Tsutsui, T.; Saito, S. *Appl. Phys. Lett.* **1989,** *55,* 1489–1491. doi:10.1063/1.101586
92. Kido, J.; Ohtaki, C.; Hongawa, K.; Okuyama, K.; Nagai, K. *Jpn. J. Appl. Phys.* **1993,** *32,* L917–L920. doi:10.1143/JJAP.32.L917
93. Kulkarni, A. P.; Tonzola, C. J.; Babel, A.; Jenekhe, S. A. *Chem. Mater.* **2004,** *16,* 4556–4573. doi:10.1021/cm049473l
94. Lee, J.; Shizu, K.; Tanaka, H.; Nomura, H.; Yasuda, T.; Adachi, C. *J. Mater. Chem. C* **2013,** *1,* 4599–4604. doi:10.1039/c3tc30699b
95. Valchanov, G.; Ivanova, A.; Tadjer, A.; Chercka, D.; Baumgarten, M. *J. Phys. Chem. A* **2016,** *120,* 6944–6955. doi:10.1021/acs.jpca.6b06680
96. Dumur, F.; Goubard, F. *New J. Chem.* **2014,** *38,* 2204–2224. doi:10.1039/c3nj01537h
97. Li, Y.; Li, X.-L.; Chen, D.; Cai, X.; Xie, G.; He, Z.; Wu, Y.-C.; Lien, A.; Cao, Y.; Su, S.-J. *Adv. Funct. Mater.* **2016,** *26,* 6904–6912. doi:10.1002/adfm.201602507
98. Sohn, S.; Koh, B. H.; Baek, J. Y.; Byun, H. C.; Lee, J. H.; Shin, D.-S.; Ahn, H.; Lee, H.-K.; Hwang, J.; Jung, S.; Kim, Y.-H. *Dyes Pigm.* **2017,** *140,* 14–21. doi:10.1016/j.dyepig.2017.01.010
99. Mayr, C.; Lee, S. Y.; Schmidt, T. D.; Yasuda, T.; Adachi, C.; Brütting, W. *Adv. Funct. Mater.* **2014,** *24,* 5232–5239. doi:10.1002/adfm.201400495
100. Mayr, C.; Schmidt, T. D.; Brütting, W. *Appl. Phys. Lett.* **2014,** *105,* 183304. doi:10.1063/1.4901341
101. Kim, K.-H.; Liao, J.-L.; Lee, S. W.; Sim, B.; Moon, C.-K.; Lee, G.-H.; Kim, H. J.; Chi, Y.; Kim, J.-J. *Adv. Mater.* **2016,** *28,* 2526–2532. doi:10.1002/adma.201504451

License and Terms

This is an Open Access article under the terms of the Creative Commons Attribution License (http://creativecommons.org/licenses/by/4.0), which permits unrestricted use, distribution, and reproduction in any medium, provided the original work is properly cited.

The license is subject to the *Beilstein Journal of Organic Chemistry* terms and conditions: (https://www.beilstein-journals.org/bjoc)

The definitive version of this article is the electronic one which can be found at: doi:10.3762/bjoc.14.18

BEILSTEIN JOURNAL OF ORGANIC CHEMISTRY

Enhanced quantum yields by sterically demanding aryl-substituted β-diketonate ancillary ligands

Rebecca Pittkowski and Thomas Strassner*

Full Research Paper

Open Access

Address:
Physical Organic Chemistry, Technische Universität Dresden, Bergstraße, 01069 Dresden, Germany

Email:
Thomas Strassner* - thomas.strassner@chemie.tu-dresden.de

* Corresponding author

Keywords:
ancillary ligand; β-diketonates; photoluminescence; platinum(II) complex; quantum yield

Beilstein J. Org. Chem. **2018,** *14,* 664–671.
doi:10.3762/bjoc.14.54

Received: 10 November 2017
Accepted: 28 February 2018
Published: 21 March 2018

This article is part of the Thematic Series "Recent advances in materials for organic light emitting diodes".

Guest Editor: E. Zysman-Colman

© 2018 Pittkowski and Strassner; licensee Beilstein-Institut.
License and terms: see end of document.

Abstract

Luminescent organometallic platinum(II) compounds are of interest as phosphors for organic light emitting devices. Their emissive properties can be tuned by variation of the ligands or by specific electron-withdrawing or electron-donating substituents. Different ancillary ligands can have a profound impact on the emission color and emission efficiency of these complexes. We studied the influence of sterically hindered, aryl-substituted β-diketonates on the emission properties of C^C* cyclometalated complexes, employing the unsubstituted methyl-phenyl-imidazolium ligand. The quantum yield was significantly enhanced by changing the auxiliary ligand from acetylacetonate, where the corresponding platinum(II) complex shows only a very weak emission, to mesityl (mes) or duryl (dur) substituted acetylacetonates. The new complexes show very efficient emission with quantum yields >70% in the sky-blue spectral region (480 nm) and short decay times (<3 μs).

Introduction

Highly luminescent platinum(II) complexes have successfully been applied for lighting applications such as organic light emitting diodes (OLEDs) [1-6]. Although OLEDs are already widely used, the development of stable and efficient blue devices remains challenging [7,8]. Tetradentate [9-11], terdentate [12-15], and bidentate [16-20] cyclometalated Pt(II) complexes were recently shown to be promising phosphorescent triplet emitters in OLEDs (PhOLEDs), which emit light with high quantum yields in the blue spectral region.

The emission properties of organometallic complexes can be tuned by employing different ligand structures. For platinum(II) complexes, the influence of both cyclometalating [21-26] and auxiliary ligand [27-32] on the emission color as well as their efficiency has been demonstrated. Phenyl-substituted *N*-heterocyclic carbenes (NHCs) as C^C* cyclometalating ligands shift the emission color towards higher energy, due to the strong donor character of NHCs compared to C^N cyclometalating ligands [33,34]. Recently, it was shown that the introduction of

sterically demanding aryl groups as substituents in acetylacetonate (acac) auxiliary ligands can have a positive influence on the emission properties of platinum(II) phosphors [35-38]. The use of mesityl and duryl groups enhanced the quantum yield of platinum complexes with a variety of C^C* cyclometalating ligands [18,39-41].

We herein present the synthesis and photophysical properties of two new C^C* cyclometalated platinum complexes. Both are based on the original 3-methyl-1-phenylimidazolium (MPIM) ligand system which together with the acac auxiliary ligand showed only a very low quantum yield of 7%. We introduced sterically demanding aryl substituted β-diketonate auxiliary ligands to further examine their influence on the emission properties of the resulting platinum(II) complexes.

Results

The mesityl- and duryl-substituted 3-methyl-1-phenylimidazole complexes **2**, Pt(MPIM)(mes) and **3**, Pt(MPIM)(dur), were synthesized from 3-methyl-1-phenylimidazolium iodide (**1**) according to a modified literature procedure (Scheme 1) [41,42]. The starting imidazolium salt **1** was prepared from phenylimidazole by addition of methyl iodide as previously described [43]. Complexes **2** and **3** were obtained as yellow solids in isolated yields of 5% and 18%, respectively (Scheme 1). They were characterized by standard methods, NMR techniques (^{1}H, ^{13}C, and ^{195}Pt) as well as mass spectrometry (ESIMS). The purity of all compounds was verified by elemental analyses. Additionally we could unequivocally determine the structural parameters of **3** by a solid-state structure (Figure 1). Details of the structure determination are given in Supporting Information File 1, Table S1.

The absorption spectra (Figure 2) were measured in dichloromethane solution at ambient temperature. The complexes show almost identical absorption behavior with only minor deviations in the absorption intensity. Both complexes exhibit a strong absorption in the ultraviolet spectral region with an intense shoulder at 241 nm. Two weak and one more intense absorption bands are additionally located at 280 nm, 293 m, and 313 nm, respectively.

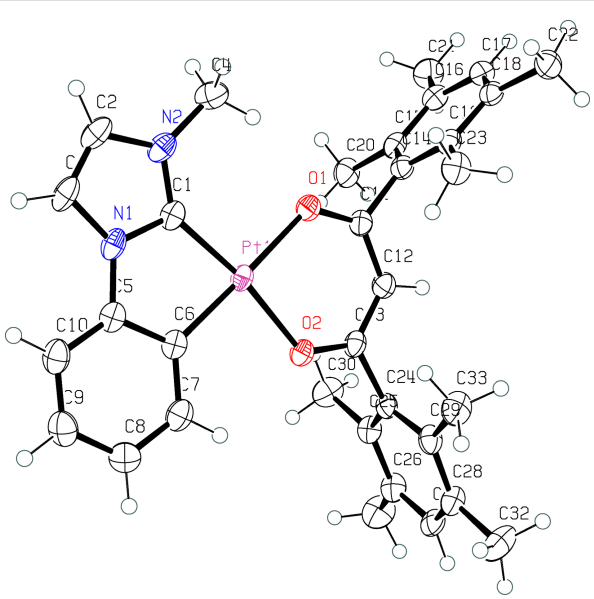
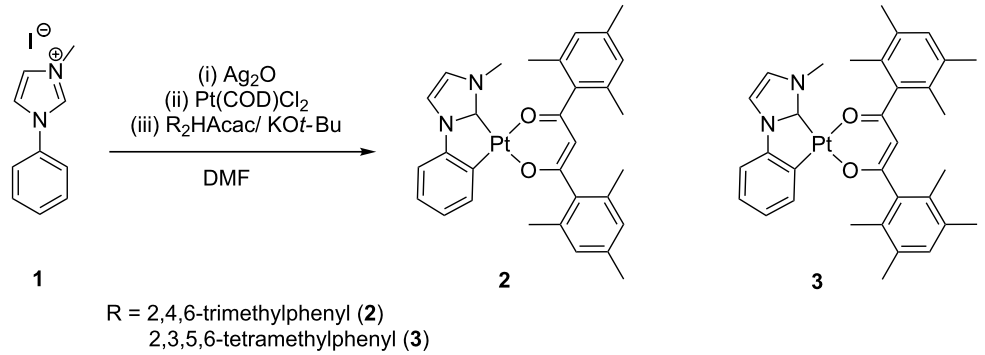


Figure 1: ORTEP representation of **3**. Thermal ellipsoids are drawn at the 50% probability level. Selected bond lengths (Å) and angles (deg): C(1)–Pt(1), 1.950(3); C(6)–Pt(1), 1.988(3); O(1)–Pt(1), 2.089(3); O(2)–Pt(1), 2.047(2); N(1)–C(1), 1.361(4); N(2)–C(1), 1.347(4); C(1)–Pt(1)–C(6), 80.17(13); O(1)–Pt(1)–O(2), 90.51(9); N(1)–C(1)–N(2), 104.8(3); O(1)–Pt(1)–C(1)–N(2), −2.7(4);

Photoluminescence spectra (Figure 3) were measured at ambient temperature in a PMMA matrix (2 wt % complex) and at 77 K in 2-MeTHF (0.5 mM). The room-temperature emission spectra of both complexes exhibit one broad, structurally unresolved band in the sky-blue spectral region.

The low-temperature emission maxima of both complexes display only a minor hypsochromic shift compared to the emission at ambient temperature: 5 nm for complex **2** and 8 nm for



Scheme 1: Synthesis of complexes **2** and **3**.

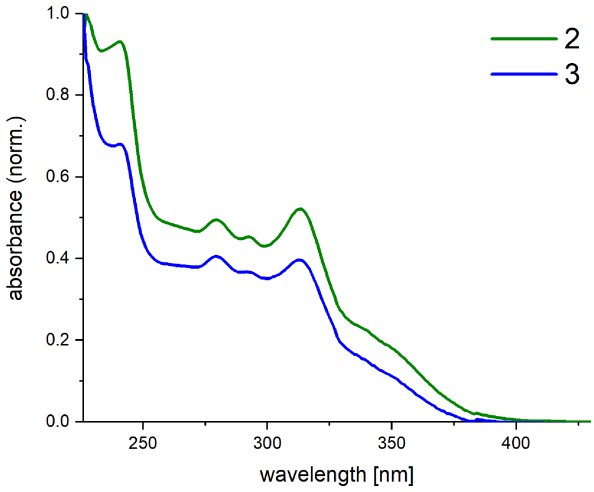


Figure 2: UV–vis absorption spectra of complexes **2** and **3** measured in dichloromethane at room temperature.

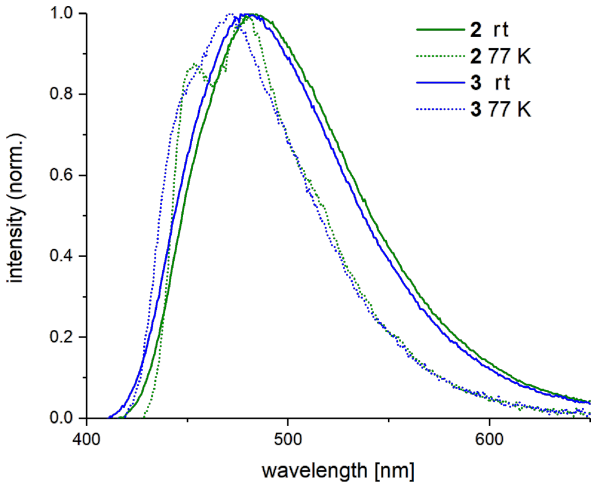


Figure 3: Emission spectra of complexes **2** and **3** measured at room temperature and 77 K, 2 wt % in a PMMA matrix and 0.5 mM in 2-MeTHF, respectively (λ_{exc} = 320 nm).

complex **3**. The emission profile of the mesityl complex **2** shows a vibronic progression with a spacing of 400 cm^{-1} between the first and second band. The low-temperature emission profile of duryl complex **3** mostly remains structurally unresolved. For both complexes, very high quantum yields of 82% (**2**) and 73% (**3**) at ambient temperatures as well as short decay times around 3 µs (Table 1) were measured. The complexes show no aggregation behavior at higher concentrations (10 wt % in PMMA and 100% amorphous film measurements, see Figures S1, S2 and Tables S2, S3 in Supporting Information File 1), which can be assigned to the steric demand of the aryl-substituted diketonate counter ligand.

Cyclic voltammograms of complexes **2** and **3** were measured in DMF with ferrocene as an internal reference. For both compounds, one irreversible oxidation wave was measured (Figure 4), which is commonly found for platinum(II) complexes [16,44]. Irreversibility of the measured signals was confirmed by variation of the scan rate (30 mV/s to 1 V/s). The peak potential of the oxidation is located at 0.69 V vs ferrocene for both complexes. No reduction was observed for both complexes in the electrochemical window of the solvent. Thus, the electrochemical behavior of the newly synthesized substances is comparable.

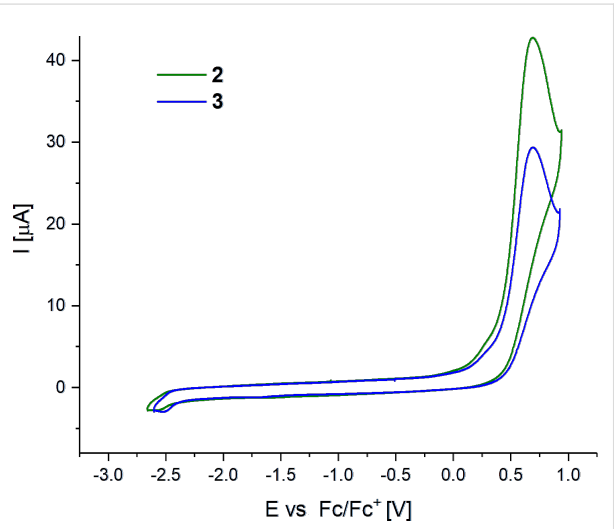


Figure 4: Cyclic voltammograms of complexes **2** and **3**, analyte concentration 10^{-4} M. Measured in DMF (0.1 M TBAP) vs Fc, v = 100 mV/s, under N_2.

Table 1: Photoluminescence data of complexes **2** and **3** (2 wt % in PMMA, λ_{exc} = 320 nm) and literature-known compound Pt(MPIM)(acac).

	CIE (x;y)[a]	λ_{em} [nm][b]	Φ [%][c]	τ_v[d]	τ_0[e]	k_r[f]	k_{nr}[g]
Pt(MPIM)(acac) [42]	0.190; 0.190	441	7	–	–	–	–
Pt(MPIM)(mes) (**2**)	0.196; 0.326	482	82	2.6	3.1	320.5	70.4
Pt(MPIM)(dur) (**3**)	0.191; 0.303	479	73	2.4	3.3	306.6	113.4

[a]CIE coordinates, [b]maximum emission wavelength, [c]absolute quantum yield ± 5% [d]decay lifetimes τ_v (excited by laser pulses 360 nm, 20 kHz) in µs, [e]$\tau_0 = \tau_v/\Phi$ in µs, [f]$k_r = \Phi/\tau_v$ in 10^3 s^{-1}, [g]$k_{nr} = (1 - \Phi)/\tau_v$ in 10^3 s^{-1}.

Discussion

Compared to the already published, structurally related 3-methyl-1-phenylimidazole platinum(II) complex with acetylacetonate as counter ligand, Pt(MPIM)(acac) [42], which shows a very weak emission (Φ = 7%), the new complexes exhibit a dramatically enhanced quantum yield (emission under UV irradiation is shown in Figure 5).

The higher emission efficiency is accompanied by a red shift in emission color of about 40 nm (Figure 6). An improved quantum yield of Φ = 30% (5 wt % in PMMA) has already been reported for a 3-methyl-1-phenylimidazolium cyclometallated platinum(II) complex by the introduction of a sterically demanding ancillary ligand (α-duryl substituted acac) in the central position of the acetylacetonate between the two C=O groups [35]. Besides an increased quantum yield, the complex displayed a small red shift (λ_{exc} = 467 nm) compared to Pt(MPIM)(acac) and a decay time of 8.7 µs. When mesityl or duryl groups replace both methyl groups of the acetylacetonate, the quantum yield is further enhanced. Such a severe influence of the mesityl- and duryl-substituted auxiliary ligands on the quantum yield is unprecedented, although enhanced quantum yields have been reported for both ligands [18,39-41]. Additionally, the decay times of Pt(MPIM)(mes) and Pt(MPIM)(dur) are shorter compared to the phosphorescence decay of the α-duryl-substituted complex (8.7 µs at 77 K in 2-MeTHF).

The observed effects can be attributed to a major influence of the counter ligand on the emission characteristics, which is further supported by the localization of spin density almost exclusively on the ancillary ligand for all three complexes discussed. The spin densities were obtained from DFT calculations with the Gaussian 09 [45] program suite, using the B3LYP[46-50] functional and 6-31G(d) [51-56] basis set with Hay–Wadt ECP (LANL2DZ) [57-59] for platinum (Figure 7).

The observed red shift in emission color is also in agreement with the results of the DFT calculations (Supporting Information File 1, Table S4) of the predicted emission wavelength, according to a previously published procedure [60]. The bathochromic shift in emission color of complexes **2** and **3** can be assigned to the delocalization of electron density on the aryl-substituted auxiliary ligands.

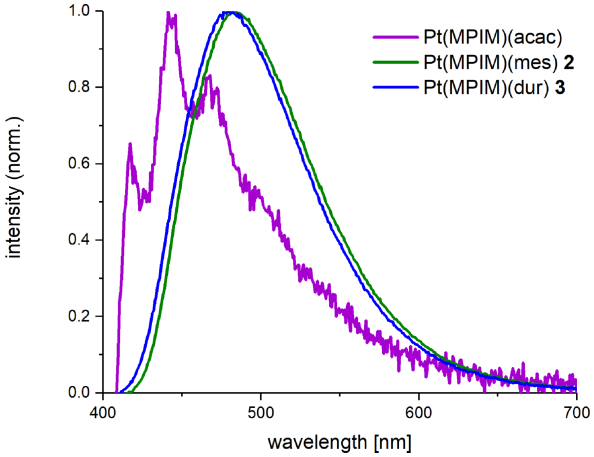


Figure 6: Photoluminescence spectra of **2** and **3** compared to the emission profile of Pt(MPIM)(acac), 2 wt % in PMMA, λ_{exc} = 320 nm.

Conclusion

As shown above, we observed an unprecedented enhancement of the quantum yield for platinum(II) complexes with 3-methyl-1-phenylimidazole as C^C* cyclometalating ligand by changing the ancillary ligand from acetylacetonate (R = CH_3) to sterically demanding aryl-substituted β-diketones (R = 2,4,6-trimethylphenyl, 2,3,5,6-tetramethylphenyl). The drastically increased quantum yield was accompanied by a shift in the emission color from the deep-blue to the sky-blue spectral region. Besides a very efficient phosphorescent emission, the two newly synthesized complexes also exhibit very short decay times of less than 3 µs. The profound impact of the counter ligand on the complexes' emission properties originates from the diketonate ligand, which was also confirmed by DFT calculations.

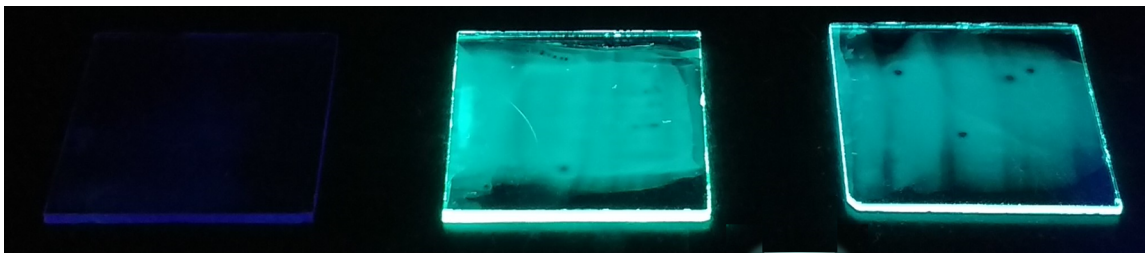


Figure 5: Thin films of Pt(MPIM)(acac) left, Pt(MPIM)(mes) (**2**) middle, and Pt(MPIM)(dur) (**3**) right, 2 wt % in PMMA under irradiation with ultraviolet light (365 nm).

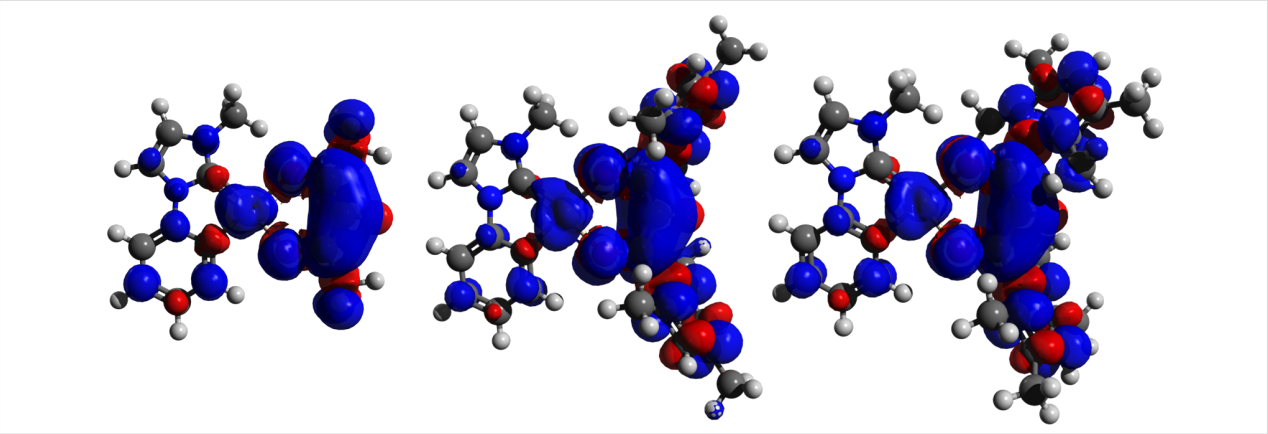


Figure 7: Localization of spin density on the complexes Pt(MPIM)(acac) left, Pt(MPIM)(mes) (**2**) middle, and Pt(MPIM)(dur) (**3**) right (B3LYP/6-31G(d), ECP LANL2DZ, isovalue 0.02).

Experimental

Both complexes were characterized by ^{1}H, ^{13}C, and ^{195}Pt NMR spectroscopy, ESIMS, and elemental analysis. Formation of the carbene complexes was verified by the disappearance of the characteristic NCHN proton signal of the imidazolium salt in the ^{1}H NMR experiment. The syntheses of the platinum complexes were performed under an argon atmosphere and by exclusion of light, using flame-dried Schlenk tubes. Solvents of at least 99.0% purity were used. DMF was dried according to standard methods and stored over molecular sieve (3 Å) under argon atmosphere. Dichloro(1,5-cyclooctadiene)platinum(II) [Pt(COD)Cl_2] was prepared following a modified literature procedure [61]. Potassium tetrachloroplatinate(II) was purchased from Pressure Chemicals (USA) and was used as received. Other chemicals were obtained from common suppliers and used without further purification. ^{1}H, ^{13}C, and ^{195}Pt NMR spectra were recorded on a Bruker NMR spectrometer. ^{1}H and ^{13}C spectra were referenced internally using the resonances of the residual solvent (^{1}H: 2.50 ppm, ^{13}C: 39.52 ppm for DMSO-d_6 and ^{1}H: 7.26 ppm, ^{13}C: 77.00 ppm for $CDCl_3$). ^{195}Pt spectra were referenced externally using potassium tetrachloroplatinate(II) in D_2O (−1617.2 ($PtCl_4^{2-}$), −2654.1 ppm ($PtCl_2$)). Chemical shifts are given in ppm downfield from TMS, coupling constants J in Hz (the signal splitting is abbreviated as followed: s = singlet, d = doublet, t = triplet, m = multiplet). Elemental analyses were performed by the analytical laboratory of the department using a Eurovektor Hekatech EA-3000 elemental analyzer. Melting points were measured on a Wagner and Munz Poly Therm A system and are not corrected.

X-ray crystallography

Crystallographic data for compound **3** were collected on Bruker D8 VENTURE Kappa Duo PHOTON200 by IμS micro-focus sealed tube Mo Kα 0.71073 Å at a temperature of 100(2) K. The absorption corrections were carried out using numerical methods. The structure was solved by direct methods (XP) and refined by full matrix least squares based on F^2 (SHELXL2014).

Photophysical characterization

Absorption spectra of all complexes were measured on a Perkin Elmer lambda 25 spectrophotometer in dichloromethane solution. Photoluminescence measurements were performed in amorphous PMMA thin films doped with the emitter. Films were prepared by doctor blading a solution of 2 wt % emitter in a 10 wt % PMMA solution in dichloromethane on a quartz substrate with a 60 μm doctor blade. Film emission was measured under nitrogen flux. Excitation was carried out at different wavelengths (Xe-lamp with monochromator) and the emission was detected with a calibrated quantum-yield detection system (Hamamatsu, model C11347). The phosphorescence decay of all complexes was measured with an Edinburgh Instruments *mini-τ* by excitation with a pulsed EPLED (360 nm, 20 kHz) and time-resolved photon counting (TCSPC). Frozen 2-MeTHF glass emission samples at 77 K were prepared by inserting a sealed quartz tube, containing the solution under argon atmosphere, into liquid nitrogen. Spectroscopic grade 2-methyltetrahydrofuran (2-MeTHF) was purchased from ABCR and used as received.

Cyclic voltammetry

Electrochemical measurements were performed with a BioLogic SP-150 potentiostat in degassed, dry *N,N*-dimethylformamide using a Pt counter electrode, a glassy carbon working electrode, and a Ag/Ag^+ pseudo reference electrode. All complexes were measured as 0.1 mM solutions with the addition of 0.1 M (n-Bu)$_4NClO_4$ as supporting electrolyte at a sweep rate of 100 mV/s. Signals were identified as irreversible by varying the scan rate between 30 mV/s and 1 V/s. All measurements were internally referenced against the Fc/Fc^+ redox

couple. For visualization, the EC-Lab software V11.01 and Origin 2017 were used.

Synthesis

(SP-4-4)-[1-Methyl-3-phenyl-1*H*-imidazolin-2-yliden-$\kappa^{C2},\kappa^{C2'}$][dimesitoylmethanato-$\kappa^{O},\kappa^{O'}$]platinum(II) (**2**)

General procedure: A flame-dried and argon-flushed Schlenk tube was charged with 1-methyl-3-phenyl-1*H*-imidazol-3-ium iodide (**1**, 230 mg, 0.8 mmol) and silver(I) oxide (100 mg, 0.4 mmol). After the addition of 20 mL of dry DMF the reaction mixture was stirred under an argon atmosphere with the exclusion of light for two hours at room temperature, then for 23 hours at 50 °C. Dichloro(1,5-cyclooctadiene)platinum(II) (300 mg, 0.8 mmol) was added at room temperature, and the mixture was stirred for two hours at 50 °C, then for 24 hours at 120 °C. Afterwards, potassium *tert*-butanolate (180 mg, 1.6 mmol) and 1,3-bis(2,4,6-trimethylphenyl)propane-1,3-dione (495 mg, 1.4 mmol) were added, and the mixture was stirred for 24 hours at room temperature and then for six hours at 110 °C; all volatiles were removed in vacuo, the crude product was washed with water and purified by flash chromatography (silica gel, DCM/isohexanes 3:1). Afterwards, it was washed with pentane and cold ethanol. The residue was fully dissolved in ethanol and recrystallized. After washing again with cold ethanol and drying in vacuo, the pure product was obtained as yellow crystals in 5% yield (25 mg, 0.04 mmol). Mp. 134 °C; ^{1}H NMR ($CDCl_3$, 300 MHz) δ (ppm) 7.71 (dd, *pseudo*-t $J_{H,Pt}$ = 24.9 Hz, J = 7.3 Hz, J = 1.2 Hz, 1H, CH_{arom}), 7.26 (d, J = 2.1 Hz, 1H, CH_{arom}), 7.06–6.88 (m, 3H, CH_{arom}), 6.85 (d, J = 9.4 Hz, 4H, CH_{arom}), 6.79 (d, J = 2.1 Hz, 1H, CH_{arom}), 5.68 (s, 1H, CH), 3.94 (s, 3H, NCH_3), 2.34 (d, J = 9.1 Hz, 12H, CH_3), 2.30 (d, J = 4.3 Hz, 6H, CH_3); ^{13}C NMR (DMSO-d_6, 75MHz) δ (ppm) 184.5 (CO), 183.6 (CO), 147.2 (NCN), 146.9 (C_{arom}), 139.2 (C_{arom}), 138.8 (C_{arom}), 137.3 (C_{arom}), 137.1(C_{arom}), 133.2 (C_{arom}), 132.9 (C_{arom}), 130.7 (CH_{arom}), 128.2 (CH_{arom}), 128.1 (CH_{arom}), 124.5 (C_{arom}), 123.5 (CH_{arom}), 123.5 (CH_{arom}), 122.3 (CH_{arom}), 115.4 (CH_{arom}), 110.8 (CH_{arom}), 106.5 (CH), 34.0 (NCH_3), 20.7 (CH_3), 20.6 (CH_3), 19.4 (CH_3), 19.2 (CH_3); ^{195}Pt NMR (DMSO-d_6, 64.52 MHz,) δ (ppm) −3368. ESIMS m/z = 660.4 $[M + H]^+$; anal. calcd for $C_{31}H_{32}N_2O_2Pt$: C, 56.44; H, 4.89; N, 4.25; found: C, 56.68; H, 5.08; N, 4.16.

(SP-4-4)-[1-Methyl-3-phenyl-1*H*-imidazolin-2-yliden-$\kappa^{C2},\kappa^{C2'}$][bis(2,3,5,6-tetramethylphenyl) propane-1,3-dionato-$\kappa^{O},\kappa^{O'}$]platinum(II) (**3**)

The product was obtained following the general procedure reported for **2** using 1-methyl-3-phenyl-1*H*-imidazol-3-ium iodide (**1**, 230 mg, 0.8 mmol) and silver(I) oxide (100 mg, 0.4 mmol), dichloro(1,5-cyclooctadiene)platinum(II) (300 mg, 0.8 mmol) together with potassium *tert*-butanolate (180 mg, 1.6 mmol) and the β-diketonate 1,3-bis(2,3,5,6-tetramethylphenyl)propane-1,3-dione (540 mg, 1.6 mmol). The crude product was washed with water, isolated by flash chromatography (silica gel, DCM/isohexanes 4:1), and washed with pentane and cold ethanol. The residue was completely dissolved in ethanol and recrystallized. After washing with cold ethanol again and drying in vacuo at 50 °C, the pure product was obtained as a yellow powder in 18% yield (79 mg, 0.14 mmol). Mp. decomp. >310 °C; ^{1}H NMR ($CDCl_3$, 300 MHz) δ (ppm) 7.72 (dd, *pseudo*-t $J_{H,Pt}$ = 26.4 Hz, J = 7.4 Hz, J = 0.9 Hz, 1H, CH_{arom}), 7.26 (d, J = 2.1 Hz, 1H, CH_{arom}), 7.06–6.88 (m, 5H, CH_{arom}), 6.79 (d, J = 2.1 Hz, 1H, CH_{arom}), 5.64 (s, 1H, CH), 3.93 (s, 3H, NCH_3), 2.31–2.16 (m, 24H, CH_3); ^{13}C NMR ($CDCl_3$, 75 MHz) δ (ppm) 185.8 (CO), 185.6 (CO), 146.8 (NCN), 142.4 (C_{arom}), 134.1 (C_{arom}), 133.7 (C_{arom}), 133.6 (C_{arom}), 132.2 (CH_{arom}), 131.1 (CH_{arom}), 131.0 (CH_{arom}), 129.9 (C_{arom}), 129.8 (C_{arom}), 129.5 (C_{arom}), 124.3 (C_{arom}), 124.1 (CH_{arom}), 123.6 (CH_{arom}), 120.8 (CH_{arom}), 114.3 (CH_{arom}), 109.9 (CH_{arom}), 107.5 (CH), 35.0 (CH_3), 19.7 (CH_3), 19.7 (CH_3), 16.5 (CH_3), 16.3 (CH_3); ^{195}Pt NMR ($CDCl_3$, 64.52 MHz) δ (ppm) −3383; ESIMS m/z = 688.4 $[M + H]^+$; anal. calcd for $C_{33}H_{36}N_2O_2Pt$: C, 57.63; H, 5.28; N, 4.07; found: C, 57.93; H, 5.46; N, 3.82.

Supporting Information

The Supporting Information contains NMR-spectra, additional figures, details of the solid state structure determination and computational details. CCDC 1823322 contains the supplementary crystallographic data for this paper. These data can be obtained free of charge via http://www.ccdc.cam.ac.uk/data_request/cif, or by emailing data_request@ccdc.cam.ac.uk, or by contacting The Cambridge Crystallographic Data Centre, 12 Union Road, Cambridge CB21EZ, UK; fax: +44 1223 336033.

Supporting Information File 1

NMR spectra, additional figures, details of the solid state structure determination and computational details.
[https://www.beilstein-journals.org/bjoc/content/supplementary/1860-5397-14-54-S1.pdf]

Supporting Information File 2

Crystallographic data.
[https://www.beilstein-journals.org/bjoc/content/supplementary/1860-5397-14-54-S2.cif]

Acknowledgements

We thank the ZIH (TU Dresden) for computational time at their high-performance computational facility and M.Sc. Johannes Soellner for his help with the solid state structure refinement.

References

1. Baldo, M. A.; O'Brien, D. F.; You, Y.; Shoustikov, A.; Sibley, S.; Thompson, M. E.; Forrest, S. R. *Nature* **1998,** *395,* 151–154. doi:10.1038/25954
2. Evans, R. C.; Douglas, P.; Winscom, C. J. *Coord. Chem. Rev.* **2006,** *250,* 2093–2126. doi:10.1016/j.ccr.2006.02.007
3. Williams, J. A. G.; Develay, S.; Rochester, D. L.; Murphy, L. *Coord. Chem. Rev.* **2008,** *252,* 2596–2611. doi:10.1016/j.ccr.2008.03.014
4. Kalinowski, J.; Fattori, V.; Cocchi, M.; Williams, J. A. G. *Coord. Chem. Rev.* **2011,** *255,* 2401–2425. doi:10.1016/j.ccr.2011.01.049
5. Li, K.; Ming Tong, G. S.; Wan, Q.; Cheng, G.; Tong, W.-Y.; Ang, W.-H.; Kwong, W.-L.; Che, C.-M. *Chem. Sci.* **2016,** *7,* 1653–1673. doi:10.1039/C5SC03766B
6. Fleetham, T.; Li, G.; Li, J. *Adv. Mater.* **2017,** *29,* 1601861. doi:10.1002/adma.201601861
7. Im, Y.; Byun, S. Y.; Kim, J. H.; Lee, D. R.; Oh, C. S.; Yook, K. S.; Lee, J. Y. *Adv. Funct. Mater.* **2017,** *27,* 1603007. doi:10.1002/adfm.201603007
8. Yook, K. S.; Lee, J. Y. *Adv. Mater.* **2012,** *24,* 3169–3190. doi:10.1002/adma.201200627
9. Hang, X.-C.; Fleetham, T.; Turner, E.; Brooks, J.; Li, J. *Angew. Chem., Int. Ed.* **2013,** *52,* 6753–6756. doi:10.1002/anie.201302541
   Angew. Chemie **2013,** *125,* 6885–6888. doi:10.1002/ange.201302541
10. Fleetham, T.; Li, G.; Wen, L.; Li, J. *Adv. Mater.* **2014,** *26,* 7116–7121. doi:10.1002/adma.201401759
11. Turner, E.; Bakken, N.; Li, J. *Inorg. Chem.* **2013,** *52,* 7344–7351. doi:10.1021/ic302490c
12. Cocchi, M.; Kalinowski, J.; Fattori, V.; Williams, J. A. G.; Murphy, L. *Appl. Phys. Lett.* **2009,** *94,* 073309. doi:10.1063/1.3086900
13. Fleetham, T.; Wang, Z.; Li, J. *Org. Electron.* **2012,** *13,* 1430–1435. doi:10.1016/j.orgel.2012.03.041
14. Develay, S.; Blackburn, O.; Thompson, A. L.; Williams, J. A. G. *Inorg. Chem.* **2008,** *47,* 11129–11142. doi:10.1021/ic8014157
15. Naziruddin, A. R.; Lee, C.-S.; Lin, W.-J.; Sun, B.-J.; Chao, K.-H.; Chang, A. H. H.; Hwang, W.-S. *Dalton Trans.* **2016,** *45,* 5848–5859. doi:10.1039/C5DT04770F
16. Brooks, J.; Babayan, Y.; Lamansky, S.; Djurovich, P. I.; Tsyba, I.; Bau, R.; Thompson, M. E. *Inorg. Chem.* **2002,** *41,* 3055–3066. doi:10.1021/ic0255508
17. Bachmann, M.; Suter, D.; Blacque, O.; Venkatesan, K. *Inorg. Chem.* **2016,** *55,* 4733–4745. doi:10.1021/acs.inorgchem.5b02962
18. Strassner, T. *Acc. Chem. Res.* **2016,** *49,* 2680–2689. doi:10.1021/acs.accounts.6b00240
19. Wang, X.; Chang, Y.-L.; Lu, J.-S.; Zhang, T.; Lu, Z.-H.; Wang, S. *Adv. Funct. Mater.* **2014,** *24,* 1911–1927. doi:10.1002/adfm.201302871
20. Fuertes, S.; Chueca, A. J.; Arnal, L.; Martín, A.; Giovanella, U.; Botta, C.; Sicilia, V. *Inorg. Chem.* **2017,** *56,* 4829–4839. doi:10.1021/acs.inorgchem.6b02826
21. Fuertes, S.; García, H.; Perálvarez, M.; Hertog, W.; Carreras, J.; Sicilia, V. *Chem. – Eur. J.* **2015,** *21,* 1620–1631. doi:10.1002/chem.201404915
22. Bossi, A.; Rausch, A. F.; Leitl, M. J.; Czerwieniec, R.; Whited, M. T.; Djurovich, P. I.; Yersin, H.; Thompson, M. E. *Inorg. Chem.* **2013,** *52,* 12403–12415. doi:10.1021/ic4011532
23. Kourkoulos, D.; Karakus, C.; Hertel, D.; Alle, R.; Schmeding, S.; Hummel, J.; Risch, N.; Holder, E.; Meerholz, K. *Dalton Trans.* **2013,** *42,* 13612–13621. doi:10.1039/c3dt50364j
24. Kumar, G. R.; Thilagar, P. *Inorg. Chem.* **2016,** *55,* 12220–12229. doi:10.1021/acs.inorgchem.6b01827
25. Li, G.; Wolfe, A.; Brooks, J.; Zhu, Z.-Q.; Li, J. *Inorg. Chem.* **2017,** *56,* 8244–8256. doi:10.1021/acs.inorgchem.7b00961
26. Hudson, Z. M.; Sun, C.; Helander, M. G.; Chang, Y.-L.; Lu, Z.-H.; Wang, S. *J. Am. Chem. Soc.* **2012,** *134,* 13930–13933. doi:10.1021/ja3048656
27. Mydlak, M.; Yang, C.-H.; Polo, F.; Galstyan, A.; Daniliuc, C. G.; Felicetti, M.; Leonhardt, J.; Strassert, C. A.; De Cola, L. *Chem. – Eur. J.* **2015,** *21,* 5161–5172. doi:10.1002/chem.201405839
28. Solomatina, A. I.; Aleksandrova, I. O.; Karttunen, A. J.; Tunik, S. P.; Koshevoy, I. O. *Dalton Trans.* **2017,** *46,* 3895–3905. doi:10.1039/C7DT00349H
29. Galstyan, A.; Naziruddin, A. R.; Cebrián, C.; Iordache, A.; Daniliuc, C. G.; De Cola, L.; Strassert, C. A. *Eur. J. Inorg. Chem.* **2015,** 5822–5831. doi:10.1002/ejic.201500949
30. Lu, W.; Mi, B.-X.; Chan, M. C. W.; Hui, Z.; Che, C.-M.; Zhu, N.; Lee, S.-T. *J. Am. Chem. Soc.* **2004,** *126,* 4958–4971. doi:10.1021/ja0317776
31. Hua, F.; Kinayyigit, S.; Cable, J. R.; Castellano, F. N. *Inorg. Chem.* **2005,** *44,* 471–473. doi:10.1021/ic048498j
32. Spencer, M.; Santoro, A.; Freeman, G. R.; Díez, Á.; Murray, P. R.; Torroba, J.; Whitwood, A. C.; Yellowlees, L. J.; Williams, J. A. G.; Bruce, D. W. *Dalton Trans.* **2012,** *41,* 14244–14256. doi:10.1039/c2dt31525d
33. Li, K.; Cheng, G.; Ma, C.; Guan, X.; Kwok, W.-M.; Chen, Y.; Lu, W.; Che, C.-M. *Chem. Sci.* **2013,** *4,* 2630–2644. doi:10.1039/c3sc21822h
34. Unger, Y.; Zeller, A.; Ahrens, S.; Strassner, T. *Chem. Commun.* **2008,** 3263–3265. doi:10.1039/b804019b
35. Ko, S.-B.; Park, H.-J.; Gong, S.; Wang, X.; Lu, Z.-H.; Wang, S. *Dalton Trans.* **2015,** *44,* 8433–8443. doi:10.1039/C4DT03085K
36. Micksch, M.; Tenne, M.; Strassner, T. *Organometallics* **2014,** *33,* 3464–3473. doi:10.1021/om500383b
37. Tronnier, A.; Heinemeyer, U.; Metz, S.; Wagenblast, G.; Muenster, I.; Strassner, T. *J. Mater. Chem. C* **2015,** *3,* 1680–1693. doi:10.1039/C4TC02575J
38. Shigehiro, T.; Yagi, S.; Maeda, T.; Nakazumi, H.; Fujiwara, H.; Sakurai, Y. *J. Phys. Chem. C* **2013,** *117,* 532–542. doi:10.1021/jp307853t
39. Soellner, J.; Tenne, M.; Wagenblast, G.; Strassner, T. *Chem. – Eur. J.* **2016,** *22,* 9914–9918. doi:10.1002/chem.201601060
40. Leopold, H.; Heinemeyer, U.; Wagenblast, G.; Münster, I.; Strassner, T. *Chem. – Eur. J.* **2017,** *23,* 1118–1128. doi:10.1002/chem.201604456
41. Pinter, P.; Mangold, H.; Stengel, I.; Münster, I.; Strassner, T. *Organometallics* **2016,** *35,* 673–680. doi:10.1021/acs.organomet.5b00982
42. Unger, Y.; Meyer, D.; Molt, O.; Schildknecht, C.; Münster, I.; Wagenblast, G.; Strassner, T. *Angew. Chem., Int. Ed.* **2010,** *49,* 10214–10216. doi:10.1002/anie.201001316
    Angew. Chem. **2010,** *122,* 10412–10414. doi:10.1002/ange.201001316
43. Berding, J.; van Paridon, J. A.; van Rixel, V. H. S.; Bouwman, E. *Eur. J. Inorg. Chem.* **2011,** 2450–2458. doi:10.1002/ejic.201100015
44. Tronnier, A.; Pöthig, A.; Metz, S.; Wagenblast, G.; Münster, I.; Strassner, T. *Inorg. Chem.* **2014,** *53,* 6346–6356. doi:10.1021/ic500971z
45. *Gaussian 09,* Revision D.01; Gaussian Inc.: Wallingford, CT, 2009.
46. Vosko, S. H.; Wilk, L.; Nusair, M. *Can. J. Phys.* **1980,** *58,* 1200–1211. doi:10.1139/p80-159

47. Becke, A. D. *J. Chem. Phys.* **1993,** *98,* 5648–5652. doi:10.1063/1.464913
48. Miehlich, B.; Savin, A.; Stoll, H.; Preuss, H. *Chem. Phys. Lett.* **1989,** *157,* 200–206. doi:10.1016/0009-2614(89)87234-3
49. Lee, C.; Yang, W.; Parr, R. G. *Phys. Rev. B* **1988,** *37,* 785–789. doi:10.1103/PhysRevB.37.785
50. Stephens, P. J.; Devlin, F. J.; Chabalowski, C. F.; Frisch, M. J. *J. Phys. Chem.* **1994,** *98,* 11623–11627. doi:10.1021/j100096a001
51. Ditchfield, R.; Hehre, W. J.; Pople, J. A. *J. Chem. Phys.* **1971,** *54,* 724–728. doi:10.1063/1.1674902
52. Hehre, W. J.; Ditchfield, R.; Pople, J. A. *J. Chem. Phys.* **1972,** *56,* 2257–2261. doi:10.1063/1.1677527
53. Hariharan, P. C.; Pople, J. A. *Chem. Phys. Lett.* **1972,** *16,* 217–219. doi:10.1016/0009-2614(72)80259-8
54. Hariharan, P. C.; Pople, J. A. *Theor. Chim. Acta* **1973,** *28,* 213–222. doi:10.1007/BF00533485
55. Hariharan, P. C.; Pople, J. A. *Mol. Phys.* **1974,** *27,* 209–214. doi:10.1080/00268977400100171
56. Rassolov, V. A.; Pople, J. A.; Ratner, M. A.; Windus, T. L. *J. Chem. Phys.* **1998,** *109,* 1223–1229. doi:10.1063/1.476673
57. Hay, P. J.; Wadt, W. R. *J. Chem. Phys.* **1985,** *82,* 270–283. doi:10.1063/1.448799
58. Wadt, W. R.; Hay, P. J. *J. Chem. Phys.* **1985,** *82,* 284–298. doi:10.1063/1.448800
59. Hay, P. J.; Wadt, W. R. *J. Chem. Phys.* **1985,** *82,* 299–310. doi:10.1063/1.448975
60. Unger, Y.; Strassner, T.; Lennartz, C. *J. Organomet. Chem.* **2013,** *748,* 63–67. doi:10.1016/j.jorganchem.2013.07.011
61. Drew, D.; Doyle, J. R. *Inorg. Synth.* **1990,** *28,* 346–349.

License and Terms

This is an Open Access article under the terms of the Creative Commons Attribution License (http://creativecommons.org/licenses/by/4.0), which permits unrestricted use, distribution, and reproduction in any medium, provided the original work is properly cited.

The license is subject to the *Beilstein Journal of Organic Chemistry* terms and conditions: (https://www.beilstein-journals.org/bjoc)

The definitive version of this article is the electronic one which can be found at: doi:10.3762/bjoc.14.54

BEILSTEIN JOURNAL OF ORGANIC CHEMISTRY

D–A–D-type orange-light emitting thermally activated delayed fluorescence (TADF) materials based on a fluorenone unit: simulation, photoluminescence and electroluminescence studies

Lin Gan, Xianglong Li, Xinyi Cai, Kunkun Liu, Wei Li and Shi-Jian Su*

Full Research Paper

Open Access

Address:
State Key Laboratory of Luminescent Materials and Devices and Institute of Polymer Optoelectronic Materials and Devices, South China University of Technology, Wushan Road 381, Tianhe District, Guangzhou 510640, Guangdong Province, P. R. China

Email:
Shi-Jian Su* - mssjsu@scut.edu.cn

* Corresponding author

Keywords:
fluorenone acceptor; orange light emission; organic light-emitting diode (OLED); thermally activated delayed fluorescence

Beilstein J. Org. Chem. **2018,** *14,* 672–681.
doi:10.3762/bjoc.14.55

Received: 15 November 2017
Accepted: 28 February 2018
Published: 22 March 2018

This article is part of the Thematic Series "Recent advances in materials for organic light emitting diodes".

Guest Editor: E. Zysman-Colman

© 2018 Gan et al.; licensee Beilstein-Institut.
License and terms: see end of document.

Abstract

The design of orange-light emitting, thermally activated, delayed fluorescence (TADF) materials is necessary and important for the development and application of organic light-emitting diodes (OLEDs). Herein, two donor–acceptor–donor (D–A–D)-type orange TADF materials based on fluorenone and acridine, namely 2,7-bis(9,9-dimethylacridin-10(9*H*)-yl)-9*H*-fluoren-9-one (27DACRFT, **1**) and 3,6-bis(9,9-dimethylacridin-10(9*H*)-yl)-9*H*-fluoren-9-one (36DACRFT, **2**), were successfully synthetized and characterized. The studies on their structure–property relationship show that the different configurations have a serious effect on the photoluminescence and electroluminescence performance according to the change in singlet–triplet splitting energy (ΔE_{ST}) and excited state geometry. This indicates that a better configuration design can reduce internal conversion and improve triplet exciton utilization of TADF materials. Importantly, OLEDs based on **2** exhibited a maximum external quantum efficiency of 8.9%, which is higher than the theoretical efficiency of the OLEDs based on conventional fluorescent materials.

Introduction

Since multilayered OLEDs were first reported by Tang in 1987 [1], organic light-emitting diodes (OLEDs) have been a research focus due to their applications in display devices and general lighting. The efficiency of OLEDs was previously limited by the statistic rule of spin multiplicity. For conventional fluorescent materials, only singlet excitons are involved in electroluminescence, leading to a theoretical maximal internal quantum efficiency (IQE_{max}) of 25% and a theoretical

maximal external quantum efficiency (EQE_{max}) of 5%, when assuming the out-coupling efficiency to be 20%. On the other hand, phosphorescent materials could utilize triplet excitons in electroluminescence processes to achieve 100% IQE_{max} [2,3]. However, the utilization of metals like iridium and platinum, which are expensive and nonrenewable, inevitably increase the cost of the final OLEDs. Alternatively, a thermally activated delayed fluorescence (TADF) material is a kind of noble-metal-free fluorescent material able to transform triplet excitons into singlet excitons through reverse intersystem crossing (RISC) to achieve 100% IQE_{max} in theory [4].

On the basis of the previous considerations, for TADF materials, the energy difference (ΔE_{ST}) between the first singlet excited state (S_1) and the first triplet excited state (T_1) must be small enough to enable the RISC process with the activation of environmental thermal energy [5]. To achieve this, electron donors (D) and electron acceptors (A) are introduced into the molecule to form an intramolecular charge transfer (ICT) state with a large twisting angle between the donor and the acceptor to achieve the separation of highest occupied molecular orbital (HOMO) and lowest unoccupied molecular orbital (LUMO) [6], which is the key to reduce the ΔE_{ST}. Therefore, D–A-type or D–A–D-type molecules are the most classical TADF molecular structures [7].

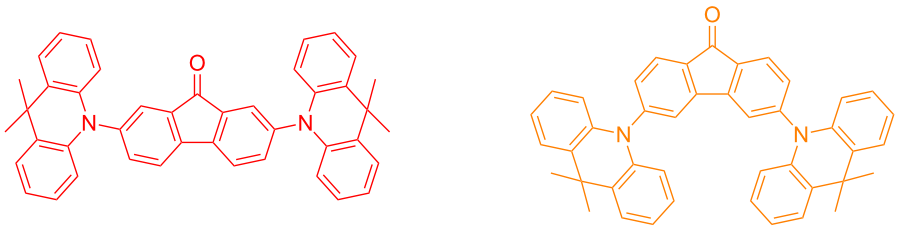
Although there have been numerous TADF materials synthesized and reported [8,9], to the best of our knowledge, orange and red TADF materials are still rarely reported in comparison with blue and green TADF materials [10,11]. It is difficult to achieve TADF in orange and red fluorescent materials not only because red TADF materials require a strong ICT state, which strongly facilitates nonradiative transition processes, but also because the energy gap law generally results in a low radiative rate constant (k_r) to compete with a large nonradiative rate constant (k_{nr}) [12]. The increasing nonradiative transition processes and large k_{nr} play a role in competition with RISC and radiative transition processes and seriously restrict the development of orange and red TADF materials [5]. Therefore, further attempts and new designs towards orange and red TADF materials are necessary.

In this work, we designed and synthetized two novel D–A–D-type orange TADF materials, namely 2,7-bis(9,9-dimethylacridin-10(9*H*)-yl)-9*H*-fluoren-9-one (27DACRFT, **1**) and 3,6-bis(9,9-dimethylacridin-10(9*H*)-yl)-9*H*-fluoren-9-one (36DACRFT, **2**, Scheme 1). The compounds are isomers with different donor–accepter bonding positions, where the fluorenone unit is a strong electron acceptor, which has not been reported in the field of TADF materials before, while acridine, one of the most commonly used donors in TADF materials, has strong electron-donating and hole-transport ability. The combination of the strong acceptor and strong donor can give a narrow energy gap and thus longer wavelength emission. Compounds **1** and **2** were thoroughly characterized by ^{1}H NMR, ^{13}C NMR and electron ionization (EI) mass spectrometry. Both of them show TADF behavior with orange emission color according to the photoluminescence spectra and time-resolved transient photoluminescence decay measurement. EQEs of 2.9% and 8.9% were achieved for the OLED devices based on **1** and **2**, respectively, which are higher than the theoretical efficiency of the OLEDs based on conventional fluorescent materials.

Results and Discussion

27DACRFT **1** and 36DACRFT **2** have similar thermal properties according to thermogravimetric analysis (TGA) and differential scanning calorimetry (DSC) measurements. They have high decomposition temperatures (T_d, corresponding to a 5% weight loss) of 361 and 363 °C, respectively. In addition, no glass-transition temperature (T_g) was found according to their DSC curves. Thanks to their amorphous characteristics, the stability of their morphology and chemical composition can be expected during the evaporation processing fabrication of OLEDs.

In order to characterize their electrochemical properties, cyclic voltammetry (CV) measurements were conducted to measure



27DACRFT, **1** 36DACRFT, **2**

Scheme 1: Molecular structures of isomers **1** and **2**.

their oxidation potentials (E_{ox}) and reduction potentials (E_{red}). Ionization potential (IP) and electron affinity (EA), which approximate to their HOMO and LUMO energy levels, are calculated from E_{red} and E_{ox}. Compounds **1** and **2** have similar HOMO and LUMO energy levels due to the same donor and acceptor in the molecules (Table 1).

Table 1: Thermal and electrochemical properties of the investigated compounds **1** and **2**.

Compound	T_d[a]/T_g[b] (°C)	IP[c] (eV)	EA[d] (eV)	E_g[e] (eV)
1	361/N.A.	−3.20	−5.10	1.90
2	363/N.A.	−3.15	−5.30	2.15

[a]Decomposition temperature (T_d) at 5 wt % weight loss obtained from TGA measurements; [b]glass-transition temperature (T_g) obtained by DSC measurements; [c]ionization potential (IP) calculated from the empirical formula: IP = −(E_{red} + 4.4) eV, the cyclic voltammetry was carried out in 0.1 M *n*-Bu_4NPF_6 in CH_2Cl_2/CH_3CN 4:1 solution; delectron affinity (EA) calculated from the empirical formula: IP = −(E_{ox} + 4.4) eV; [e]energy gap (E_g) estimated from cyclic voltammetry measurements.

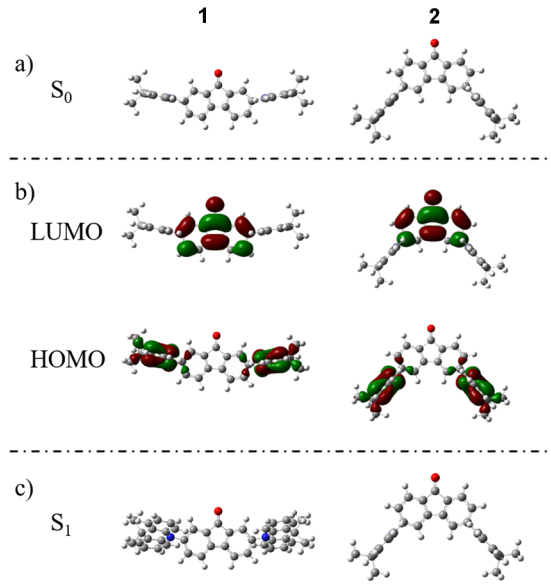


Figure 1: (a) The optimized S_0 geometries of **1** (left) and **2** (right) on B3LYP/6-31G* level in gas phase; (b) The frontier molecular orbital distributions of **1** and **2**; (c) The optimized S_1 geometries in TD-DFT on m062x/6-31G* level.

The molecular geometry of **1** and **2** in the ground state and excited state were simulated by density functional theory (DFT) and time-dependent density functional theory (TD-DFT) calculations, respectively. The ground state (S_0) geometries were optimized on B3LYP/6-31G* level in gas phase, while the lowest triplet excited state (T_1) energy levels and the singlet excited state (S_1) geometries of those molecules were optimized by TD-DFT on m062x/6-31G* level based on the optimized ground state geometries. The optimized geometries of S_0 and S_1 are shown in Figure 1.

The optimized geometries in S_0 are shown in Figure 1a, and all the data are summarized in Table 2. Large twisting angles (θ) of 89.33° and 88.80° between the donor units and the accepter units were estimated for compound **1** and **2**, respectively. As shown in Figure 1b, HOMOs and LUMOs are mainly located on the acridine unit and the fluorenone unit, respectively, which contribute to small ΔE_{ST}. The existence of a very small overlap of HOMOs and LUMOs is advantageous to retain high photoluminescence (PL) quantum yields [13-15]. The calculated ΔE_{ST} of **1** and **2** are 0.33 and 0.27 eV, which are small enough to achieve TADF behavior.

As shown in Figure 1c, the twisting angle (θ') of **1** in S_1 is 63.74°, which is much smaller than its θ in S_0, meanwhile, the conformation of the acridine units in **1** is also changed in S_1 as a result of vibrational relaxation and internal conversion (IC), which means the S_0 geometry of **1** becomes unstable when the molecule is excited and the wave function distribution is changed. The different twisting angles between S_0 and S_1 may reduce its PL property according to the energy gap law [16] as vibrational relaxation and intersystem crossing (IC) processes can consume the energy in S_1, leading to increased nonradiative deactivation [17], reduced PL quantum yield, and thus reduced singlet exciton utilization. On the contrary, the geometry of **2** is hardly changed when excited. Thus, compound **2** shows more potentiality in the application of OLEDs for its better configuration.

Table 2: The calculated HOMO, LUMO, twisting angles (θ, θ'), bond lengths (l, l'), ΔE_{ST} and dipole moment in gas phase for S_0 and in solution for S_1, from DFT and TD-DFT.

Compound	S_0						S_1	
	HOMO (eV)	LUMO (eV)	θ (°)	l (Å)	ΔE_{ST} (eV)	Dipole moment (D)	θ' (°)	l' (Å)
1	−5.00	−2.61	89.33	1.433	0.33	3.501	63.74	1.419
2	−5.03	−2.61	88.80	1.434	0.27	1.814	89.36	1.434

Ultraviolet–visible (UV–vis) absorption and PL spectra in dilute solutions of **1** and **2** (10^{-5} M) are presented in Figure 2. Both compounds **1** and **2** have similar absorption peaks at around 345 and 456 nm. The peaks at around 456 nm result from their ICT states from the donor to the acceptor, while the absorption below 380 nm is caused by their short π-conjugation. It is obvious that **2** has not only a higher oscillator strength (f) than **1** from its transition of charge-transfer states, but also a weaker oscillator strength from its local excited (LE) states. It could be considered that **2** has a better configuration, which is advantageous to intramolecular charge transfer compared with **1**, which coincides with the conclusion from DFT calculation.

The PL spectra of the materials in different solvents were also measured. However, no emission was observed in the dilute solutions of dichloromethane (DCM) and tetrahydrofuran (THF) because vibrational relaxation and internal conversion are promoted to reduce the PL intensity. Both compounds **1** and **2** show almost the same PL spectra in dilute solutions of toluene and *n*-hexane. The photoluminescence spectra of the *n*-hexane solutions show a peak at 517 nm with a shoulder at 545 nm, which can be considered as the radiative transition of ^{1}LE states. Noticeably, the charge-transfer process is limited in *n*-hexane because of its lower polarity. Only one peak at 593 nm was observed for the dilute toluene solutions of both molecules with the typical PL spectra from the radiative transition of ICT states, which could be the evidence of the existence of strong ICT states of both molecules. More importantly, both materials achieve orange luminescence in a dilute solution of toluene, which could be attributed to the strong electron-withdrawing ability and excess conjugation length of fluorenone plane compared with conventional benzophenone acceptor [18].

In addition, low temperature photoluminescence (LTPL) spectra of the materials in toluene at 77 K were measured. The energy levels of S_1 and T_1 were determined from the onset of the prompt and delayed emission peaks, respectively. As shown in Figure 3, both T_1 states of the materials could be confirmed as ^{3}CT character from their delayed photoluminescence spectra without any well-defined vibronic structure [7]. The ΔE_{ST} of **1** and **2** are 0.19 and 0.09 eV, respectively, indicating that compound **2** may have a much more efficient RISC process than **2** [19,20] (Table 3).

To gain a further understanding of the photophysical properties of **1** and **2** in solid state, two doped films in 4,4'-dicarbazolyl-1,1'-biphenyl (CBP) were vacuum co-deposited at a concentration of 8 wt % for photoluminescence quantum yield (PLQY) and time-resolved transient photoluminescence decay measurements. The concentration of the doped films was optimized to ensure complete energy transfer between the host and the guest. PLQY measurements of **1**:CBP and **2**:CBP are 7% and 26%, respectively. The PLQY measurements of the doped films with lower concentration show varying degrees of deviation due to the incomplete energy transfer and the obvious luminescence from CBP (PLQY of **1** and **2** doped in CBP with 1 wt % are 2%

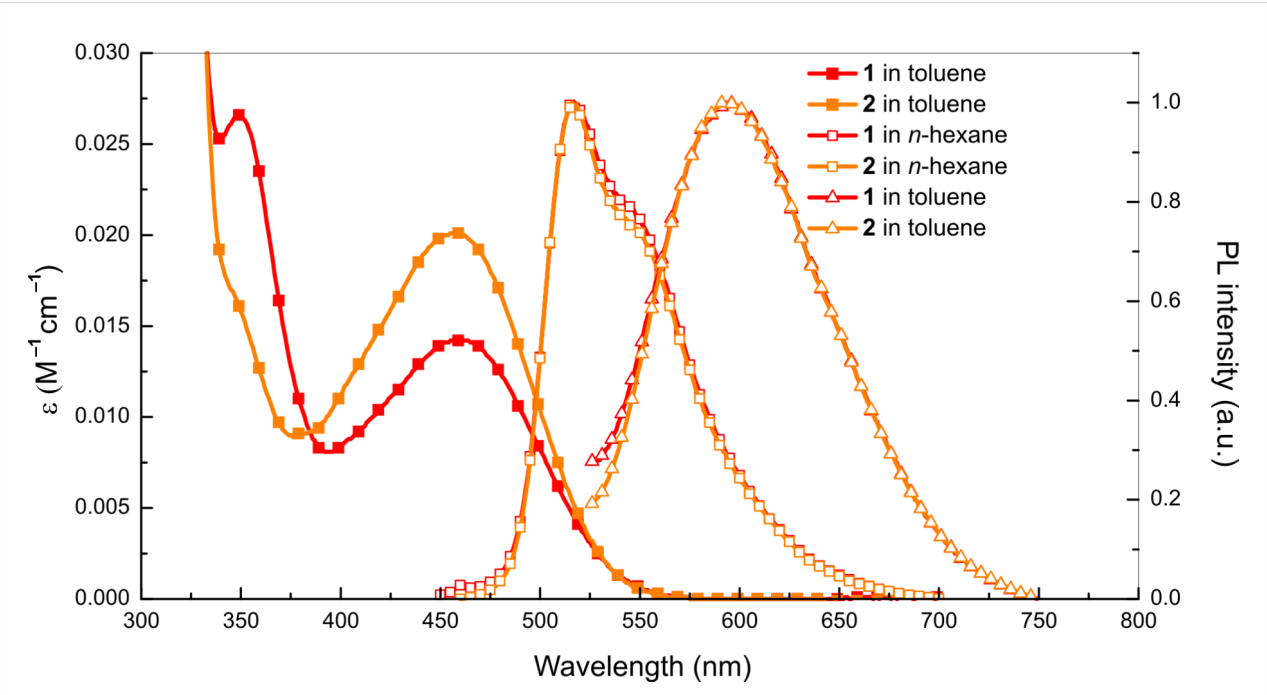


Figure 2: UV–vis (solid point) and photoluminescence (hollow point) spectra of **1** and **2** in dilute solution.

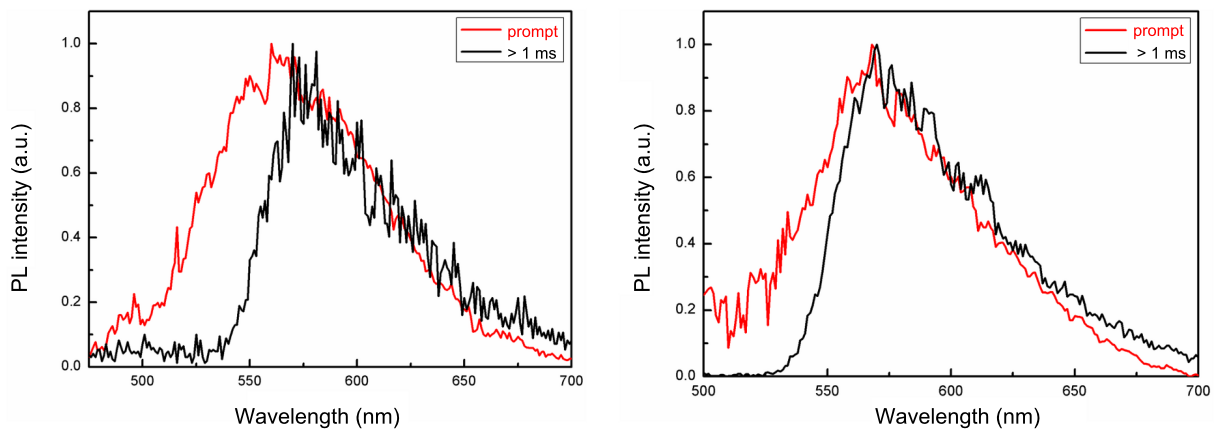


Figure 3: The low temperature photoluminescence spectra of **1** (left) and **2** (right) in toluene at 77 K.

Table 3: Photophysical properties of the investigated molecules **1** and **2**.

Compound	λ_{abs}[a] (nm)	λ_{em}[b] (nm)	λ_{em}[a] (nm)	λ_{em}[c] (nm)	E_g[d] (eV)	Φ_{PL}[c] (%)	ΔE_{ST}[e] (eV)
1	345, 456	517, 545	593	593	2.32	7	0.19
2	345, 456	517, 545	593	581	2.32	26	0.09

[a]Ultraviolet–visible absorption spectra and photoluminescence spectra measured in toluene; [b]photoluminescence (PL) spectra measured in *n*-hexane; [c]photoluminescence spectra and PL quantum yields measured in doped film 8 wt % in CBP; [d]energy gap (E_g) calculated from the empirical formula: $E_g = 1240/\lambda_{abs\text{-}onset}$, where $\lambda_{abs\text{-}onset}$ is the onset of ultraviolet–visible absorption spectra. [e]ΔE_{ST} is calculated from the onset of photoluminescence spectra at 77 K.

and 10%, respectively). As shown in Supporting Information File 1, both PL spectra of the doped films of **1**:CBP and **2**:CBP show red-shift from their PL spectra in *n*-hexane, which could be considered as the influence from aggregation. As mentioned above, **1** and **2** show nearly the same PL spectra in their dilute toluene solution. However, the PL spectrum of **2** is slightly blue-shifted from its PL spectrum in toluene, while **1**:CBP shows alike spectra with **1** in toluene. It could be considered as the solid-state solvation effect [21], as **2** and **1** have different dipole moment of 1.814 D and 3.501 D, respectively from DFT calculation, owing to their different configurations.

The doped film **2**:CBP shows a typical TADF behavior as shown in Figure 4b, according to the time-resolved transient photoluminescence decay measurement. The proportion of delayed fluorescence increases rapidly with improved temperature from 77 to 250 K and slowly by acceleration of the nonradiative transition rate when the temperature is higher than 250 K. On the other hand, **1**:CBP hardly shows a TADF behavior when the temperature is below 300 K, as shown in Figure 4c.

The signals are characterized by noise rather than delayed fluorescence when the temperature is lower than room temperature due to its low PLQY. Delayed fluorescence can be only observed when the temperature is above 300 K. This could be attributed to the large ΔE_{ST} and low PLQY of **1** which requires more energy to achieve RISC process from T_1 to S_1. According to the integration and the lifetime of the prompt and delayed components of the time-resolved transient PL decay curves at room temperature, the PLQY of their respective components and rate constant of different kinetic processes were calculated, as shown in Table 4.

The rate constants were calculated following Equations 1–4 below [5,7,16].

$$k_r = \Phi_{PF} / \tau_{PF} \quad (1)$$

$$\Phi = k_r / \left(k_r + k_{nr}\right) \quad (2)$$

$$\Phi_{PF} = k_r / \left(k_r + k_{isc} + k_{nr}\right) \quad (3)$$

$$k_{risc} = k_P k_d \Phi_{TADF} / k_{isc} \Phi_{PF} \quad (4)$$

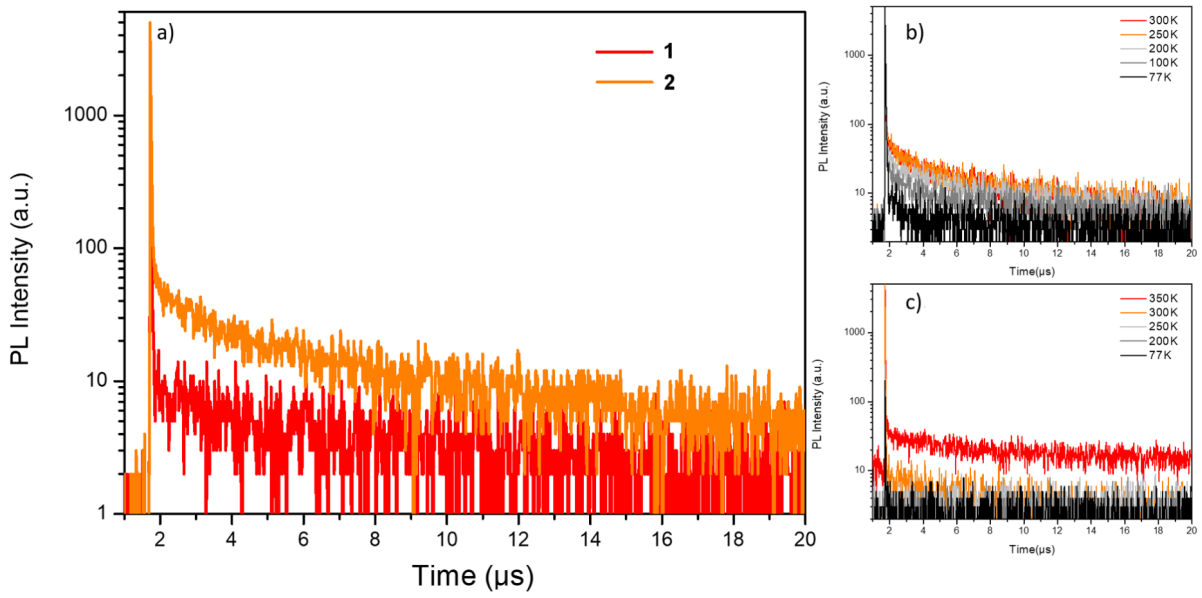


Figure 4: (a) Time-resolved transient photoluminescence decay spectra of the doped films (8 wt % in CBP) measured in N_2 at 300 K; time-resolved transient photoluminescence decay spectra of (b) **2**:CBP and (c) **1**:CBP measured in N_2 at different temperatures.

Table 4: Photophysical properties of the **1** and **2** doped in CBP films (8 wt %) at room temperature.

Compound	Φ	$Φ_{PF}$	$Φ_{TADF}$	$τ_{PF}$ (ns)	$τ_{TADF}$ (μs)	k_r (10^6 s^{-1})	k_{nr} (10^7 s^{-1})	k_{isc} (10^7 s^{-1})	k_{risc} (10^5 s^{-1})
1	0.07	0.06	0.01	11.6	10.6	5.2	6.91	1.23	1.10
2	0.26	0.16	0.10	18.5	4.28	8.6	2.45	2.07	3.81

where k_r, k_{nr}, k_{isc}, and k_{risc} represent the rate constant of radiative, nonradiative, intersystem crossing and reverse intersystem crossing, respectively; Φ, $Φ_{PF}$, $Φ_{TADF}$, $τ_{PF}$ and $τ_{TADF}$ represent the photoluminescence quantum yield, quantum yield of the prompt component, quantum yield of the delayed component, and lifetimes of the prompt and delayed components, respectively. As shown in Table 4, **2** has a significantly larger k_{nr} than **2**, which is consistent with the DFT simulation. On the other hand, a much lower k_{risc} and longer $τ_{TADF}$ was acquired by **1**:CBP than **2**:CBP, as a result of the blocked reverse intersystem crossing and the large $ΔE_{ST}$. Further, the existence of strong IC and vibrational relaxation processes of **1** is proved by its large k_{nr} and low PLQY. In contrast, owing to the relatively small $ΔE_{ST}$, k_{risc} of **2** is higher and $τ_{TADF}$ is relatively shorter than **1**. The short $τ_{TADF}$ not only signifies efficient utilization of singlet excitons, but is also advantageous in reducing the triplet exciton concentration and efficiency roll-off in the OLED devices.

Finally, electroluminescent properties of **1** and **2** were characterized in a device structure of ITO/TAPC (25 nm)/1 wt % emitter in CBP (35 nm)/TmPyPB (55 nm)/LiF (1 nm)/Al, where 1,1-bis(4-(di-*p*-tolylamino)phenyl)cyclohexane (TAPC), 4,4'-bis(9*H*-carbazol-9-yl)biphenyl (CBP), 1,3,5-tri[(3-pyridyl)-phen-3-yl]benzene (TmPyPB) and LiF play the roles of hole transport layer, host material, electron transport layer and electron injection layer, respectively [22]. The energy level diagrams and the chemical structures of the materials utilized are shown in Figure 5.

TAPC and TmPyPB also play the role of exciton blocking layer at the same time because of their high T_1 energy level. Carriers will also be trapped by the emitter directly because of the energy level difference between CBP and the emitter, which makes it possible for the OLEDs with such a low emitter concentration to achieve complete energy transfer. The performance of the fabricated devices is summarized in Table 5 while the *J*–*V*–*L* (current density–voltage–luminance) and EQE–current density characteristics of the devices are shown in Figure 6.

A significantly higher performance was observed from the device based on **2** with a maximal current efficiency (CE_{max}) of

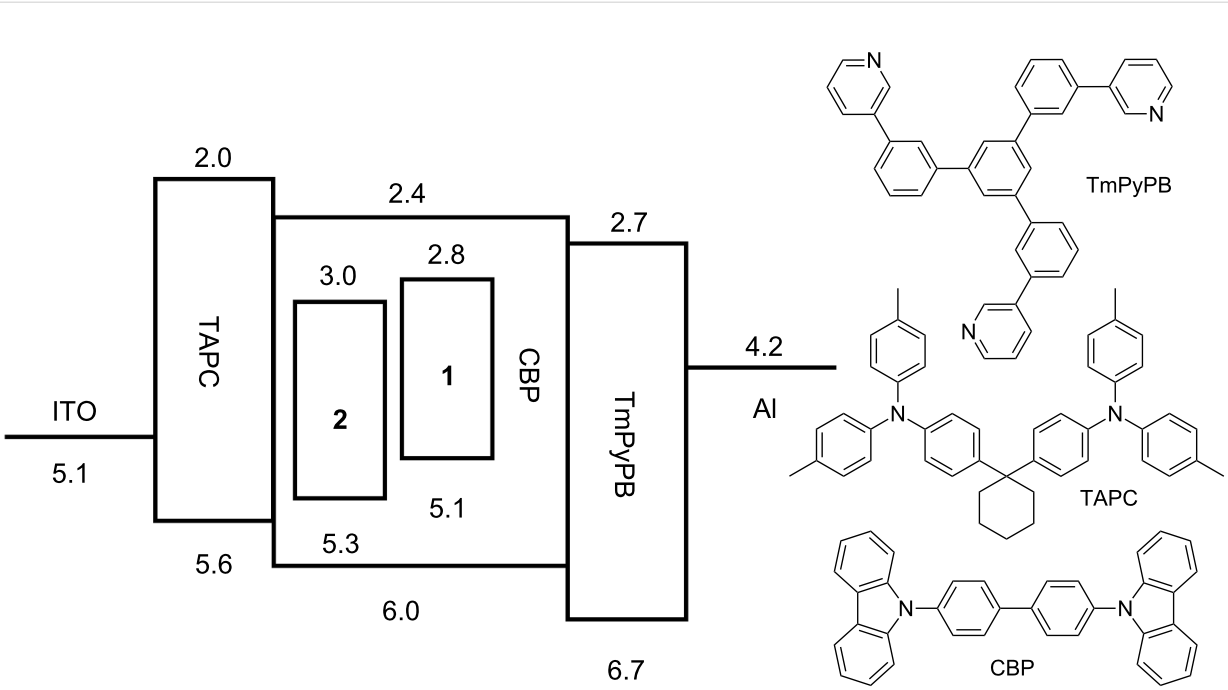


Figure 5: Energy level (eV) diagrams of OLED devices and the chemical structures of the materials utilized for device fabrication.

Table 5: Summary of the device performances of the OLEDs based on **1** and **2**.

Device[a]	V_{on}[b] (V)	CE_{max} (cd/A)	PE_{max} (lm/W)	EQE_{max} (%)	at 100 cd/m^2		at 1000 cd/m^2	
					V (V)	EQE (%)	V (V)	EQE (%)
1	3.8	5.70	4.98	2.93	6.1	1.77	9.2	0.67
2	3.6	21.84	19.11	8.92	5.0	7.53	6.7	4.55

[a]The device structure is ITO/TAPC (25 nm)/CBP:**1** or **2** (1 wt %, 35 nm)/TmPyPB (55 nm)/LiF (1 nm)/Al. [b]At the luminance 1 cd/m^2.

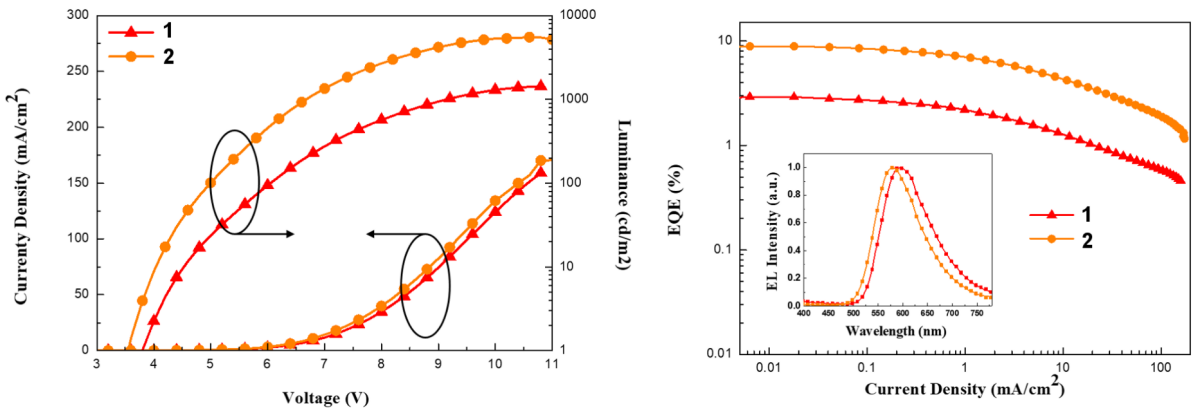


Figure 6: *J*–*V*–*L* (current density–voltage–luminance) (left) and EQE–current density characteristics of the devices (right). Inset: Electroluminescence spectra of the devices at a luminance of 1 cd m^{-2}.

21.84 cd/A, maximal power efficiency (PE_{max}) of 19.11 lm/W and maximal external quantum efficiency (EQE_{max}) of 8.92%, which is higher than the theoretical maximal external quantum efficiency of the OLEDs based on conventional fluorescent emitter. Meanwhile, the device based on **1** shows poor performance due to its low PLQY and nonobvious TADF behavior. Moreover, the efficiency roll-off of the device based on **2** was reduced compared with the **1**-based device. The EQE of the **2**-based device is still over half of its EQE_{max} at a brightness of 100 cd/m^2, while the EQE of **1** at the same brightness is only about 22% of its EQE_{max}. According to the previous study, triplet–triplet annihilation (TTA) might be the main cause of efficiency roll-off in the TADF-OLEDs when the triplet exciton concentration increases with brightness and current density [23,24]. The efficiency roll-off caused by the TTA process of TADF-OLEDs could be analyzed by the TTA model using Equation 5 [25,26] below:

$$\eta/\eta_0 = J_0 / 4J\left[\sqrt{1+8J/J_0}-1\right] \quad (5)$$

where η_0 represents the EQE without the influence of TTA, and J_0 represents the current density at the half maximum of the EQE; η and J represent the EQE with the influence of TTA and the corresponding current density, respectively. As shown in Figure 7, both devices show good agreement with the TTA model fitted curves at low current density because TTA process is the leading factor to the efficiency roll-off of TADF-OLEDs when the exciton concentration is low. With the increase of exciton concentration, singlet–triplet annihilation (STA), singlet–polaron annihilation (SPA) and triplet–polaron annihilation (TPA) may also have serious impact to the efficiency roll-off, which cause the TTA model fitted curves to deviate from the actual value. The device based on **2** shows a better agreement with the fitted curve in higher current density while the device based on **1** does not. In addition, **2** has a better triplet exciton utilization ability to reduce the efficiency roll-off, which comes to the same conclusion with the analysis of their photophysical properties.

Conclusion

In summary, two novel D–A–D-type orange-emitting TADF materials, namely 2,7-bis(9,9-dimethylacridin-10(9*H*)-yl)-9*H*-fluoren-9-one (27DACRFT, **1**) and 3,6-bis(9,9-dimethylacridin-10(9*H*)-yl)-9*H*-fluoren-9-one (36DACRFT, **2**), with the fluorenone unit as acceptor and the acridine as donor, were synthetized. Compounds **1** and **2** are isomers but show greatly different performance in terms of both photoluminescence and electroluminescence. It has been shown that the fluorenone unit is a promising acceptor for orange TADF materials, which aids

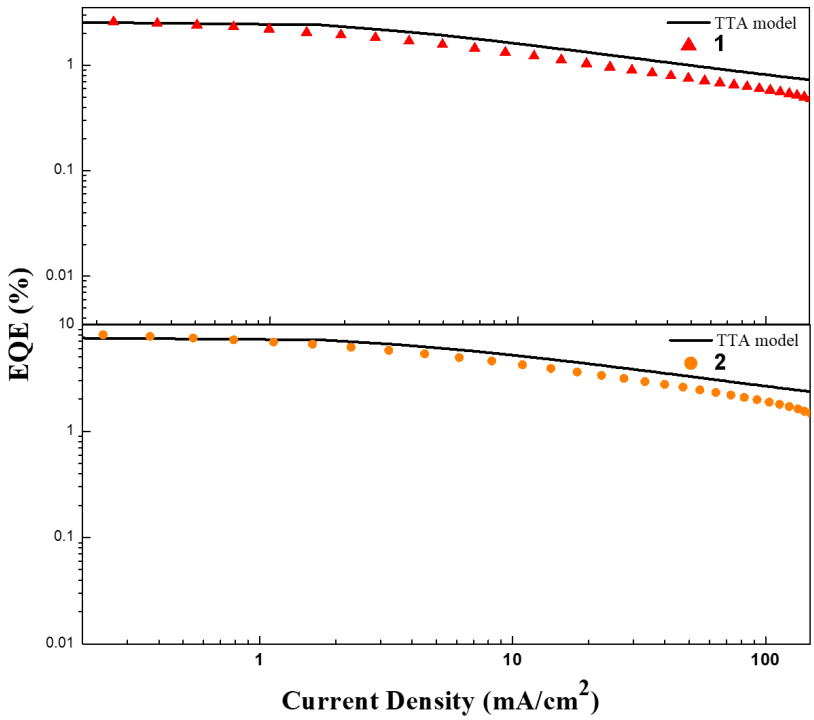


Figure 7: EQE–current density characteristics of the devices based on **1** (top) and **2** (bottom). The solid lines represent the simulated EQE by employing the TTA model.

in the design of the TADF behavior and luminescence color of **1** and **2**. Owing to the strong electron-withdrawing ability and extended conjugation length of fluorenone unit, the emission peaks of both materials show obvious red-shifts from other TADF materials based on carbonyl acceptor [27,28]. According to the DFT and TD-DFT simulation and photophysical characterization, **2** shows a smaller singlet–triplet energy difference (ΔE_{ST}) and a larger radiative rate constant (k_r) to give reduced internal conversion, promoted RISC process, and thus a better triplet exciton utilization ability. Maximum EQE values of 8.9% and 2.9% were achieved for the OLED devices based on **2** and **1**, respectively. Efficiency roll-off, which is considered to be the result of TTA, is also reduced more effectively for the OLEDs based on **2**.

Experimental

^{1}H and ^{13}C NMR spectra were measured on a Bruker NMR spectrometer with tetramethylsilane (TMS) as the internal standard. TGA and DSC measurements were performed on a Netzsch TG 209 and a Netzsch DSC 209 under N_2, respectively. A CHI600D electrochemical work station with a platinum working electrode and a platinum wire counter electrode at a scanning rate of 100 mV s^{-1} against a Ag/Ag^+ (0.1 M of $AgNO_3$ in acetonitrile) reference electrode were utilized for cyclic voltammetry measurements. UV–vis absorption spectra were measured using a HP 8453 spectrophotometer and PL and LTPL spectra were measured with a Jobin-Yvon spectrofluorometer. PLQY spectra were measured on a Hamamatsu absolute PL quantum yield spectrometer C11347. Transient PL spectra were measured with an Edinburgh FL920 fluorescence spectrophotometer. The current density–voltage–luminance characteristics of the OLED devices were measured with a Keithley 2420 and Konica Minolta chromameter CS-200. The EL spectra were measured with a Photo Research PR705 device.

Supporting Information

Supporting Information File 1

Experimental and additional information.
[https://www.beilstein-journals.org/bjoc/content/supplementary/1860-5397-14-55-S1.pdf]

Acknowledgements

The authors greatly appreciate financial support from the National Key R&D Program of China (2016YFB0401004), the National Natural Science Foundation of China (51625301, 51573059 and 91233116), 973 Project (2015CB655003), and Guangdong Provincial Department of Science and Technology (2016B090906003 and 2016TX03C175).

ORCID® iDs

Shi-Jian Su - https://orcid.org/0000-0002-6545-9002

References

1. Tang, C. W.; VanSlyke, S. A. *Appl. Phys. Lett.* **1987,** *51,* 913–915. doi:10.1063/1.98799
2. Baldo, M. A.; Brien, D. F.; You, Y.; Shoustikov, A.; Sibley, S.; Thompson, M. E.; Forrest, S. R. *Nature* **1998,** *395,* 151–154. doi:10.1038/25954
3. Ma, Y.; Zhang, H.; Shen, J.; Che, C. *Synth. Met.* **1998,** *94,* 245–248. doi:10.1016/S0379-6779(97)04166-0
4. Uoyama, H.; Goushi, K.; Shizu, K.; Nomura, H.; Adachi, C. *Nature* **2012,** *492,* 234–238. doi:10.1038/nature11687
5. Cai, X.; Li, X.; Xie, G.; He, Z.; Gao, K.; Liu, K.; Chen, D.; Cao, Y.; Su, S.-J. *Chem. Sci.* **2016,** *7,* 4264–4275. doi:10.1039/C6SC00542J
6. Cui, L.-S.; Nomura, H.; Geng, Y.; Kim, J. U.; Nakanotani, H.; Adachi, C. *Angew. Chem., Int. Ed.* **2017,** *56,* 1571–1575. doi:10.1002/anie.201609459
7. Zhang, Q.; Li, B.; Huang, S.; Nomura, H.; Tanaka, H.; Adachi, C. *Nat. Photonics* **2014,** *8,* 326–332. doi:10.1038/nphoton.2014.12
8. Yang, Z.; Mao, Z.; Xie, Z.; Zhang, Y.; Liu, S.; Zhao, J.; Xu, J.; Chi, Z.; Aldred, M. P. *Chem. Soc. Rev.* **2017,** *46,* 915–1016. doi:10.1039/C6CS00368K
9. Wong, M. Y.; Zysman-Colman, E. *Adv. Mater.* **2017,** *29,* 1605444.
10. Li, C.; Duan, R.; Liang, B.; Han, G.; Wang, S.; Ye, K.; Liu, Y.; Yi, Y.; Wang, Y. *Angew. Chem.* **2017,** *129,* 11683–11687. doi:10.1002/ange.201706464
11. Data, P.; Pander, P.; Okazaki, M.; Takeda, Y.; Minakata, S.; Monkman, A. P. *Angew. Chem., Int. Ed.* **2016,** *55,* 5739–5744. doi:10.1002/anie.201600113
12. Tsuboyama, A.; Iwawaki, H.; Furrgori, M.; Mukaide, T.; Kamatani, J.; Igawa, S.; Moriyama, T.; Miura, S.; Takiguchi, T.; Okada, S.; Hoshino, M.; Ueno, K. *J. Am. Chem. Soc.* **2003,** *125,* 12971–12979. doi:10.1021/ja034732d
13. Hatakeyama, T.; Shiren, K.; Nakajima, K.; Nomura, S.; Nakatsuka, S.; Kinoshita, K.; Ni, J.; Ono, Y.; Ikuta, T. *Adv. Mater.* **2016,** *28,* 2777–2781. doi:10.1002/adma.201505491
14. Endo, A.; Sato, K.; Yoshimura, K.; Kai, T.; Kawada, A.; Miyazaki, H.; Adachi, C. *Appl. Phys. Lett.* **2011,** *98,* 083302. doi:10.1063/1.3558906
15. Li, J.; Zhang, Q.; Nomura, H.; Miyazaki, H.; Adachi, C. *Appl. Phys. Lett.* **2014,** *105,* 013301. doi:10.1063/1.4887346
16. Zhang, Q.; Kuwabara, H.; Potscavage, W. J., Jr.; Huang, S.; Hatae, Y.; Shibata, T.; Adachi, C. *J. Am. Chem. Soc.* **2014,** *136,* 18070–18081. doi:10.1021/ja510144h
17. Li, Y.; Li, X.-L.; Chen, D.; Cai, X.; Xie, G.; He, Z.; Wu, Y.-C.; Lien, A.; Cao, Y.; Su, S.-J. *Adv. Funct. Mater.* **2016,** *26,* 6904–6912. doi:10.1002/adfm.201602507
18. Cai, X.; Chen, D.; Gao, K.; Gan, L.; Yin, Q.; Qiao, Z.; Chen, Z.; Jiang, X.; Su, S.-J. *Adv. Funct. Mater.* **2018,** *28,* 1704927. doi:10.1002/adfm.201704927
19. Pan, K.-C.; Li, S.-W.; Ho, Y.-Y.; Shiu, Y.-J.; Tsai, W.-L.; Jiao, M.; Lee, W.-K.; Wu, C.-C.; Chung, C.-L.; Chatterjee, T.; Li, Y.-S.; Wong, K.-T.; Hu, H.-C.; Chen, C.-C.; Lee, M.-T. *Adv. Funct. Mater.* **2016,** *26,* 7560–7571. doi:10.1002/adfm.201602501
20. Cai, X.; Gao, B.; Li, X.-L.; Cao, Y.; Su, S.-J. *Adv. Funct. Mater.* **2016,** *26,* 8042–8052. doi:10.1002/adfm.201603520
21. Liu, W.; Zheng, C.-J.; Wang, K.; Chen, Z.; Chen, D.-Y.; Li, F.; Ou, X.-M.; Dong, Y.-P.; Zhang, X.-H. *ACS Appl. Mater. Interfaces* **2015,** *7,* 18930–18936. doi:10.1021/acsami.5b05648

22. Su, S.-J.; Chiba, T.; Takeda, T.; Kido, J. *Adv. Mater.* **2008,** *20,* 2125–2130. doi:10.1002/adma.200701730
23. Murawski, C.; Leo, K.; Gather, M. C. *Adv. Mater.* **2013,** *25,* 6801–6827. doi:10.1002/adma.201301603
24. Zhao, H.; Wang, Z.; Cai, X.; Liu, K.; He, Z.; Liu, X.; Cao, Y.; Su, S.-J. *Mater. Chem. Front.* **2017,** *1,* 2039–2046. doi:10.1039/C7QM00195A
25. Baldo, M. A.; Forrest, S. R. *Phys. Rev. B* **2000,** *62,* 10958–10966. doi:10.1103/PhysRevB.62.10958
26. Xie, G.; Li, X.; Chen, D.; Wang, Z.; Cai, X.; Chen, D.; Li, Y.; Liu, K.; Cao, Y.; Su, S.-J. *Adv. Mater.* **2016,** *28,* 181–187. doi:10.1002/adma.201503225
27. Rajamalli, P.; Senthilkumar, N.; Huang, P.-Y.; Ren-Wu, C.-C.; Lin, H.-W.; Cheng, C.-H. *J. Am. Chem. Soc.* **2017,** *139,* 10948–10951. doi:10.1021/jacs.7b03848
28. Rajamlli, P.; Thangaraji, V.; Senthilkumar, N.; Ren-Wu, C.-C.; Lin, H.-W.; Cheng, C.-H. *J. Mater. Chem. C* **2017,** *5,* 2919–2926. doi:10.1039/C7TC00457E

License and Terms

This is an Open Access article under the terms of the Creative Commons Attribution License (http://creativecommons.org/licenses/by/4.0), which permits unrestricted use, distribution, and reproduction in any medium, provided the original work is properly cited.

The license is subject to the *Beilstein Journal of Organic Chemistry* terms and conditions: (https://www.beilstein-journals.org/bjoc)

The definitive version of this article is the electronic one which can be found at: doi:10.3762/bjoc.14.55

BEILSTEIN JOURNAL OF ORGANIC CHEMISTRY

Two novel blue phosphorescent host materials containing phenothiazine-5,5-dioxide structure derivatives

Feng-Ming Xie[1,2], Qingdong Ou[3], Qiang Zhang[1,2], Jiang-Kun Zhang[1,2], Guo-Liang Dai[1,2], Xin Zhao[*1,2] and Huai-Xin Wei[*1,2]

Full Research Paper

Open Access

Address:
[1]College of Chemistry, Biology and Material Engineering, Suzhou University of Science and Technology, Suzhou, Jiangsu 215009, P.R. China, [2]Jiangsu Key Laboratory of Environmental Functional Materials, Suzhou, Jiangsu 215009, P.R. China and [3]Department of Materials Science and Engineering, Monash University, Clayton, Victoria 3800, Australia

Email:
Xin Zhao[*] - zhaoxinsz@126.com; Huai-Xin Wei[*] - hxwei@usts.edu.cn

* Corresponding author

Keywords:
host materials; phenothiazine; phosphorescence; synthesis

Beilstein J. Org. Chem. **2018,** *14,* 869–874.
doi:10.3762/bjoc.14.73

Received: 12 November 2017
Accepted: 03 April 2018
Published: 17 April 2018

This article is part of the Thematic Series "Recent advances in materials for organic light emitting diodes".

Guest Editor: E. Zysman-Colman

© 2018 Xie et al.; licensee Beilstein-Institut.
License and terms: see end of document.

Abstract

Two novel D–A bipolar blue phosphorescent host materials based on phenothiazine-5,5-dioxide: 3-(9*H*-carbazol-9-yl)-10-ethyl-10*H*-phenothiazine-5,5-dioxide (CEPDO) and 10-butyl-3-(9*H*-carbazol-9-yl)-10*H*-phenothiazine-5,5-dioxide (CBPDO) were synthesized and characterized. The photophysical, electrochemical and thermal properties were systematically investigated. CEPDO and CBPDO not only have a high triplet energy but also show a bipolar behavior. Moreover, their fluorescence emission peaks are in the blue fluorescence region at 408 nm and the fluorescence quantum efficiency (Φ) of CEPDO and CBPDO were 62.5% and 59.7%, respectively. Both CEPDO and CBPDO showed very high thermal stability with decomposition temperatures (T_d) of 409 and 396 °C as well as suitable HOMO and LUMO energy levels. This preferable performance suggests that CEPDO and CBPDO are alternative bipolar host materials for the PhOLEDs.

Introduction

Since 1987, the Tang group [1] firstly reported double organic light-emitting diodes (OLEDs) with ultra-thin film by using vacuum evaporation technology. It has attracted much attention to develop it. In recent years, OLEDs have been rapidly developed and widely used in lighting and display because of many unique performance advantages such as wide viewing angle (≥170°), fast response (1 μs scale), high luminous efficiency, low drive voltage (3–10 V), thickness (less than 2 mm), lightweightness and flexibility [2-6]. Compared with traditional fluorescence OLEDs which only utilize singlet (25%) excitons for electroluminescence, PhOLEDs can simultaneously harvest both the singlet and triplet (75%) excitons through spin-orbit

coupling (SOC), and obtain nearly 100% of the internal quantum efficiency (IQE). Thus, most of researchers have focused on phosphorescent organic light-emitting diodes (PhOLEDs) all over the world [7,8]. With the deepening of this research, the performance of red and green electroluminescent devices has been able to meet the commercial requirements, but the blue electroluminescent devices have several weaknesses such as low efficiency and poor stability and so on, which hinder its development. It has been proved that the selection of proper materials for each layer is very important for achieving highly efficient PhOLEDs. In particular, the design of host materials plays a critical role in the determination of the devices performance. Therefore, it is beneficial to develop new blue phosphorescent host materials with high-performance for blue PhOLEDs [9-12].

Generally, ideal host materials are required to fulfill several requirements [13,14]: i) the triplet energy level (E_T) should be higher for efficient energy transfer to the guest; ii) suitable energy levels appropriately aligned with those of the neighboring active layers for efficient charge carrier injection to achieve a low operating voltage; iii) good and balanced charge carrier transport properties for the hole–electron recombination process; iv) good thermal and morphological stability for the vacuum deposition method to prolong the device operational lifetime.

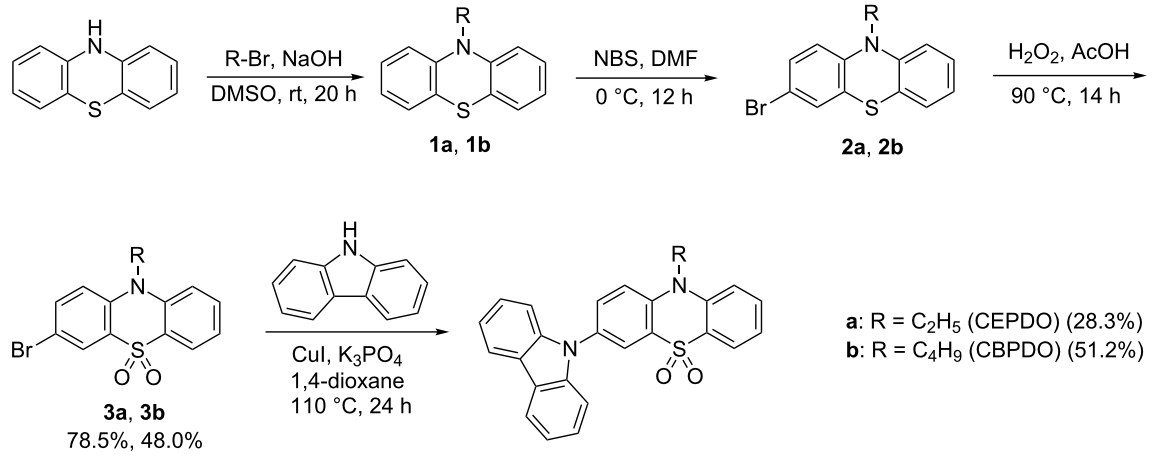
Carbazole groups are widely used in host materials because of their high triplet energy levels and high hole mobility [15]. The Lee group [16] linked carbazolyl groups to diphenyl phosphoramines to design asymmetric (9-phenyl-9*H*-carbazole-2,5-diyl)bis(diphenylphosphine oxide) (PCPOs) with a higher triplet energy level (2.80 eV) and a glass transition temperature (140 °C). The maximum external quantum efficiency (EQE) of PhOLEDs was 31.4%, which was prepared by PCPO as a bipolar host material. Kim et al. [17] reported that the bipolar host material 9-(4-(9*H*-pyrido[2,3-*b*]indol-9-yl)phenyl)-9*H*-3,9'-bicarbazole (pBCb2Cz) has a high triplet energy level (2.93 eV), which is the main material of blue PhOLEDs, and the EQE of the device is 23.0%. The Suh group [18] reported that the EQE of the prepared device of the bipolar host material *N*-(3,5-di(9*H*-carbazol-9-yl)phenyl)-*N*-(pyridin-2-yl)pyridin-2-amine (DCPPy) based on carbazole group is 21.6%. The Wang group [19] designed a host material with symmetrical structure based on phenothiazine-5,5-dioxide. But the host materials with asymmetric structure based on the phenothiazine-5,5-dioxide were rarely reported. For obtaining a high triplet energy level and good stability, herein, with phenothiazine-5,5-dioxide as acceptor (A) and carbazole as donor (D), and introducing an alkane chain group to the host materials for better film-forming properties, two novel blue phosphorescent host materials, CEPDO and CBPDO, were synthesized. At the same time, the photophysical properties, electrochemical properties and their thermal stability were studied and the expected results were obtained.

Results and Discussion

Synthesis and theoretical calculations

The synthesis route for CEPDO and CBPDO is shown in Scheme 1. The detailed synthesis procedures and characterizations are given in Supporting Information File 1.

In order to further understand the structural properties of the materials and the possibility of charge transfer from donor to acceptor on electronic excitation, the electronic structure of the materials were analyzed by density functional theoretical (DFT) calculations using the Gaussian 09 program package. The electron density distributions and energy levels of the HOMO and LUMO are displayed in Figure 1.



Scheme 1: Synthetic routes of CEPDO and CBPDO.

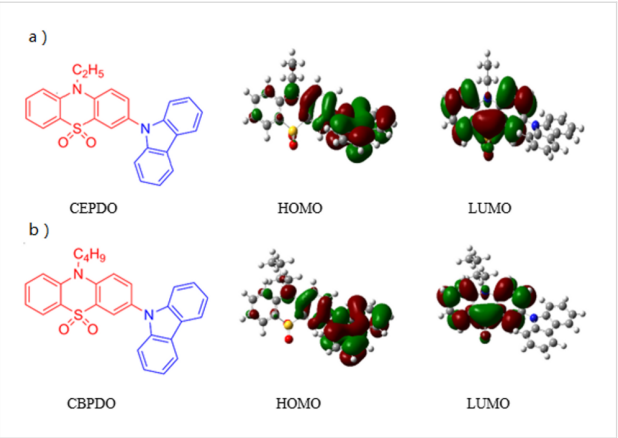


Figure 1: Structures and molecular orbitals of (a) CEPDO and (b) CBPDO.

The HOMOs of CEPDO and CBPDO are mainly distributed over the electron-donating carbazole moiety and slightly extended to the phenyl ring. The LUMOs are mostly localized on the phenothiazine-5,5-dioxide, based on the DFT calculation. There is a small degree of spatial overlap between the HOMO and LUMO in these two molecules. The separated HOMO and LUMO resulted from the strong electron-donating nature of the carbazole unit and electron-withdrawing ability of the phenothiazine-5,5-dioxide unit, thus realized the orbital separation of hole and electron transport in the same molecule. This indicated CEPDO and CBPDO have bipolar characteristic.

Photophysical properties

Figure 2 presents the UV–vis absorption, photoluminescence and phosphorescence (77 K) spectra of CEPDO (a) and CBPDO (b) in solution, respectively. Obviously, the strong absorption peak at 236 nm can be ascribed to the π→π* transition of carbazole moiety of the molecules, and the weaker absorptions around 295 nm assign to the n→π* transition of the conjugation of the whole molecule.

The optical bandgap (E_g) of the two substances were all calculated to be 3.32 eV from the UV–vis absorption spectra of CEPDO and CBPDO. Upon photoexcitation of 330 nm at room temperature, both CEPDO and CBPDO exhibited a FL spectrum with peaks at 408 nm and emitted blue fluorescence. The fluorescence quantum efficiencies (Φ) of CEPDO and CBPDO were 62.5% and 59.7%, respectively, by using quinine sulfate as a reference [20]. Compared with CEPDO, the longer alkyl chain of CBPDO led to a corresponding increase in Φ value. Therefore, CEPDO and CBPDO are promising photoelectric materials. To obtain the triplet energy level, their low-temperature Phos spectra were measured in a 2-methyltetrahydrofuran solution at 77 K which are also shown in Figure 2. The phosphorescence emission peaks were at 440 nm and 439 nm, respectively. According to the onset of their phosphorescence spectra, the calculated triplet energy levels (E_T) of CEPDO and CBPDO were identical at 2.82 eV, which matched with the blue phosphorescent guest material FIrpic (2.65 eV), dark blue phosphorescent guest material FCNIrpic (2.74 eV) and FIr6 (2.73 eV). The high E_T was attributed to the insulated carbazole moieties. Hence, both CEPDO and CBPDO are expected to be applied to PhOLED as a blue phosphorescent host material.

Electrochemical properties

The electrochemical properties of CEPDO and CBPDO were studied by cyclic voltammetry (CV) measurements in deoxygenated DCM solution with 0.1 M tetrabutylammonium hexafluorophosphate as the supporting electrolyte. The cyclic voltammograms are shown in Figure 3.

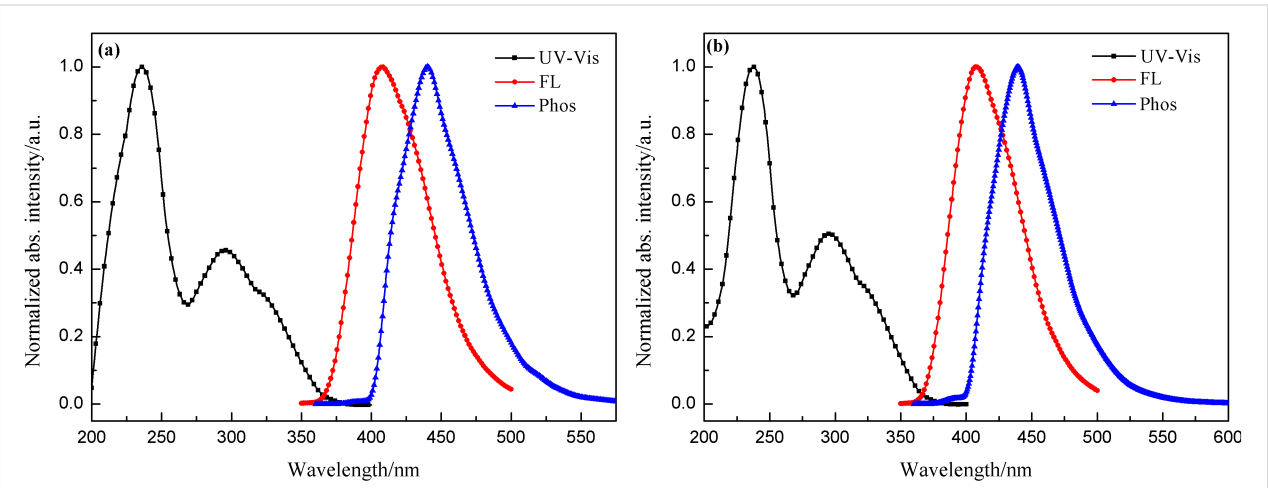


Figure 2: UV–vis absorption and photoluminescence spectra in DCM solution (1×10^{-5} M and 1×10^{-6} M, respectively) at room temperature, phosphorescence spectra in 2-MeTHF solution (1×10^{-3} M) at 77 K of CEPDO (a) and CBPDO (b).

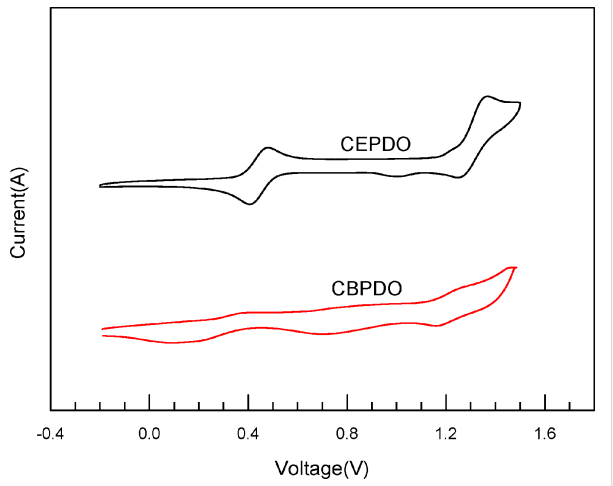


Figure 3: Cyclic voltammograms for CEPDO and CBPDO in DCM solution.

Cyclic voltammetry was measured with a glassy carbon working electrode, a platinum wire counter electrode, a saturated Ag/AgCl reference electrode, ferrocenium-ferrocene (Fc^+/Fc) as the internal standard and tetrabutylammonium hexafluorophosphate (0.1 M) as the supporting electrolyte.

The onset potential (E^{onset}_{ox}) of the first oxidation wave for CEPDO and CBPDO are utilized to estimate the HOMO energy level according to the equation $E_{HOMO} = -e(E^{onset}_{ox} + 4.8)$ as ca. −5.63 and −5.64 eV, respectively. And both HOMO energy levels are matched with the functional function of the anode ITO (−4.5 to −5.0 eV). The LUMO energy levels of CEPDO and CBPDO are estimated from the half-potential to be −2.31 eV and −2.32 eV, respectively, which are matched with the LUMO energy level of electron injection material TAZ and favorable for electron injection and transmission [21]. Therefore, we successfully synthesized two novel bipolar host materials with higher triplet energy by choosing suitable donor and acceptor units.

Thermal properties

The thermal properties of CEPDO and CBPDO were determined by thermogravimetric analysis (TGA) and differential scanning calorimetry (DSC) under nitrogen atmosphere at a scanning rate of 10 °C/min and the results are shown in Figure 4. Both CEPDO and CBPDO show very high thermal stability with decomposition temperatures (T_d) of 409 and 396 °C and glass transition temperatures (T_g) of 167 and 138 °C, respectively. Compared to the introduction of ethyl groups, the introduction of normal butyl groups to the phenothiazine-5,5-dioxide moieties appears to decrease the T_d and T_g of CEPDO by 13 °C and 29 °C, respectively, relative to those of CBPDO. The reason may be the *n*-butyl chain is longer. It reduces the polarity and intermolecular forces of molecules. The high thermal values ensure high thermostability and that the amorphous structure can form homogeneous and stable films by vacuum deposition to improve the lifetime of the PhOLEDs. The photophysics, electrochemical and thermal properties of CEPDO and CBPDO are summarized in Table 1.

Conclusion

In summary, we have designed and synthesized two bipolar host materials CEPDO and CBPDO. CEPDO and CBPDO not only have a high triplet energy but also show a bipolar behavior. Moreover, their fluorescence emission peaks are blue fluorescence at 408 nm and the fluorescence quantum efficiency (Φ) of CEPDO and CBPDO are 62.5% and 59.7%, respectively. Both CEPDO and CBPDO show very high thermal stability with T_d of 409 and 396 °C, T_g of 167 and 138 °C, respectively, and also appear suitable HOMO and LUMO energy levels. Hence,

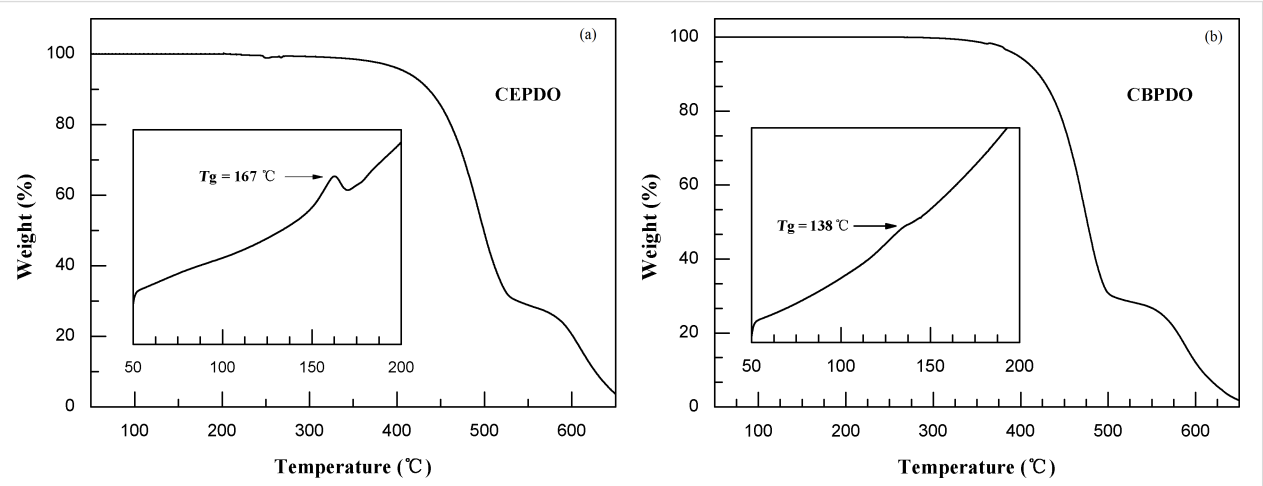


Figure 4: DSC and TGA curves of CEPDO and CBPDO.

Table 1: Photophysics, electrochemical and thermal properties of CEPDO and CBPDO.

compound	λ_{abs}[a] /nm	λ_{onset}[b] /nm	λ_{emt}[c] /nm	λ_{phos}[d] /nm	Φ[e] /%	E_{onset}[f] /eV	E_g[g] /eV	E_t[h] /eV	$E_{HOMO/LUMO}$[i] /eV	$T_{d/g}$[j] /°C
CEPDO	236	373	408	440	49	1.23	3.32	2.82	−5.63/−2.31	409/167
CBPDO	236	372	408	439	69	1.24	3.32	2.82	−5.64/−2.32	396/138

[a]The absorption maximum of the UV–vis spectrum; [b]estimated from the onset of the UV–vis spectrum; [c]emission fluorescence maximum at room temperature; [d]phosphorescence emission peak at 77 K; [e]fluorescence quantum yield; [f]first oxidation peak potential; [g]$E_g = 1240/\lambda_{onset}$; [h]$E_T = 1240/\lambda_{phos}$; [i]$E_{HOMO}$: measured from the oxidation potential in 10^{-3} M DCM solution by cyclic voltammetry, $E_{LUMO} = E_g + E_{HOMO}$; [j]decomposition temperature (T_d) with 5% loss, glass transition temperature (T_g).

CEPDO and CBPDO are two promising blue phosphorescent host materials for PhOLEDs.

Supporting Information

Supporting Information File 1

Experimental part and copies of NMR spectra.
[https://www.beilstein-journals.org/bjoc/content/supplementary/1860-5397-14-73-S1.pdf]

Acknowledgements

We acknowledge financial supports from the National Natural Science Foundation of China (No. 61705154), the Project of natural science Foundation of the Jiangsu Higher Education Institutions, (No. 17KJB140022); Suzhou University of Science and Technology (No. 331512301), the Natural Science Foundation of Jiangsu Province (No. BK20150282), Applied Basic Research Project of Suzhou (No. SYG201440), Graduate Research and Innovation Project of Jiangsu Province (SKCX16_060).

ORCID® iDs

Qiang Zhang - https://orcid.org/0000-0002-8173-8722

References

1. Tang, C. W.; VanSlyke, S. A. *Appl. Phys. Lett.* **1987,** *51,* 913–915. doi:10.1063/1.98799
2. Rajamalli, P.; Senthilkumar, N.; Gandeepan, P.; Huang, P.-Y.; Huang, M.-J.; Ren-Wu, C.-Z.; Yang, C.-Y.; Chiu, M.-J.; Chu, L.-K.; Lin, H.-W.; Cheng, C.-H. *J. Am. Chem. Soc.* **2016,** *138,* 628–634. doi:10.1021/jacs.5b10950
3. Baldo, M. A.; O'Brien, D. F.; You, Y.; Shoustikov, A.; Sibley, S.; Thompson, M. E.; Forrest, S. R. *Nature* **1998,** *395,* 151–154. doi:10.1038/25954
4. Lin, T.; Zhang, T.; Song, Q.; Jin, F.; Liu, Z.; Su, Z.; Luo, Y.; Chu, B.; Lee, C. S.; Li, W. *Org. Electron.* **2016,** *38,* 69–73. doi:10.1016/j.orgel.2016.08.001
5. Kim, K.-H.; Yoo, S.-J.; Kim, J.-J. *Chem. Mater.* **2016,** *28,* 1936–1941. doi:10.1021/acs.chemmater.6b00478
6. Feng, M. Q.; Tang, J. X.; Liao, L. S. *Imaging Sci. Photochem.* **2017,** *35,* 26–33.
7. Dos Santos, P. L.; Ward, J. S.; Bryce, M. R.; Monkman, A. P. *J. Phys. Chem. Lett.* **2016,** *7,* 3341–3346. doi:10.1021/acs.jpclett.6b01542
8. Wang, F.; Tao, Y.; Huang, W. *Acta Chim. Sin.* **2015,** *73,* 9–22. doi:10.6023/A14100716
9. Xiao, L.; Chen, Z.; Qu, B.; Luo, J.; Kong, S.; Gong, Q.; Kido, J. *Adv. Mater.* **2011,** *23,* 926–952. doi:10.1002/adma.201003128
10. Seino, Y.; Sasabe, H.; Pu, Y.-J.; Kido, J. *Adv. Mater.* **2014,** *26,* 1612–1616. doi:10.1002/adma.201304253
11. Tao, Y.; Yang, C.; Qin, J. *Chem. Soc. Rev.* **2011,** *40,* 2943–2970. doi:10.1039/c0cs00160k
12. Chaskar, A.; Chen, H.-F.; Wong, K.-T. *Adv. Mater.* **2011,** *23,* 3876–3895. doi:10.1002/adma.201101848
13. Zhao, Z.; Yu, G.; Chang, Q.; Liu, X.; Liu, Y.; Wang, L.; Liu, Z.; Bian, Z.; Liu, W.; Huang, C. *J. Mater. Chem. C* **2017,** *5,* 7344–7351. doi:10.1039/C7TC01594A
14. Sun, Q.; Cui, L.-S.; Xie, Y.-M.; Liang, J.-J.; Jiang, Z.-q.; Liao, L.-s.; Fung, M.-K. *Org. Electron.* **2017,** *48,* 112–117. doi:10.1016/j.orgel.2017.05.034
15. Baryshnikov, G. V.; Bondarchuk, S. V.; Minaeva, V. A.; Ågren, H.; Minaev, B. F. *J. Mol. Model.* **2017,** *23,* 55. doi:10.1007/s00894-017-3234-y
16. Kim, M.; Lee, J. Y. *Adv. Funct. Mater.* **2014,** *24,* 4164–4169. doi:10.1002/adfm.201304072
17. Kim, S. J.; Kim, Y. J.; Son, Y. H.; Hur, J. A.; Um, H. A.; Shin, J.; Lee, T. W.; Cho, M. J.; Kim, J. K.; Joo, S.; Yang, J. H.; Chae, G. S.; Choi, K.; Kwon, J. H.; Choi, D. H. *Chem. Commun.* **2013,** *49,* 6788–6790. doi:10.1039/c3cc42569j
18. Park, S.-R.; Kim, S.-M.; Kang, J.-H.; Lee, J.-H.; Suh, M. C. *Dyes Pigm.* **2017,** *141,* 217–224. doi:10.1016/j.dyepig.2017.02.014
19. Zheng, Y.; Xie, Q.; Wang, B. *Chin. J. Org. Chem.* **2015,** *36,* 803–811.
20. Yang, X.; Pan, Z. T.; Ma, Y. J. *Anal. Sci.* **2003,** *16,* 588–589.
21. Li, J.; Zhang, Z.; Han, C.; Ding, D.; Zhao, Y.; Huang, W.; Xu, H. *J. Mater. Chem. C* **2015,** *3,* 6709–6716. doi:10.1039/C5TC01179E

License and Terms

This is an Open Access article under the terms of the Creative Commons Attribution License (http://creativecommons.org/licenses/by/4.0), which permits unrestricted use, distribution, and reproduction in any medium, provided the original work is properly cited.

The license is subject to the *Beilstein Journal of Organic Chemistry* terms and conditions: (https://www.beilstein-journals.org/bjoc)

The definitive version of this article is the electronic one which can be found at: doi:10.3762/bjoc.14.73

BEILSTEIN JOURNAL OF ORGANIC CHEMISTRY

Recent advances in phosphorescent platinum complexes for organic light-emitting diodes

Cristina Cebrián*[1] and Matteo Mauro*[2]

Review

Open Access

Address:
[1]Université de Lorraine, CNRS, L2CM, F-57000 Metz, France and [2]Université de Strasbourg, CNRS – Institut de Physique et Chimie des Matériaux de Strasbourg (IPCMS), UMR 7504, 23 rue du Loess, F-67000 Strasbourg, France

Email:
Cristina Cebrián* - cristina.cebrian-avila@univ-lorraine.fr;
Matteo Mauro* - mauro@unistra.fr

* Corresponding author

Keywords:
cyclometalating ligands; electroluminescence; OLED; phosphorescence; platinum complexes

Beilstein J. Org. Chem. **2018,** *14,* 1459–1481.
doi:10.3762/bjoc.14.124

Received: 19 January 2018
Accepted: 23 May 2018
Published: 18 June 2018

This article is part of the Thematic Series "Recent advances in materials for organic light emitting diodes".

Guest Editor: E. Zysman-Colman

© 2018 Cebrián and Mauro; licensee Beilstein-Institut.
License and terms: see end of document.

Abstract

Phosphorescent organometallic compounds based on heavy transition metal complexes (TMCs) are an appealing research topic of enormous current interest. Amongst all different fields in which they found valuable application, development of emitting materials based on TMCs have become crucial for electroluminescent devices such as phosphorescent organic light-emitting diodes (PhOLEDs) and light-emitting electrochemical cells (LEECs). This interest is driven by the fact that luminescent TMCs with long-lived excited state lifetimes are able to efficiently harvest both singlet and triplet electro-generated excitons, thus opening the possibility to achieve theoretically 100% internal quantum efficiency in such devices. In the recent past, various classes of compounds have been reported, possessing a beautiful structural variety that allowed to nicely obtain efficient photo- and electroluminescence with high colour purity in the red, green and blue (RGB) portions of the visible spectrum. In addition, achievement of efficient emission beyond such range towards ultraviolet (UV) and near infrared (NIR) regions was also challenged. By employing TMCs as triplet emitters in OLEDs, remarkably high device performances were demonstrated, with square planar platinum(II) complexes bearing π-conjugated chromophoric ligands playing a key role in such respect. In this contribution, the most recent and promising trends in the field of phosphorescent platinum complexes will be reviewed and discussed. In particular, the importance of proper molecular design that underpins the successful achievement of improved photophysical features and enhanced device performances will be highlighted. Special emphasis will be devoted to those recent systems that have been employed as triplet emitters in efficient PhOLEDs.

Introduction

Photoactive TMCs have attracted enormous attention in the last two decades because of their peculiar photophysical and rich redox properties, which make them appealing from both fundamental research and technological applications points of view. Nowadays, several research groups have devoted much effort in exploring a large variety of classes of luminescent TMCs with closed-shell d^6, d^8 and d^{10} electronic configurations [1-5]. The concomitant presence of a heavy metal ion and coordinated π-conjugated chromophoric ligands enriches the photophysical features displayed by TMCs when compared to classical organic luminophors. Indeed, apart from ligand centred (LC) and intraligand charge transfer (ILCT) states, admixing of the metal and ligand orbitals close to the frontier region results in excited states featuring a certain degree of metal contribution. In particular, metal-to-ligand charge transfer (MLCT), ligand-to-metal charge transfer (LMCT), ligand-to-ligand charge transfer (LLCT) and metal centred (MC) states actively contribute to the richer photophysical and photochemical features of TMCs and to their resulting properties, also in terms of electrochemistry. Additionally, the presence of a heavy metal atom induces spin-orbit coupling (SOC) effects to such an extent that intersystem crossing (ISC) processes become thus competitive over other radiationless deactivation pathways owing to relaxation of spin rules. In this way, long-lived and low energy lying excited states with triplet (T_n states) character are accessible and can be efficiently populated. The subsequent deactivation from the lowest lying T_1 state into the electronic ground state (S_0) through radiative channels, $T_1 \rightarrow S_0$, occurs with decay kinetics between hundreds of nanoseconds to several microseconds, constituting a formally spin-forbidden transition (phosphorescence). Structural modification of the TMCs and proper tailoring of coordinated ligands can independently act on the nature, energy and topology of frontier orbitals. In fact, a fine modulation is achieved through a precise energetic positioning and mixing of different excited states, as well as tuning of the energetic band gap between S_0 and the lower-lying singlet and triplet manifold excited states. This approach did successfully yield phosphorescent TMCs with an emission wavelength tuneable over the entire visible spectrum and beyond; together with compounds with photoluminescence quantum yield (PLQY) approaching unity. These peculiar features have greatly fuelled the still growing interest in luminescent TMCs for its potential employment in applications and real-market technology including photocatalysis [6], bio-imaging [7,8], and solar-energy conversion [9], just to cite a few.

Thompson and Forrest reported in 1998 on the first example of a phosphorescent emitter, namely 2,3,7,8,12,13,17,18-octaethyl-21*H*,23*H*-porphyrin platinum(II) (Pt(OEP)), used as dopant for the fabrication of an efficient (external quantum efficiency, EQE, ca. 4%) OLED device [10]. Since that pioneering work, an impressive amount of research effort has been devoted in the last two decades to seeking for TMCs that display better device performances. In this respect, iridium(III) and platinum(II) derivatives undoubtedly play leading roles as electro-active materials in light-emitting devices. Their outstanding photophysical and electrochemical features enabled fabrication of PhOLEDs and LEECs [11] with enhanced device performances in terms of efficiency, operating lifetime and colour purity. In electrophosphorescent devices, the triplet nature of excited states localized on the active TMCs allows harvesting of both singlet and triplet electro-generated excitons through either direct trapping or energy transfer processes. As a consequence, the theoretical internal quantum efficiency rises from 25%, which corresponds to purely fluorescent-based devices from a first approximation spin statistics, up to 100%. Nonetheless, EQEs are typically upper limited to values of ca. 20–25% owing to differences in the refractive index of organic materials commonly employed and suboptimal light outcoupling. In spite of that, highly performing vacuum-processed devices with record EQEs up to 54% have been reported to date for PhOLEDs based on Ir(III) with optimized light outcoupling [12]. On the other hand, an impressive EQE value as high as 38.8% [13] and 55% [14] have been recently achieved in platinum(II)-based OLEDs without and with outcoupling elements, respectively, via engineering of transition dipole moment orientation in the device active matrix.

Owing to the enormous interest they are currently attracting, the scope of the present review article is to highlight the current trends and achievements in the field of phosphorescent platinum complexes for PhOLEDs with a special emphasis on the most recent advances. It should be noted that this contribution is not indented to be comprehensive and readers are invited to refer elsewhere for previous examples of platinum emitters [15-18]. In particular, we will focus our attention on recently reported Pt(II) complexes by breaking down the different classes into those containing monodentate, bidentate, tridentate and tetradentate chromophoric ligands, in order to put in context and compare their photophysical and electroluminescent properties. Finally, some very recent and interesting examples of Pt(IV) compounds as triplet emitters in OLEDs, a class of compound that has been much less explored, will also be reviewed. PhOLED performances of devices comprising the examples reviewed herein are summarised in Table 1.

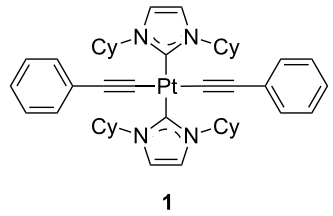
Review

Platinum(II) complexes

Platinum complexes bearing mono-dentate ligands

Platinum(II) complexes bearing monodentate ligands are likely to have very poor luminescent properties. In these complexes,

the molecular flexibility as a consequence of the low denticity favors efficient thermal deactivation via MC excited states and other nonradiative relaxation pathways. Schanze and co-workers have demonstrated, however, that it is possible to obtain satisfactory photo- and electroluminescence from *trans*-platinum(II) complex **1** bearing only monodentate ligands (Figure 1) [19]. In this derivative, the MC states were efficiently destabilized by selecting strong σ-donating NHC and –C≡C–R ligands. The presence of the two bulky cyclohexyl substituents on the imidazolylidene moiety contributed to rigidify the structure, as well as avoid detrimental intermolecular interactions. Though being weakly emissive in THF solution, the compound exhibited a narrow deep blue photoluminescence (CIE = 0.14, 0.12) with a PLQY of 0.30 in PMMA films. Multilayer vacuum-processed OLEDs were fabricated to test the electroluminescence performance of this complex. A remarkable value of 8% of EQE was attained, but a severe roll-off efficiency was observed with an EQE value dropping to 2% at a practical brightness of 500 cd m^{-2}. Nevertheless, this work opens the door for a novel design of highly efficient deep-blue phosphors.



1

Figure 1: Molecular structure of neutral platinum(II) complex **1** bearing four monodentate ligands; cy = cyclohexyl [19].

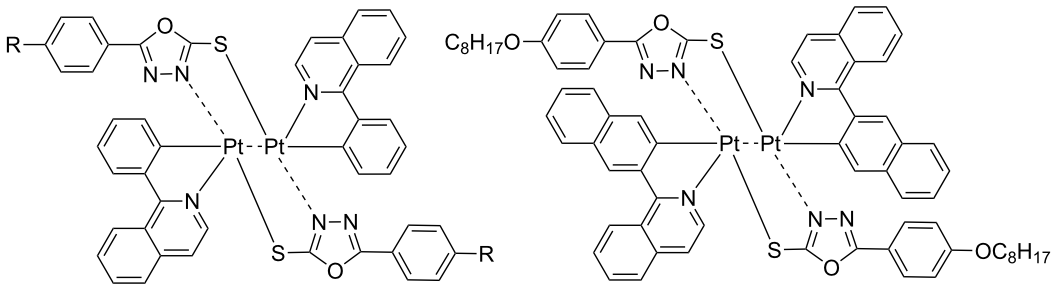
More complex structures based on dinuclear platinum(II) complexes have also been recently described [20]. Upon using two 1,3,4-oxadiazole-2-thiol as bridging ligands coordinating two Pt(II) centers in a monodentate fashion, Zhu and co-workers have reported on dimeric structures, namely **2** and **3**, exhibiting an interaction between the two metallic centres (Pt···Pt distance of ca. 3 Å) (Figure 2). The appearance of a triplet metal–metal-to-ligand charge transfer (^{3}MMLCT) transition led to NIR emission with PLQY of ca. 0.31. These bimetallic compounds were tested as dopants in solution-processed PLED, achieving EQE values up to 5.2% at 100 mA cm^{-2}, even though with relatively high turn-on voltages of 10.4–14.6 V. However, molecular aggregation was observed at dopant concentrations above 12 wt %.

Although (hetero-)metallic clusters are beyond the scope of this review, it is worth to mention some recent reports from Chen and co-workers on trimetallic systems based on $PtAu_2$ [21,22] and $PtAg_2$ [23,24] core. Motivated by very high PLQYs in doped films, OLED devices were fabricated showing remarkable efficiency attaining EQE of 21.5% at a luminance of 1029 cd m^{-2} with small roll-off [21]. These performances are the best reported so far for such a practical luminance.

Systems based on bidentate ligands

In the past, the most common synthetic strategy to obtain luminescent platinum(II) complexes has been the use of π-conjugated chelating ligands with a bidentate motif bearing π-accepting (hetero)aromatic units. Compared to monodentate ligands, the more rigid structure of the bidentate motif is expected to reduce excited-state molecular distortion and access to quenching channels to some extent. On the other hand, the appearance of new low-lying excited states associated to the π molecular orbitals typically results into efficient emission due to their larger radiative decay rates [25].

Though limited in the 1980s by their sensitive synthesis via lithiated species, archetypical luminescent platinum(II) complexes were based on 2-phenylpyridine (ppy) and its derivatives. The combination of the strong σ-donor effect of the phenylate and the π-accepting character of the pyridine ring results in a high ligand-field for the coordinated metal, thus



2a: R = H,
2b: R = $C_8H_{17}O$

3

Figure 2: Chemical structure of the dinuclear Pt complexes **2a–b** and **3** [20].

raising the energy of quenching d–d states while lowering emissive MLCT and LC excited states. Alternatively, the use of *N*-deprotonable azole units has also been largely explored due to the fact that it can exert similar effects to ppy-like ligands [16]. Nevertheless, easier deprotonation of the N–H site in comparison with ppy chelates notably widens applicability and increases the chemical structure diversity of the final luminophors, e.g., for complexating metal ions less prone to undergo cyclometallation reactions. Extensive work based on azolate-type of ligands has been developed by the group of Chi [16] who has recently described a series of neutral platinum(II) complexes bearing isoquinolylpyrazolates, complexes **4**–**7** in Figure 3 [26]. Control on the intermolecular interactions was exerted through the substitution pattern, yielding solids that exhibited mechano- and solvatochromic properties. Indeed, bathochromic shifts in the emission energy were observed upon either grinding or incrementing solvent polarity. This emission was attributed to a radiative transition with triplet metal–metal-to-ligand charge transfer character (^{3}MMLCT), which ultimately strongly depends on the platinum···platinum intermolecular distance. These compounds were also suitable OLED dopants, achieving high EQE of 8.5–11.5%. Nevertheless, the electroluminescence was slightly broader than the corresponding photoluminescence due to incomplete suppression of the intermolecular interactions.

Taking advantage of the easy generation of anionic ligands from azoles, the same group described the preparation of neutral platinum(II) complexes resulting from the combination of dianionic with neutral chelates (Figure 4) [27]. Compounds **8** and **9** were weakly emissive in solution. Nevertheless, the solid-state emission of these particular heteroleptic complexes was switched on notably. Apart from reduced geometry distortions within a rigid environment, the presence in some cases of interligand H-bonding interactions further contributed to efficiently suppress nonradiative decay channels. More importantly, these supplementary interactions reinforced the ligand–metal bond, which explains well the remarkable phosphorescence efficiency obtained in solid-state thin films being PLQY of 0.52 and 0.83 for **8** and **9**, respectively. Such findings prompted the authors to fabricate non-doped OLEDs with an architecture as follows: ITO/MoO_3 (2 nm)/1,4-bis(1-naphthylphenylamino)biphenyl (NPB) (25 nm)/1,3-bis(9-carbazolyl)benzene (mCP) (8 nm)/complex **8** or **9** (40 nm)/tris[3-(3-pyridyl)mesityl]borane (3TPyMB) (50 nm)/LiF (1 nm)/Al. The OLED based on **8** displayed orange-red electroluminescence (EL) with EQE of 19.0%, current efficiency (CE) of 21.0 cd A^{-1}, power efficiency (PE) of 15.5 lm W^{-1} and brightness as high as 43000 cd m^{-2}. On the other hand, yellow emitting OLED were obtained for **9** with EQE of 7.1%, CE of 21.0 cd A^{-1}, PE of 11.3 lm W^{-1} and brightness of 5100 cd m^{-2}. The better performances of **8** over **9** were ascribed to a shorter exciton lifetime that contributes to reduce detrimental nonradiative processes such as triplet–triplet annihilation (TTA) and triplet–polaron annihilation (TPA).

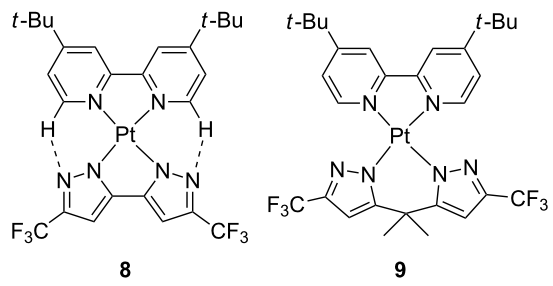


Figure 4: Selected neutral platinum(II) complexes featuring dianionic biazolate and neutral bipyridines [27].

On the other hand, strong σ-donor NHC carbenes ligands could be regarded as the neutral variant of phenylate-like counterparts [28-30]. Apart from the strong σ-donor ability, the great

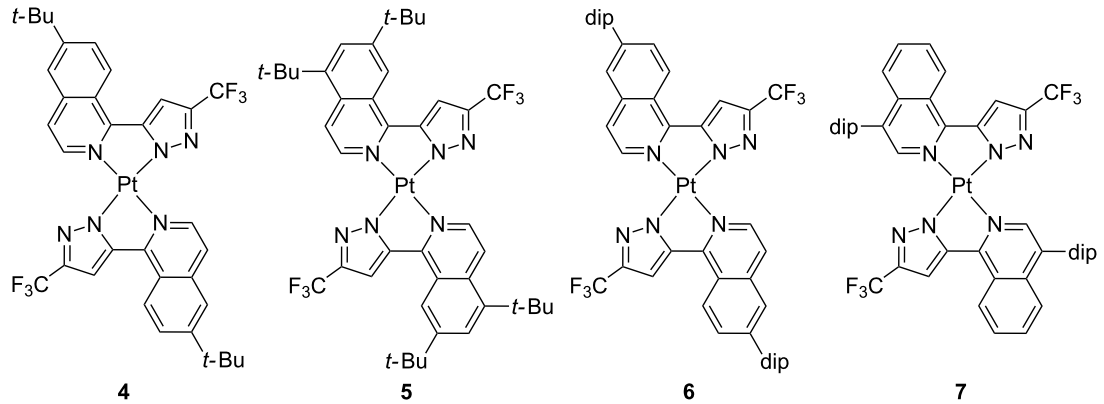


Figure 3: Molecular structure of platinum(II) complexes bearing isoquinolinylpyrazolates; dip = 2,6-diisopropylphenyl [26].

interest for these ligands relies on the robustness that they confer to the resulting complexes, upon coordination onto both early [31] and late transition metals [32,33]. In this regard, the group of Chi employed carbene-based chelates as neutral imine substitutes in an attempt to further improved the stability and the performances of their N···H–C stabilized phosphors (Figure 5) [34,35]. Either when one, compound **10** [34], or two, compound **11** [35], carbene moieties were used, the resulting platinum compounds were basically nonemissive in solution. On the contrary, they became strong emitters in the solid state owing to the switching of the nature of the excited state that becomes ^{3}MMLCT in nature. Their EL properties were evaluated by fabrication of non-doped OLEDs. Compound **10** was embedded into an OLED device with the following configuration ITO/MoO_3 (1 nm)/TAPC (65 nm)/mCP (8 nm)/**10** (pure/nondoped, 30 nm)/3TPYMB (50 nm)/LiF (1 nm)/Al (120 nm), where TAPC is 1,1-bis[(di-4-tolylamino)phenyl]cyclohexane, and serve either as the hole- or electron-transport layers. A highly efficient yellow-emitting device was obtained with EQE = 25.9% and CE = 90 cd A^{-1} at 100 cd m^{-2} (EQE = 24.4%, CE = 85 cd A^{-1} at 1000 cd m^{-2}); one of the best performances ever reported for a non-doped OLED. On the other hand, device architecture for compound **11** was as follows: ITO/TAPC with 20 wt % MoO_3 (20 nm)/TAPC (40 nm)/2,6-bis(3-(9*H*-carbazol-9-yl)phenyl)pyridine (26DCzppy) with 8 wt % of **11** (20 nm)/1,3,5-tris[(3-pyridyl)phen-3-yl]benzene (TmPyPB) (50 nm)/LiF (0.8 nm)/Al (150 nm). The associated OLED performances for **11** were lower respect to those of the former compound, yielding a green-yellow emission with EQE = 12.5%, CE = 44.0 cd A^{-1} and PE = 28.0 lm W^{-1} for **11a**, and EQE = 11.2%, CE = 40.6 cd A^{-1} and PE = 25.8 lm W^{-1} for **11b**. In consequence, the use of only one carbene moiety seemed to afford very appealing photophysical features both for display and lighting applications.

The beneficial effect of carbene moieties on the photophysical features of the dopant was also shown by Strassner and co-workers [36-38]. Compared with previously reported imidazolylidene and triazolylidene acetylacetonate (acac) platinum(II) complexes, complexes **12** bearing 1,3-thiazol-2-ylidene carbenes outperformed the former when evaluating the photophysical properties (Figure 6) [37]. The intermolecular interaction was finely tuned as a function of the steric hindrance of the acac-type ancillary ligand, which had a profound impact on the emission quantum yield. Characterization of the electroluminescence performances of these complexes in mixed-matrix OLED led to EQE values as high as 12.3%, CE of 37.8 cd A^{-1} and PE of 24.0 lm W^{-1} at 300 cd m^{-2} for complex **12f**.

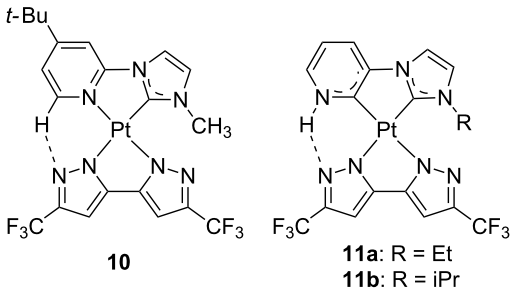


Figure 5: Selected neutral platinum(II) complexes from bipyrazolate and carbene-based chelates [34,35].

In spite of typical TTA processes at high concentrations for phosphorescent dopants, azolate-containing platinum(II) complexes have recently shown great potentiality for the fabrication of non-doped OLEDs. In fact, Wang and collaborators reported a red-emitting device based on $Pt(fppz)_2$ [39], where fppz is 3-(trifluoromethyl)-5-(2-pyridyl)-1*H*-pyrazolate, that attained remarkable EQE of 31% [40] (see Figure 7 for the chemical structure of the complex). With the aim of correlating molecular structure, photophysical properties and OLED performances, Chi, Kim and co-workers analyzed the X-ray structures of $Pt(fppz)_2$ (**13**) and other related platinum(II) complexes **14** and **15** in both single crystal and thin film samples (Figure 7) [13]. They observed different degrees of crystallinity as a function of the substrates, though the crystal pattern of the investigated compounds was not affected. More interestingly, upon analysis of angle-dependent emission intensities at various wavelengths along with the birefringence of the films, the authors concluded that the arrangement of the complexes within

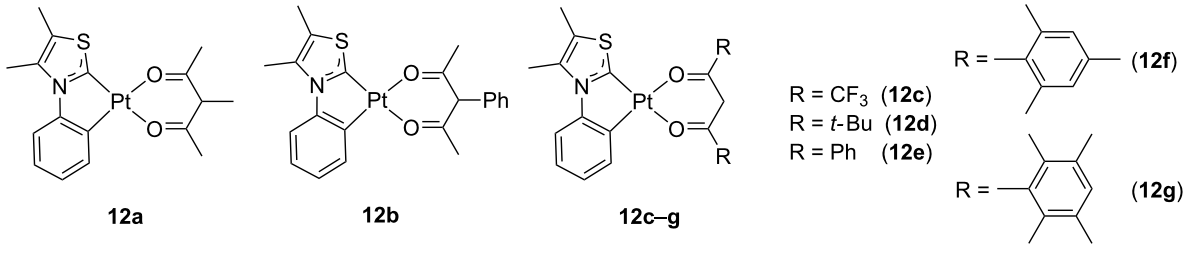


Figure 6: Cyclometalated thiazol-2-ylidene platinum(II) complexes with different acetylacetonate ligands [37].

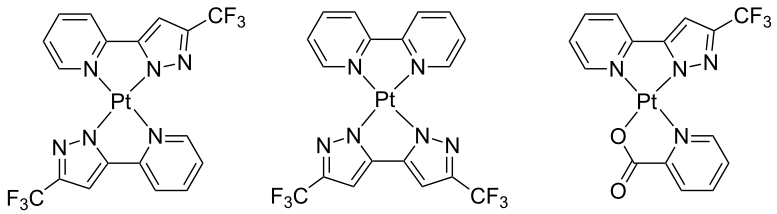


Figure 7: Neutral platinum(II) complexes **13**–**15** bearing azolate ligands [13].

the films was crucial for the PLQY attained. In the remarkable case of the crystalline film of complex $Pt(fppz)_2$, the molecular plane of the square-planar compound was mostly perpendicular respect to the substrate and hence, the ^{3}MMLCT photoluminescence dipole lies almost parallel to it. The architecture of the fabricated OLEDs using phosphor **13** as emitting layer was ITO (100 nm)/TAPC (80 nm)/4,4',4''-tri(9-carbazoyl)triphenylamine (TCTA) (10 nm)/$Pt(fppz)_2$ neat (30 nm)/1,3-bis(3,5-di(pyridin-3-yl)phenyl)benzene (BMPYPB) (15 nm)/BMPYPB:1 wt % Rb_2CO_3 (40 nm)/Al (100 nm). These devices exhibited an outstanding EQE value as high as 38.8%, which approaches the maximum EQE estimated value of ca. 45%. This latter could be achieved in the case of a phosphor with 100% of PLQY with a fully parallel emitting dipole.

The beneficial effect of the emitting dipole orientation on the light outcoupling efficiency was further illustrated in a following work by the group of Chi [14]. Exploiting the strong tendency to form ordered structures, a new series of platinum(II) bearing fluorinated 2-pyrazinylpyrazoles was developed, namely complexes **16**–**18** in Figure 8. Upon aggregation, very efficient NIR emission arising from a ^{3}MMLCT excited state with PLQY as high as 0.81 was obtained. As aforementioned, the perpendicular molecular arrangement, together with a highly ordered structure, allowed the exciton to diffuse over long distances with minimal vibrational relaxation to the ground state. Among these dopants, incorporation of **16** into an optimized planar non-doped OLED structure with architecture as follows ITO (100 nm)/1,4,5,8,9,11-hexaazatriphenylene hexacarbonitrile (HATCN) (10 nm)/NPB (50 nm)/mCP (15 nm)/**16** (20 nm)/2,2′,2″-(1,3,5-benzenetriyl)-tris(1-phenyl-1*H*-benzimidazole) (TPBi) (60 nm)/8-hydroxyquinolatolithium (Liq) (2 nm)/Al (100 nm), led to an EQE of 24 ± 1%. This result was even improved when a light outcoupling hemisphere structure was employed, achieving outstanding values of EQE up to 55 ± 3%. This performance is the highest reported so far for a NIR OLEDs. Therefore, these works nicely showed how both crystallinity and molecular orientation are key parameters that can make great differences for the resulting thin-film optoelectronic performances.

Apart from display applications, general lighting efficiency currently constitutes a main concern of our society and white-emitting OLEDs (WOLEDs) represent a valuable alternative because of their energy-saving potential. In this regard, development and improvement of white-light emitting devices attracts considerable interest. Nowadays, two main fabrication strategies seemed to be the most promising ones such as i) including either three (RGB) or two emitting components (sky-blue-orange); ii) using a phosphorescent material to partially down-convert UV or blue light from a LED source; the latter seems a promising option to date. The group of Sicilia has recently applied some cyclometallated platinum(II) complexes bearing NHC ligands to develop WOLEDs, whose chemical structure is sketched in Figure 9 [41]. Depending on the π-conjugation of the NHC-based bidentate ligand, emitting

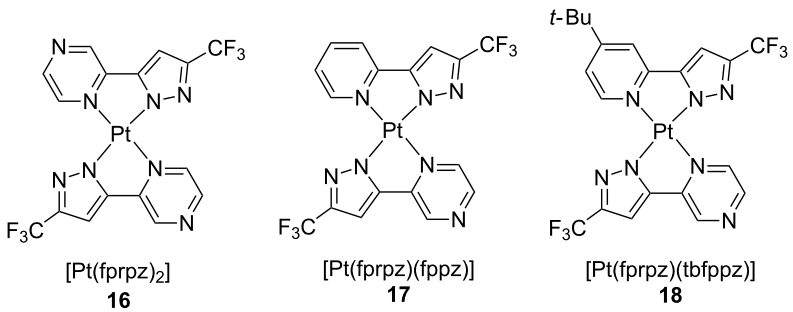
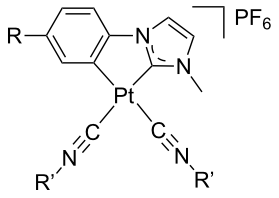
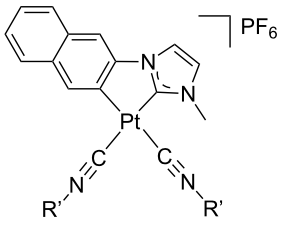


Figure 8: Chemical structure of neutral platinum(II) complexes **16**–**18** bearing azine-pyrazolato bidentate ligands [14].

complexes with luminescence varying from blue (**19** and **20**) to yellow (**21**) were obtained. Several devices were prepared following a remote phosphor configuration, which places the phosphors spatially separated from the LED source. The associated values of correlated colour temperature (CCT), colour rendering index (CRI) and luminous efficacy of the radiation (LER) were acceptable, proving the suitability of these systems for lighting applications. Nevertheless, a fast degradation of the emission was observed under device operation.



R = COOEt; R' = *t*-Bu (**19a**), Xyl (**19b**)
R = CN; R' = *t*-Bu (**20a**), Xyl (**20b**)



R' = *t*-Bu (**21a**), Xyl (**21b**)

Figure 9: Molecular structure of carbene-containing cyclometallated alkynylplatinum(II) complexes **19**–**21** [41].

Systems based on tridentate ligands

During the last two decades, platinum(II) complexes bearing tridentate ligands have been extensively investigated as well. Compared to their mono- and bidentate counterparts, a threefold chelating motif imposes higher geometrical rigidity, which is expected to further decrease molecular distortions. The overall stability of the resulting compound is increased, thus helping to greatly suppress nonradiative deactivation pathways. Although 2,2':6',2"-terpyridines showed widespread use in coordination chemistry [42,43], the bite angle of such class of tridentate ligands is not ideal for a square-planar geometry, leading to longer bond lengths when compared with their bidentate congeners. As a consequence, ligand-field is reduced and the presence of low-lying d–d excited states provide easy access to nonradiative deactivation channels [25,44].

Nevertheless, the use of multidentate chromophoric ligands that are able to provide metal–ligand bonds with higher covalent character, as for instance cyclometalating ligands, has proven to be a successful strategy for improving the luminescence properties due to the energetic destabilization of quenching MC states [45,46].

Complexes based on C^N^N ligands

Following the seminal work of von Zelewski [47,48] on platinum(II) complexes bearing C-deprotonated 2-phenylpyridines (C^N), the development of tridentate analogues has received a great deal of attention in the recent past. Early reports were based on 6-phenyl-2,2'-bipyridine, namely C^N^N [49,50]. In spite of the strong ligand field exerted by the cyclometalating moiety, this type of complexes resulted to be rather weakly emissive due to large structural distortion of the emitting triplet excited state. Nevertheless, Che and co-workers demonstrated that extending the π-conjugation of the cyclometalated ligand led to enhanced phosphorescence quantum yields [51,52]. Indeed, the increased conjugation resulted in a modification of the frontier molecular orbitals and prevention of Jahn–Teller distortions.

Recently, Che and co-workers reported a series of asymmetric tridentate C^N^N platinum(II) complexes with π-extended moieties, compounds **22** (Figure 10) [53]. Depending on the ancillary ligand, these complexes showed emission arising from several contributions, being ^{3}MLCT and ^{3}ILCT, together with ^{3}XLCT or ^{3}LLCT, where XLCT is a halogen-to-ligand charge transfer, with PLQY values approaching unity for some derivatives. Different structural isomers were synthesized, including a π-conjugated fragment attached at different positions of the employed tridentate ligand. The best results were obtained when the azine moiety isoquinolin-3-yl was used due to the minimization of the repulsions within the tridentate scaffold as well as with the ancillary ligands. Based on these initials results, new structural variations were investigated at both the cyclometalating and the ancillary ligands. As for the former, a clear impact on the emission colour was observed due to the participation of the cyclometalating unit to the HOMO frontier orbital. Thus, an emission ranging from green to yellow and finally to red was obtained going from phenyl, thiophene and benzothiophene cyclometalating rings, respectively. On the contrary, the ancillary ligand had a remarkable effect on the emission efficiency. In the case of pentafluorophenylacetylide, the change in the nature of the emitting excited state led to an almost negligible k_{nr} value, which resulted in an outstanding PLQY close to unity. The most promising complexes were selected by the authors as dopants for OLED fabrication and their chemical structure is displayed in Figure 10. Four devices with the configuration of ITO/TAPC (50 nm)/ TCTA:**22** (2–4 wt %, 10 nm)/ TmPyPB (50 nm)/LiF (1 nm)/Al (100 nm) were fabricated, attaining CE of 23.1–76.7 cd A^{-1} and PE of 10.4–45.0 lm W^{-1}. While devices fabricated with **22a**,**b** as dopant exhibited yellowish-green emission, those embedding **22c**,**d** showed satu-

rated red colour. As for the maximum EQE, very high values up to 22.8% were achieved. These values are among the highest ones reported for platinum(II) complexes as dopant materials. It is worth to note that optimized PhOLED device embedding complex **22c** at doping concentration of 4 wt % showed an EQE of 22.1% that compares well with the best red-emitting iridium(III)-based devices.

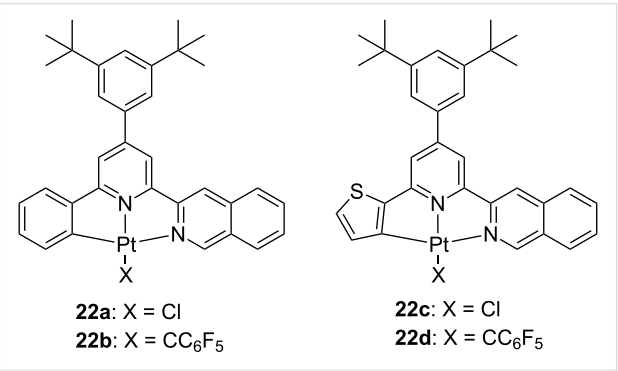


Figure 10: Chemical structure of platinum(II) complexes **22a–d** bearing asymmetric C^N^N tridentate ligands [53].

Complexes based on N^C^N ligands

Although formally bearing similar coordinating units, platinum(II) complexes bearing symmetrical N^C^N ligands resulted in better emitters than those bearing the corresponding C^N^N motif. For instance, while [Pt(C^N^N)Cl] (C^N^N = 6-phenyl-2,2'-bipyridine) possess a rather low emission (PLQY = 0.025) in degassed CH_2Cl_2 solution at room temperature [50], [Pt(N^C^N)Cl], where N^C^N is a bis-cyclometalating 2,6-dipyridylbenzene type of ligand (complexes **23**), displays a much higher PLQY reaching 0.60 in similar conditions, as for instance compound **23a** [54]. The chemical structure of complexes **23** is shown in Figure 11. These distinct results can be interpreted as follows. A shorter Pt–C bond length was observed for the N^C^N-containing complex, revealing a stronger interaction with the metallic ion. As a consequence, a higher d–d splitting could be foreseen, thereby reducing the possibility of a non-radiative deactivation channel of the emitting excited-state. On the other hand, [Pt(N^C^N)Cl] displayed a metal-perturbed $^3\pi$–π^* emission as also demonstrated by the relatively high radiative rate constant value. The combination of these two factors explained well the aforementioned good emission efficiencies. As a result, N^C^N-coordinated complexes have found numerous applications as emitting materials in areas such as emitters in PhOLEDs [55,56] and luminescent probes in bio-imaging [57-59]. Noteworthy, NIR-emitting OLED were fabricated by using complexes **23g** and **23h**, which presented a π-delocalized substituent at the 5-position of the central phenyl ring. As the parent complex **23a**, excimer formation via metal–metal interactions was observed for both derivatives at high concentrations or in neat films. Nevertheless, the increased conjugation within the chromophoric ligand led to a lower emission energy, which fell into the NIR region. The structure of the optimized vacuum-processed OLED was as follows: ITO (120 nm)/Mo_2O_x (2 nm) / TCTA (80 nm) /**23g** or **23h** (15 nm)/TPBi (25 nm)/LiF (0.5 nm)/Al (100 nm). Complex **23g** attained remarkable performances for this class of Pt(II)-based compounds, with an EQE of 1.2% at a current density of 10 mA cm^{-2} and an electroluminescence intensity of about 10 mW cm^{-2} at 9 V.

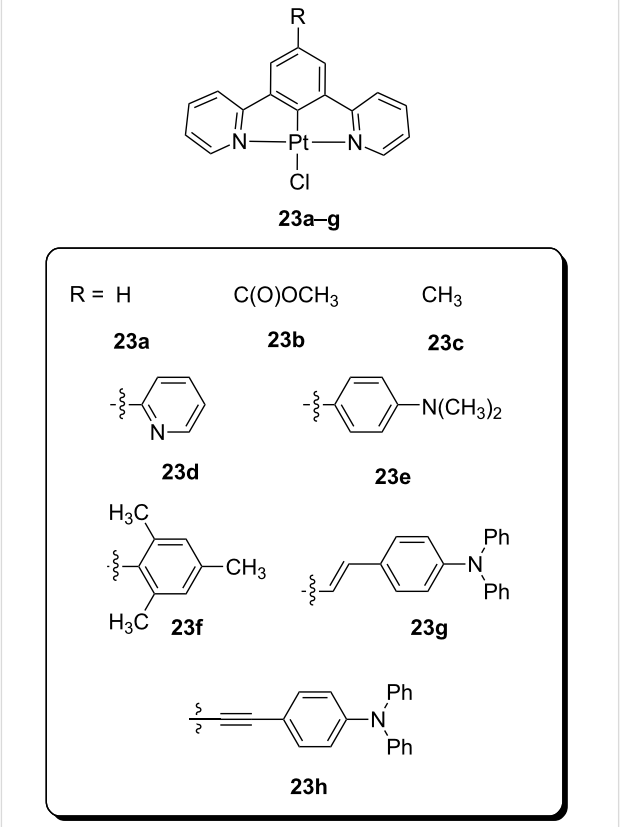


Figure 11: Chemical structure of platinum(II) complexes **23** bearing *bis*-cyclometalating 2,6-dipyridylbenzene type of ligands [54-56].

Due to the triplet character of typical platinum(II) complex emission, these metal-based dopant phosphors are typically dispersed in high triplet energy hosts to suppress energy transfer processes onto the host matrix that detrimentally affect the final performances [60]. Alternatively, development of emissive complex incorporated in a dendritic structure allows controlling both charge transport and light emission in a single material [61]. In this regard, Yam and co-workers reported on a series of dendritic carbazole-based alkynylplatinum(II) complexes with cyclometalated 2,6-bis(*N*-alkylbenzimidazol-2'-yl)benzene (bzimb) as the N^C^N tridentate ligand [62]. These complexes were found to be highly emissive with PLQYs of up to 0.80 in

solid-state thin films. Contrarily to other alkynylplatinum(II) complexes, their emission was ascribed to an admixture of ^{3}IL/^{3}MLCT since no influence of the dendrimeric ancillary ligand was observed. Nevertheless, upon increasing the dopant concentration in thin films up to 50 wt %, a new low-energy band was observed that was attributed to the formation of excimeric species. Nonetheless, it is worth to note that this excimeric emission was reduced on increasing the generation of the ancillary ligand, highlighting the importance of this molecular design strategy towards highly efficient dopants. The interesting photophysical properties of these compounds prompted the evaluation of their electroluminescence performances in OLED devices. Solution-processed green-emitting PhOLEDs were prepared with the structure of ITO/poly(ethylenedioxythiophene):poly(styrene sulfonic acid) (PEDOT:PSS 70 nm)/mCP:**24** 5–50 wt % (60 nm)/SPPO13 (30 nm)/LiF (0.8 nm)/Al (100 nm), where SPPO13 is 2,7-bis(diphenylphosphoryl)-9,9′-spirobifluorene. For all devices, emission similar to those recorded in solution was obtained independently of the doping concentration. Moreover, the decreasing driving voltages measured were ascribed to better charge transport properties in the emissive layer upon increasing the dendron generation. However, the best hole-electron current balance was achieved for a platinum(II) complex with the second generation dendrimeric structure (Figure 12), yielding a maximum CE and EQE of 37.6 cd A^{-1} and 10.4%, respectively. This enhanced

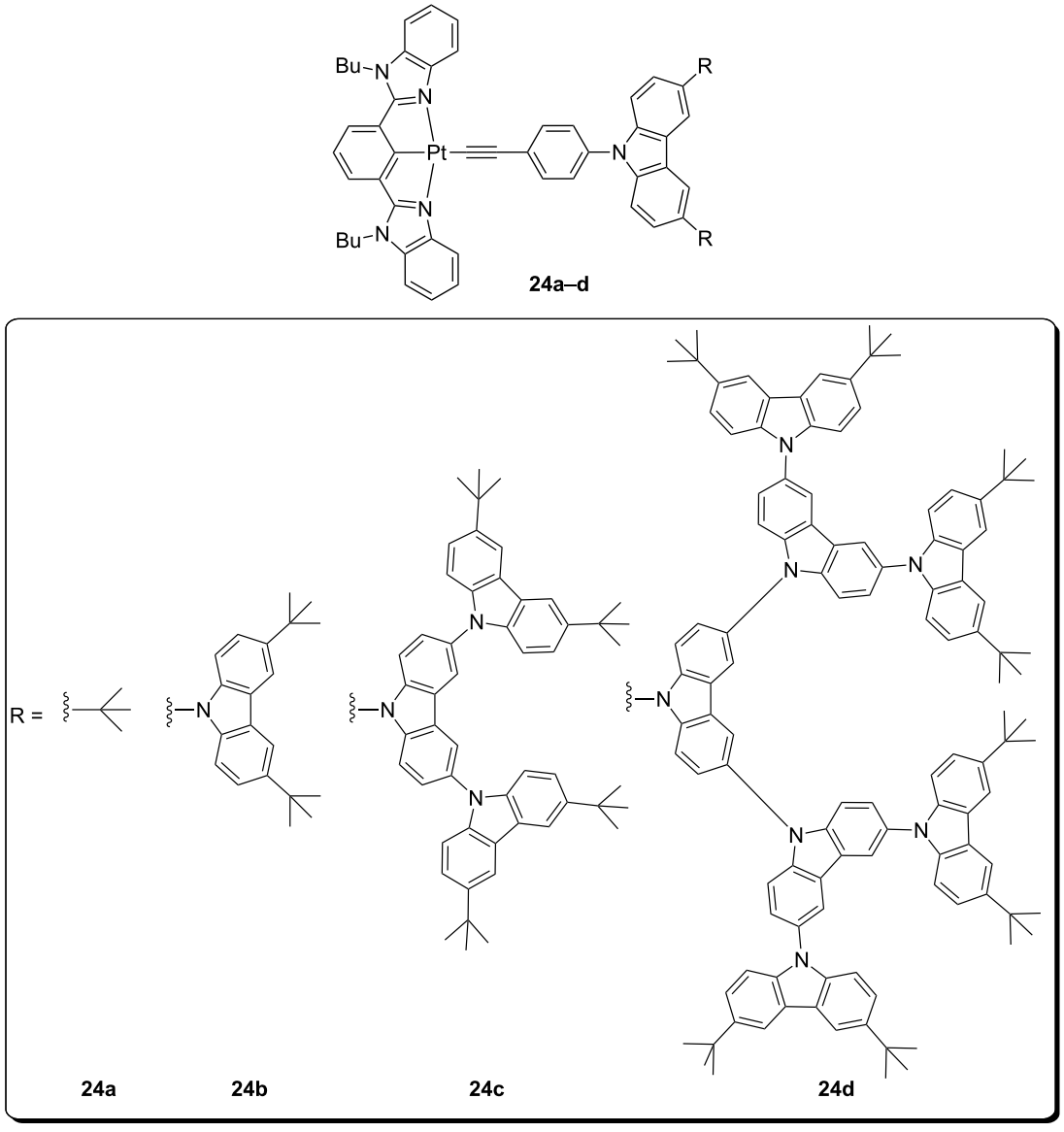


Figure 12: Molecular structure of dendritic carbazole-containing alkynyl-platinum(II) complexes **24a–d** [62].

performance highlights the beneficial effect of employing emitters with a dendrimeric design. Indeed, these results were among the best values ever reported for PhOLEDs based on metal-containing dendrimers, and even compared well with vacuum-deposited devices of non-dendritic structurally-related platinum(II) complexes.

As a further development of the work, the same group reported very recently another family of platinum(II) complexes containing both electron-donor and electron-acceptor moieties embedded within the dopant structure (Figure 13) [63]. This bipolar character was intended to reduce the TTA phenomena commonly experienced at high current density that leads to severe roll-off efficiency of OLEDs [64]. In particular, carbazole-based donor moieties and either phenylbenzimidazole (PBI) or oxadiazole (OXD) accepting units were selected as the hole-transporting and electron-transporting moiety, respectively. Two linkage fashions were explored between these donor-acceptor groups, namely *meta*- and *para*-substitution. As expected, the intramolecular charge transfer character was less prominent in the absorption features of compounds with *meta*-linkages. Nevertheless, all compounds showed a ^{3}IL/^{3}MLCT emission in the green region, that resembled well that of other complexes bearing the bzimb tridentate ligand, with no influence of the connecting mode. Moreover, successful energy transfer was achieved upon doping thin films of TCTA:SPPO13 with the tridentate platinum complex, and high PLQY in the range 0.62–0.75 were achieved. These promising results prompted the authors to fabricate PhOLED devices employing these new bipolar emitters. The device architecture was as follows: ITO/PEDOT:PSS (70 nm)/**25**:TCTA:SPPO13 5–20 wt %:1:1 (60 nm)/1,3-bis(3,5-bis(pyridine-3-yl)phenyl)benzene (BmPyPhB; 30 nm)/LiF (0.8 nm)/Al (100 nm). The differences in molecular design became more evident under operational

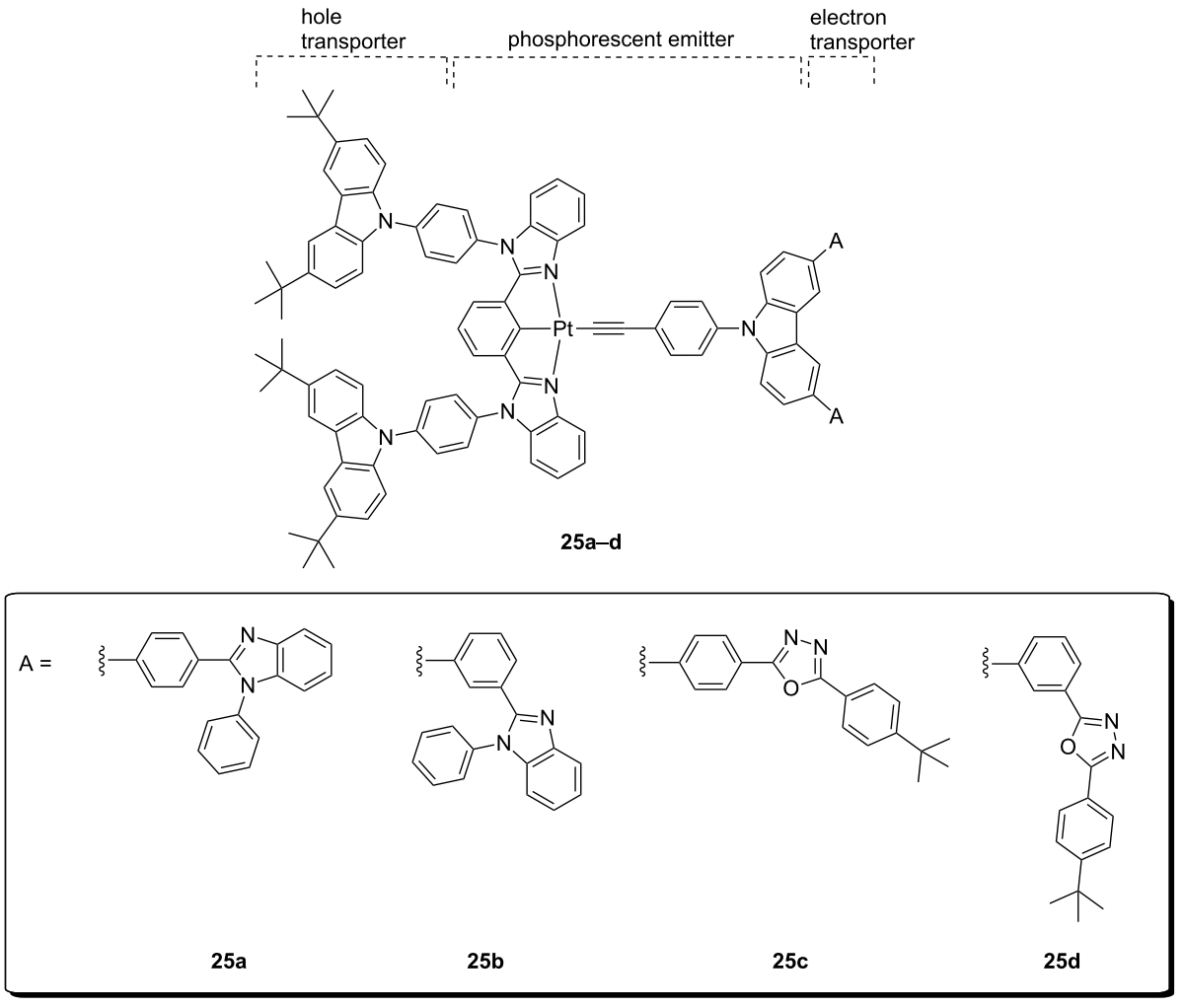


Figure 13: Molecular structure of bipolar alkynyl-platinum(II) complexes **25** bearing carbazole and electron-accepting phenylbenzimidazole or oxadiazole moities [63].

device conditions. The emitters with OXD units performed better than those with PBI units. On the other hand, a remarkable increase of CE and EQE was obtained going from *para*- to *meta*-linkage. As a result, CE as high as 57.4 cd A^{-1} were reached along with a EQE of 16.0%, for the *meta*-connected OXD-containing platinum(II) dopant at 15 wt %. These interesting results demonstrated the beneficial effects of bipolar metal-based emitters for high-performing optoelectronic devices.

In another study from the group of Yam, the bipolar design was conceived to finely tune the emission energies of the compounds [65]. Two series of platinum(II) alkynyl (compounds **26**) and carbazoyl (compounds **27**) complexes were reported, which included different donor and/or acceptor groups on the ancillary ligand (Figure 14). As expected, their emission behavior was strongly dependent on the nature of this latter, displaying different combinations of π–π* and charge-transfer triplet excited states, together with a broad emission ranging from the green to the red portion of the spectrum. Interestingly, a solution-processed OLED fabricated with a complex bearing a carbazoyl ancillary ligand showed concentration-dependent electroluminescence. In addition, a change in nature of the emission from ^{3}IL to ^{3}MLCT/^{3}LLCT character was observed upon increasing doping concentration from 5 to 20 wt %. Moderate performances were attained at this latter concentration, with CE of 24.0 cd A^{-1} and EQE of 7.2%. Alternatively, these compounds were successfully employed in the fabrication of organic memories, which demonstrates the great versatility of this class of platinum(II)-containing materials.

Complexes based on bis-anionic C^N^C and N^N^N ligands

In an attempt to further destabilize the d–d excited states, doubly cyclometalating 2,6-diphenylpyridine [66,67] and their extended π-conjugated analogues have been employed as C^N^C tridentate ligands for platinum(II) complexes. Nevertheless, the resulting complexes resulted to be almost nonemissive in solution at room temperature in spite of the stronger ligand-field exerted. Similar to the case of C^N^N type of ligands, a significant structural distortion is the main factor that accounts for this low emission efficiency. However, Che and co-workers demonstrated that extension of the π-conjugation at the tridentate ligand, together with the use of heterocyclic moieties such as thiophene or carbazole, clearly favours the luminescence properties of these type of platinum(II) complexes [68].

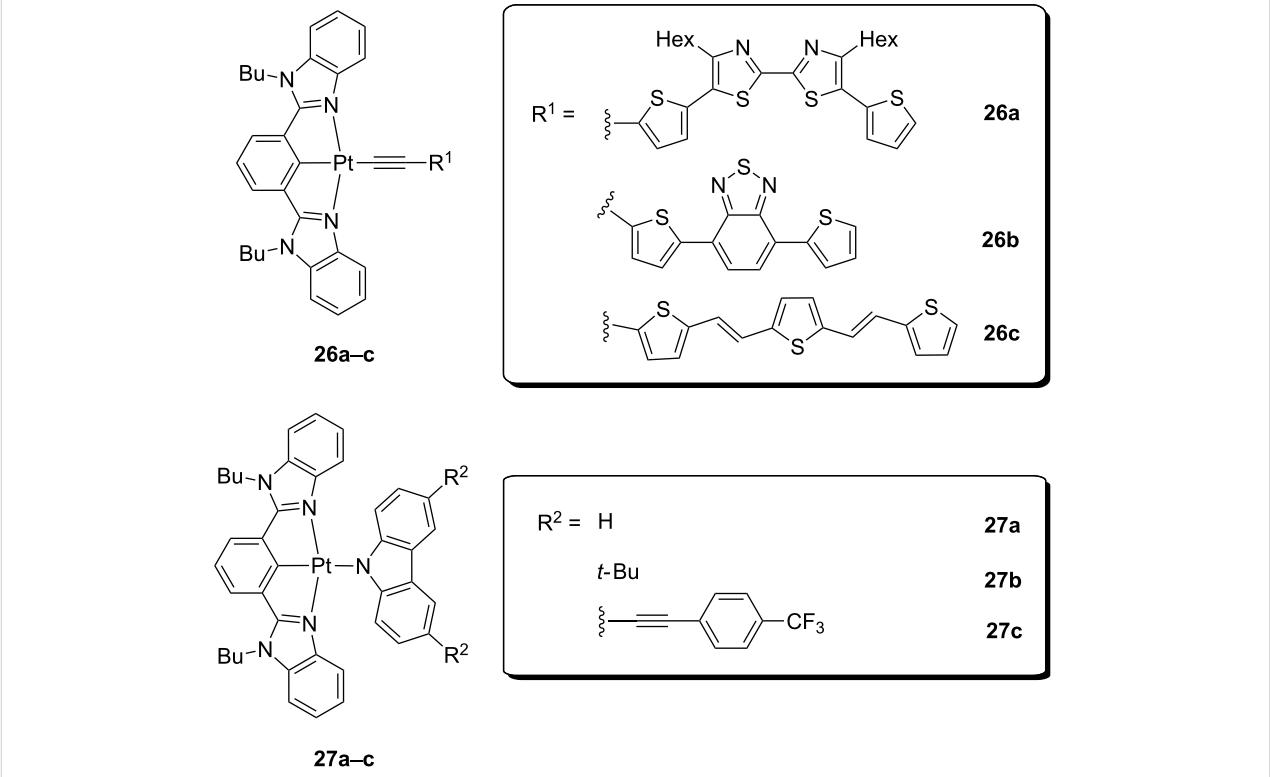


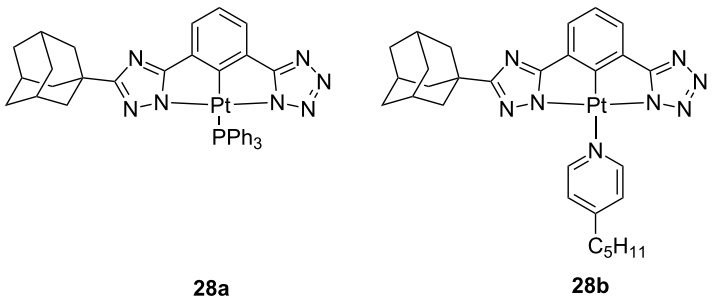
Figure 14: Molecular structures of neutral platinum(II) complexes comprising donor-acceptor alkynyls (**26**) or electron-rich carbazoles (**27**) as ancillary ligands [65].

As aforementioned, N-deprotonable azole units constitute a compelling alternative to C-cyclometalating ligands [16]. In this regard, dianionic tridentate N^N^N ligands bearing pyrazolate [69], triazolate [69-73] or tetrazolate [74] units have been used to successfully prepare highly luminescent neutral platinum(II) complexes in dilute solution and/or as aggregated state. Due to their promising emitting features, these complexes have also been employed as phosphors in optoelectronic devices [71,72]. Neutral platinum(II) complexes with an asymmetrical triazolate- and tetrazolate-containing tridentate ligand, complexes **28**, were also reported [75] (Figure 15). These green emitters were used to fabricate solution-processed PhOLEDs, displaying performances as high as their vacuum-processed structurally-related analogues, with a maximum PE of 16.4 lm W^{-1}, CE of 15.5 cd A^{-1} and EQE of 5.6% obtained for derivative **28b**. These performances are amongst the highest EQE values for solution-processed platinum-based OLEDs.

Systems based on tetradentate ligands

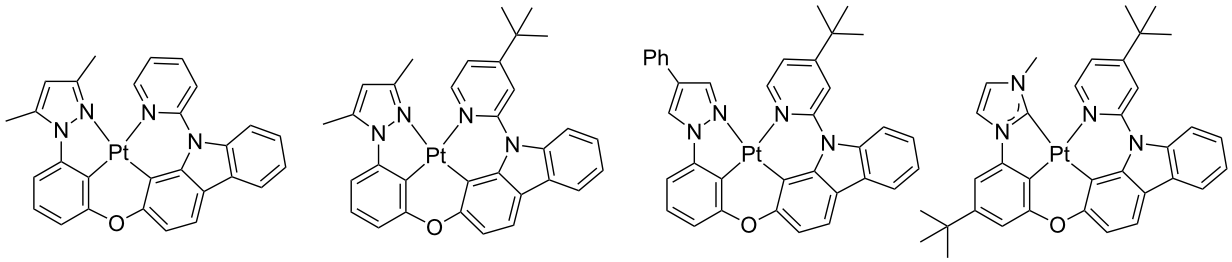
Tetradentate ligands have attracted an increased attention due to the even higher rigidity of the chromophoric scaffold that helps to suppress nonradiative decay pathways induced by large distortions around the metal atom [76,77].

Following on their strategy of employing rigid N^C^C^N and C^C^C^N ligands bearing either methyl-2-phenylimidazole or phenylpyrazole moieties [78], Li and co-workers recently reported on a series of tetradendate platinum(II) complexes **29**–**32** that displayed narrow emission spectral bandwidth (Figure 16) [79]. In such derivatives, the introduction of an electron-donating moiety, such as a *tert*-butyl group, onto the pyridyl ring of the tetradentate scaffold induces a larger energy separation between the carbazolepyridine and the phenylpyrazolate moieties. In consequence, spectra are narrowing and a higher colour purity can be achieved by reducing vibronic sideband contributions to the overall emission spectrum. The complexes displayed PLQY above 0.7 in PMMA thin-film with λ_{em} maxima centred at ca. 450 nm. OLED devices employing complexes **30**–**32** as emitting materials were fabricated with the following architecture: ITO/HATCN (10 nm)/NPD (40 nm)/TAPC (10 nm)/Pt complex 2 wt %: 26mCPy (25 nm)/DPPS (10 nm)/BmPyPB (40 nm)/LiF/Al, where 26mCPy, DPPS are 2,6-bis(*N*-carbazolyl)pyridine and diphenyl-bis[4-(pyridin-3-yl)phenyl]silane, respectively. All the investigated derivatives showed an EL spectrum similar to the PL emission band indicating efficient suppression of the spectral broadening thanks to the bulky *tert*-butyl groups. Thus, "pure" blue electrolumines-



28a **28b**

Figure 15: Chemical structure of the asymmetric Pt(II) derivatives **28** bearing triazole and tetrazole moieties onto a tridentate ligand [75].



PtON1 **29** PtON1-*t*-Bu **30** PtON6-*t*-Bu **31** PtON7-dtb **32**

Figure 16: Molecular structure of the tetradentate platinum complexes **29**–**32** bearing N^C^C^N and C^C^C^N ligands [79].

cence with CIE_y coordinate <0.1 and EQE of 17.2% were achieved for derivative **32** bearing a NHC ligand. Interestingly, upon increasing doping concentration from 2 to 6 wt % and employing TAPC and a higher bandgap electron transporting material 2,8-bis(diphenylphosphoryl)dibenzothiophene (PO15) at 1:1 ratio as co-host, peak EQE of 24.8% was achieved without significantly affecting colour purity.

Variation of the emissive moiety from the methylimidazole or phenylpyrazole to the 4-phenylpyridyl carbazole afforded compound **33** (Figure 17). This complex displayed an emission maximum at 602 nm in CH_2Cl_2 arising from an excited state with strong ^{3}MLCT character with PLQY of 0.34 (Figure 17) [80]. OLEDs were fabricated with device architecture as follows: ITO/HATCN(10 nm)/NPD(40 nm)/TrisPCz (10 nm)/**33** 10 wt %:CBP(25 nm)/BAlq(10 nm)/BPyTP(40 nm)/LiF(1 nm)/Al(100 nm), where TrisPCz, CBP and BAlq is 9,9′,9″-triphenyl-9*H*,9′*H*,9″*H*-3,3′:6′3″-tercarbazole, 4,4′-bis(*N*-carbazolyl)biphenyl and bis(2-methyl-8-quinolinolato)(biphenyl-4-olato)aluminum, respectively. The devices showed orange-red electroluminescence with remarkable estimated 97% operational lifetime, LT_{97}, over 600 hours at 1000 cd cm^{-2} and peak EQE of 10.8%. Nonetheless, further improvement of the device efficiency upon variation of host material increased the EQE value up to 21.5% when a dopant concentration of 2 wt % and the ambipolar Bebq2 host were employed instead, where Bebq2 is bis(benzo[*h*]quinolin-10-olato-κN,κO)beryllium(II). In spite of that, much lower LT_{97} values were observed most likely due to a higher charge and exciton concentration in the host layer at such low doping concentration. Such compound represents the most stable Pt(II) complex used as emissive material in an OLED device to date.

Compound **33** together with **34** and **29** were subsequently employed by the same authors as red, green and blue emissive materials, respectively, for the fabrication of white-light OLEDs (WOLEDs) [81]. Upon optimization of the device architecture in terms of doping concentration, layer thickness and stacking order of each of the emissive materials, WOLED devices with the following architecture ITO/HATCN/NPD/TAPC/complex **33** 6 wt %:26mCPy (3 nm)/complex **29** 6 wt %:26mCPy (20 nm)/complex **34** 6 wt %:26mCPy (2.5 nm)/DPPS/BmPyPB/LiF/Al showed CIE (x, y) coordinates of 0.35, 0.35, CRI of 80 and maximum EQE of 21.0%. However, a large efficiency roll-off was observed at higher current density due to increased charge and exciton trapping.

Further modification of the structure of complex **33** resulted in the related compound **35** that showed a more intense (PLQY = 0.63) and orange-red emission band with the maximum centered at 582 nm and an excited state lifetime of 7.3 μs in CH_2Cl_2 at room temperature [82]. EL performances were investigated in a charge balanced OLED device, with bi-layer EML architecture comprising two different dopant concentrations in

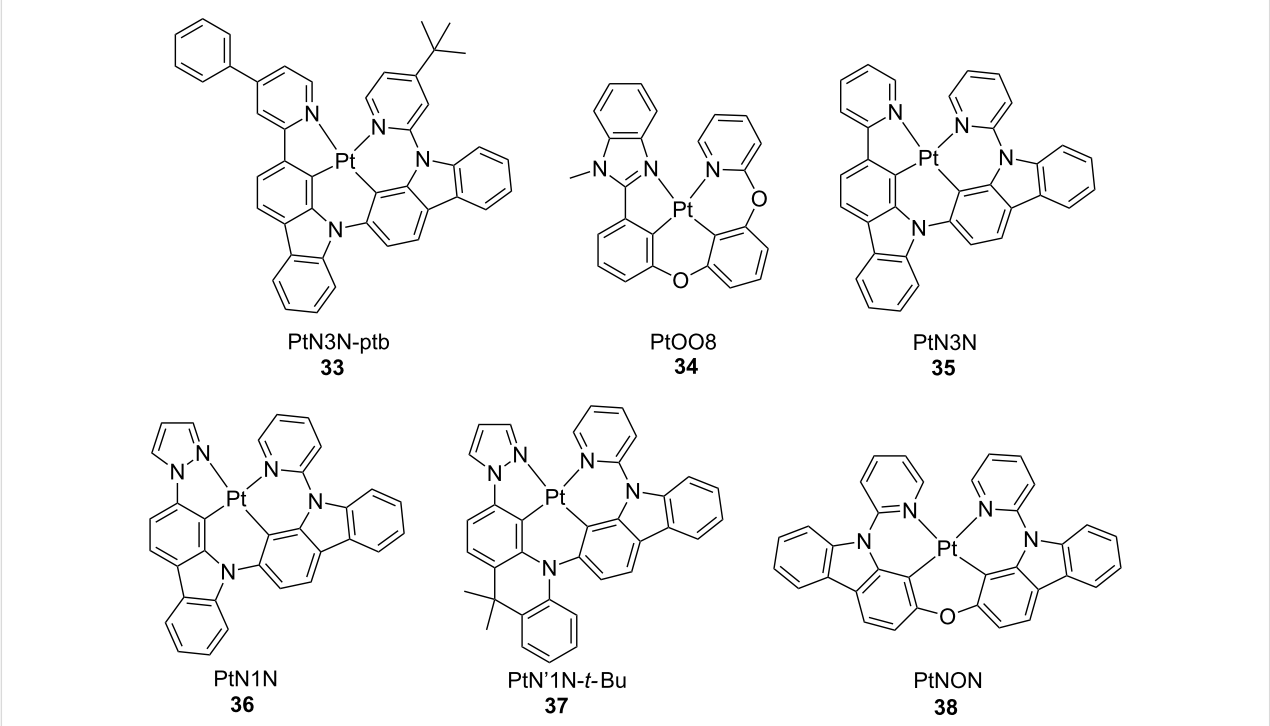


Figure 17: Chemical structure of the tetradentate Pt complexes **33**–**38** based on N^C^C^N-type of ligands [80-84].

order to shift exciton formation zone deeper into the emissive layer (device configuration: ITO/HATCN/NPD/TrisPCz/compound **35** 20 wt %:CBP/compound **35** 6 wt %:CBP/BAlq/BPyTP/LiF/Al). Such devices displayed EL spectra that was slightly broader than PL emission due to the relatively high dopant concentration with an estimated LT_{97} = 2057 h and EQE = 15.3% at 1000 cd m^{-2}.

Seeking for stable and efficient blue emitter for OLED devices and following the previous work on the red-emissive compound **33** and the green-emissive derivative **36** that showed a peak EQE of 14.3% [83], Li and co-workers developed a novel blue-emitting tetradentate platinum complex, namely **37**. The excited state of this compound was raised by breaking the π-conjugation of the carbazole moiety upon introduction of 9,10-dihydro-9,9-dimethylacridine moiety, where the two methyl groups were introduced to minimize oxidation of the benzyl carbon under device operation (Figure 17) [84]. Compound **37** exhibited a maximum of emission at 486 nm with a spectrum characterized by vibronic features, most likely due to the increased flexibility of the acridine moiety that imparted a more distorted excited state geometry compared to the carbazole-based counterpart. Upon device optimization, **37** resulted to be a rather efficient sky-blue triplet emitter. In particular, OLEDs with the following architecture ITO/HATCN (10 nm)/NPD (40 nm)/TrisPCz (10 nm)/complex **37** 10 wt %:mCBP (25 nm)/mCBT (8 nm)/BPyTP (40 nm)/LiF (1 nm)/Al (100 nm) were fabricated that showed peak EQE = 17.8% and LT_{70} of 482 h at 1000 cd m^{-2}.

A similar strategy based on the rupture of the π-conjugation in a cyclometalating ligand was employed by the same authors to achieve blue emission in symmetric tetradentate platinum(II) complexes **38** bearing six-membered pyridyne-carbazole chelating rings [85]. This latter compound showed modest (PLQY = 0.31) photoluminescence peaking at 508 nm in CH_2Cl_2 solution at room temperature. Interesting, drop-casted PMMA thin-film prepared at 5 wt % doping level exhibited hypsochromically shifted emission (λ_{em} = 474 nm) with much higher intensity (PLQY = 0.83) making such compound a valuable candidate for blue-emitting OLEDs. Upon embedding compound **38** at 6 wt % doping level in a charge and exciton confining structures with the following architecture ITO/HATCN (10 nm)/NPD (40 nm)/TAPC(10 nm)/complex **38**: 26mCPy (25 nm)/DPPS (10 nm)/BmPyPB (40 nm)/LiF/Al, OLED devices with peak EQE of 24.4% were fabricated. Such efficiency is comparable to the best blue iridium and platinum complexes reported so far.

Two different classes of tetradentate platinum derivatives bearing N^C^C^N rigid ligands were recently reported by Wang and co-workers, bearing either bis(1,2,3-triazolylphenyl) [86] or bis(1,2,4-triazolylphenyl) ligands [87]. Examples of the former class, namely complexes **39** and **40**, are displayed in Figure 18. In particular, these complexes were designed to reduce excited-state distortions by bearing a macrocyclic chelating ligand and either ether, methylene or carbonyl bridging units. The derivatives showed bright blue phosphorescence centred at λ_{em} ca. 448–470 nm depending on the bridging unit. Such blue emission was retained when the complexes were embedded in PMMA rigid matrix. Interestingly, macrocyclic derivatives possessed higher PLQY in solution with values of 0.58–0.62 when compared to non-macrocyclic counterparts that was attributed to the enhanced structural rigidity imposed by the cyclic structure. By employing complex **39** as emissive material OLED devices with the following architecture were fabricated: ITO/NPB (50 nm)/mCP (10 nm)/9,9′-(4,4′-(phenylphosphoryl)bis(4,1-phenylene))bis(9*H*-carbazole) (BCPO):complex **39** *x* wt % (20 nm)/bis[2-(diphenylphosphino)phenyl] ether oxide (DPEPO) (10 nm)/TPBi (30 nm)/LiF (1 nm)/Al (100 nm) with doping level *x* of 2, 5 and 10 wt %. EL spectra showed an emission peak at λ_{EL} = 452 nm that did not show any dependency on the doping concentration and a rather low turn-on voltage of 3.2 V. The best EL performances were recorded for the OLED device at 10 wt % doping level that showed peak brightness, CE and PE of 10680 cd m^{-2}, 11 cd A^{-1} and 10.8 lm W^{-1}, respectively, and EQE value of 9.7%. In a second set of deep-blue OLED devices, maximum EQE of 15.4% were achieved at brightness of 490 cd m^{-2}.

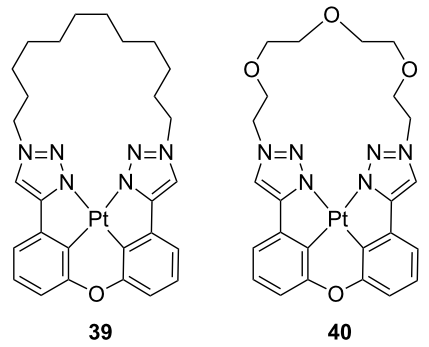


Figure 18: Chemical structure of the macrocyclic tetradentate platinum complexes reported by Wang and co-workers [86].

Other classes of tetradendate platinum(II) complexes bearing N^C^C^N chromophoric ligands have been recently reported by Fan and coworkers [88,89]. In order to prevent detrimental intermolecular interactions which might largely affect colour purity and emission efficiency in a condensed state, as well as increase solubility of the complex, the authors developed a series of (2-phenylbenzimidazole)-based tetradentate Pt(II) complexes bearing a diisopropylphenyl group, which is orthog-

onally oriented with respect to the molecular plane [88]. The three complexes featured 2-pyridylcarbazole (**41**), 2-thiazolylcarbazole (**42**) and 2-oxazolylcarbazole (**43**) moieties employed as the luminophoric motifs that were linked to the 2-phenylbenzimidazole unit through an ether bridge (Figure 19). The three complexes exhibited high thermal stability since thermogravimetric analysis (TGA) showed a weight loss of only 5% at temperatures in the range 436–463 °C. An intense and structured emission in the green region with λ_{em} = 500–507 nm and PLQY = 0.6–0.78 was recorded when the complexes were used as dopant in PMMA thin-film. DFT calculations helped to ascribe the nature of the frontier molecular orbitals as being carbazole/phenoxy and phenylbenzimidazole for HOMO and LUMO, respectively.

OLED devices were fabricated employing complexes **41**–**43** as emitting dopants with the following architecture ITO/HATCN (10 nm)/TAPC (40 nm)/TCTA (10 nm)/26mCPy:complex **41**–**43** *x* wt % (20 nm)/TmPyPB (45 nm)/Liq (2 nm)/Al (120 nm) with doping level *x* of 8, 10, 15 and 20 wt %. Even for the highest doping level investigated, i.e., 20 wt %, the EL emission was similar to the PL spectra observed in dilute condition, which suggests that the steric hindrance imparted by the diisopropylphenyl group is important for avoiding intermolecular interactions. Furthermore, OLED using complex **41** as emitting materials showed good performances with maximum EQE of 22.3%.

In a following study, a second series of tetradentate platinum complexes bearing a pyrazolo[1,5-*f*]phenanthridine moiety and with a general coordination motifs of the type $N_{pyridine}$^C_{phenyl}^C_{phenyl}^$N_{pyrazole}$ was reported by the same group, namely complexes **44**–**46** (Figure 19) [89]. The complexes showed moderate to intense sky-blue emission with PLQY in the range 0.2–0.7 and high thermal stability. Unfortunately, going from dilute solution to neat solid-state samples, PLQY values dramatically dropped to values as low as 0.10–0.02 that might point to strong intermolecular interaction and TTA phenomena. The tendency toward aggregation for complex **44** and **46** in condensed phase was also evidenced in the EL spectra. Although its shape was independent from the doping ratio, a bathochromically shift was observed along with a featureless emission profile. In sharp contrast, compound **45** displayed an EL emission maximum similar to that observed for the solution sample, indicating a much less pronounced aggregation. OLED devices were fabricated with the following configuration comprising different doping level: ITO/HATCN (10 nm)/TAPC (45 nm)/TCTA (10 nm)/host material:complex **44**–**46** *x* wt % (20 nm)/TmPyPB (50 nm)/Liq (2 nm)/Al (110 nm), where host was CBP for **44** and **46** and 26mCPy for compound **45**. Devices based on **44** at doping ratio as high as 30 wt % achieved the highest EL efficiencies amongst the three investigated complexes with CE, PE and EQE of 58.0 cd A^{-1}, 51.6 lm W^{-1} and 16.4%, respectively.

The same authors have recently reported on another class of asymmetric [90] platinum complexes featuring tertiary arylamine motifs and their chemical structure is displayed in Figure 20. Such complexes, whose structure is derived from the parental symmetric systems previously reported by Huo and

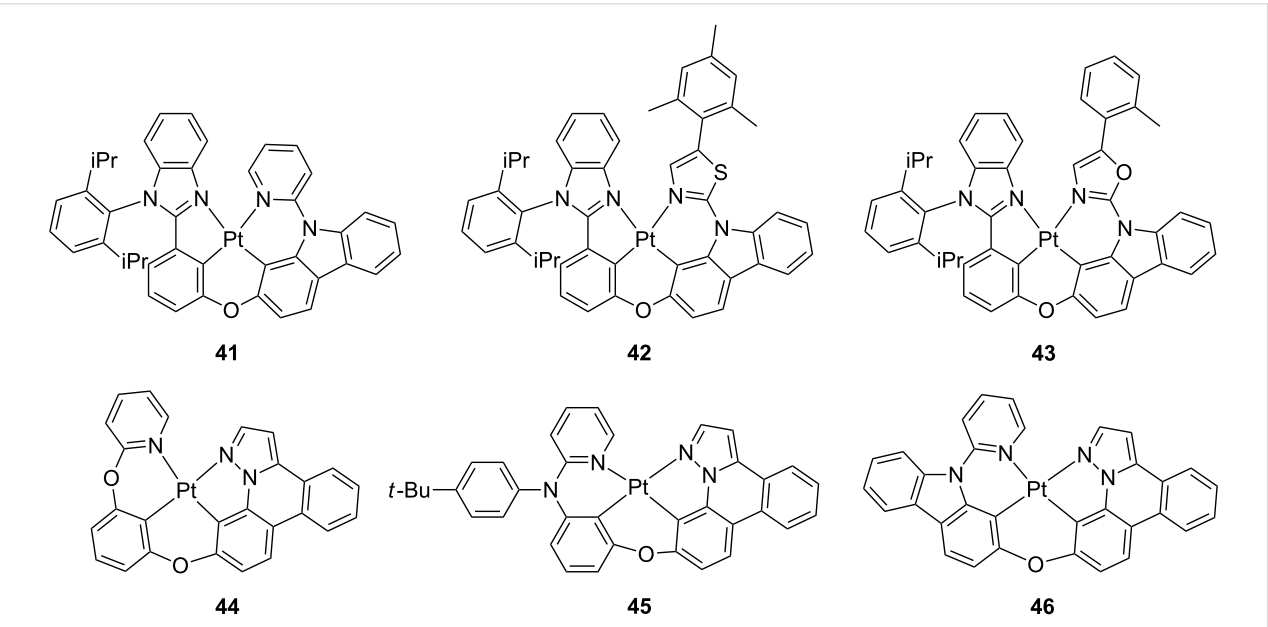


Figure 19: Molecular structure of complex **41–46** [88,89].

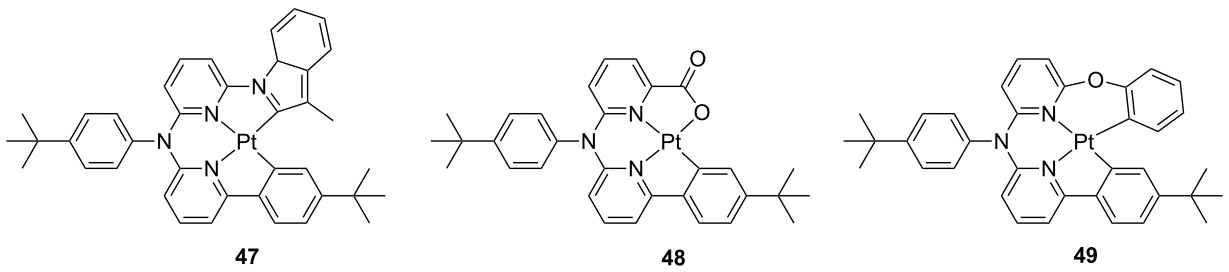


Figure 20: Molecular structure of asymmetric derivatives **47–49** based on triaryl-type of bridge [90].

co-workers [91], bear a 3-methylindole, a carboxylic and a dangling phenoxy moiety, complex **47**, **48** and **49**, respectively, resulting in a general ligand structure with general formula being either C^N^N^C or C^N^N^O.

The compounds displayed moderate emission in the green-yellow portion of the visible spectrum with λ_{em} maximum peaking at 504–513 nm and PLQY of 0.27–0.47, attributable to an excited state with main LC character as suggested by the vibronic profile of the spectrum, repectively. Employment of these complexes as triplet emitters in OLEDs with configuration ITO/HATCN (10 nm)/TAPC (40 nm)/TCTA/mCP: platinum complex 10 wt %/TmPyPb (40 nm)/Liq (2 nm)/Al (120 nm) afforded electroluminescent devices with peak EQE of 13.3% and 13.6% for **48** and **49**, respectively. Even a higher peak EQE value of 16.3% was achieved for devices fabricated with **47** at similar doping level, although colour purity of the device resulted to be affected due to the fact that the EL emission resembles the PL spectra recorded in doped PMMA thin films rather than solution sample. This spectral broadening and shift is most likely due to the establishment of intermolecular interactions at such high doping level.

Indeed, platinum(II) complexes are well known to show both ground state aggregation phenomena including formation of metallophilic $d^8\cdots d^8$ interactions and/or π–π stacking of the coordinating ligands [67,92] as well as excited-state interactions such as formation of excimers [93,94]. Although they may be usefully employed to shift both absorption and emission spectra, obtain long-range ordered luminescent supramolecular architectures and fabricate white-light emitting devices, aggregation phenomena of luminophors is typically considered detrimental due to the TTA and aggregation cause quenching (ACQ) processes that might take place. Thus, several strategies have been employed to date to avoid platinum emitters in close proximity, including introduction of bulky groups such as adamantyl [71] and spiro moieties [95]. By introducing on N^C^N^O tetradentate motifs both *tert*-butyl and spiro groups, Fan and co-workers recently reported on two platinum complexes, **50**–**51**, bearing a phenylpicolinate moiety. Their chemical structure is sketched in Figure 21 [96]. The complexes displayed structured luminescence with moderate PLQY (ca. 0.2) and relatively long lived-excited state lifetime in the range 8.4–11.6 μs. It is worth to notice that the presence of several bulky groups successfully suppressed aggregation as demonstrated by the similar PL spectra recorded in dilute CH_2Cl_2 and solid-state samples. Upon host material and doping ratio optimization, OLED devices achieved maximum EQE of 22.9% for complex **50** with relatively low roll-off efficiency that is attributed to the reduced quenching processes at high current density imparted by the bulky groups.

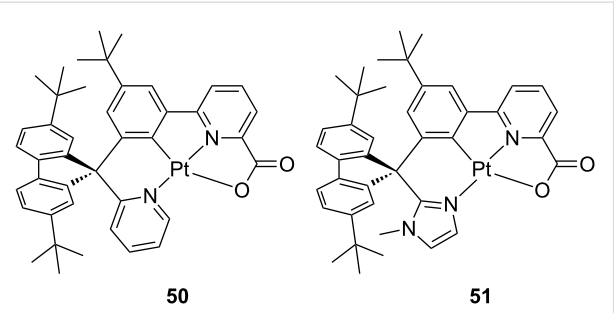


Figure 21: Chemical structure of the asymmetric tetradentate derivatives **50** and **51** based on spirofluorene linkage [96].

Spirofluorene and spiroacridine groups were also employed by Chi and co-workers on azolate-based tetradendate platinum complexes bearing either N_{trz}^N_{py}^N_{py}^N_{trz} (**52**) and N_{pz}^N_{py}^N_{py}^N_{pz} type (**53** and **54**) of ligands where trz and pz and py is a trifluoromethyltriazolate, trifluoromethylpyrazolate and pyridine ring, respectively [97] (Figure 22). This strategy has proven to enhance solubility and processability during device fabrication as demonstrated for a related Os(II) compound [98].

Photophysical characterization showed that complexes **52**, **53** and **54a** exhibited a structured and intense (PLQY = 0.58–0.8) blue emission with emission maxima at 452–465 nm. Complex

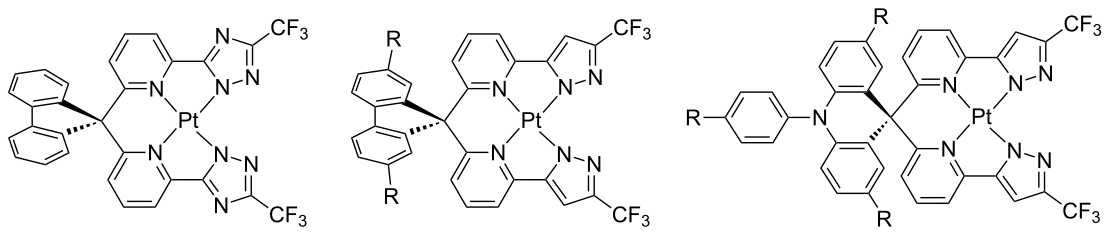


Figure 22: Molecular structure of the pyridylazolate-based complexes **52**–**54** reported by Chi and co-workers [97].

54b was characterized by a large solvatochromic effect as a consequence of the large variation of the transition dipole moment from S_0 to T_1 states of 29.33 D. Indeed, while a structured phosphorescence ascribed to a ^{3}LC/^{3}MLCT transition has been observed in cyclohexane, a much broader and featureless profile is recorded in CH_2Cl_2 and ethanol, which underlies involvement of an emitting excited state with sizeable ILCT character becoming stabilized in such more polar solvents. The two derivatives displaying the highest PLQY among the series, namely **53b** and **54b**, were employed as triplet emitters in OLED device with architecture comprising an enlarged carrier recombination zone, such as ITO/TAPC (40 nm)/mCP:platinum complex 8 wt % (17 nm)/DPEPO platinum complex 8 wt % (3 nm)/TmPyPB (50 nm)/LiF (0.8 nm)/Al (150 nm). Devices fabricated with complex **54b** showed the highest peak efficiency of 15.3% with lower roll-off that was attributed to the better charge transport ability of compound **54b**. Furthermore, by combination of sky-blue emitter **53b** and **54b** and a red emitting osmium complex reported elsewhere [99], WOLED with a sandwiched recombination zone blue/red/blue emitters displayed warm-white emission with peak EQE of 12.7, CRI of 64 and CIE coordinate of 0.365, 0.376 at 1000 cd m^{-2}.

Achieving efficient electroluminescence into the deep red and NIR region represents a challenging research topic of current interest, and only few examples are reported up to now showing remarkable performances [14]. Such challenge mainly arises from the intrinsic increase of the nonradiative rate constant upon decreasing the energy gap between excited and ground state that follows an exponential law known as energy gap law (EGL) [100]. In this respect, Su, Zhu and co-workers reported on two series of salophen-based tetradentate platinum(II) complexes decorated with donor–acceptor moieties such as triphenylaminophenazine [101] and triphenylaminobenzothiadiazole [102] and their chemical structure is shown in Figure 23.

All the complexes displayed long-lived red-to-NIR emissions in both solution and solid-state samples. The deepest red maximum was recorded for complex **57** with a maximum centred at λ_{em} = 697 nm arising from a triplet excited state with admixed MLCT/ILCT character as a consequence of the large donor–acceptor character of the ligand [102]. By employing complex **57** as triplet emitter in solution-processed OLED featuring a single-emissive layer, devices with architecture ITO/PEDOT (40 nm)/PVK:OXD-7:Pt complex 1–4 wt % (50 nm)/TPBI (30 nm)/Ba (4 nm)/Al (100 nm) were fabricated showing emission maximum λ_{EL} = 703 nm and peak EQE of 0.88% with relatively low roll-off efficiency upon increasing current density.

Platinum(IV) complexes

The first examples of luminescent platinum compounds with +IV oxidation states were reported by Balzani and von Zelewski back in the late 80s [103]. The complexes contained bis-cyclometalating (C^N) ligands of the general formula Pt(C^N)$_2$(CH_2Cl)Cl and were prepared by a photooxidative addition of CH_2Cl_2 onto the corresponding bis-cyclometalated Pt(II) parental complexes. Although Pt(IV) complexes have attracted great attention in cancer therapy [104-106], only in the very recent past they are receiving increasing interest as luminescent compounds [107,108]. Such derivatives are characterized by long-lived triplet-manifold π–π* excited states with either ^{3}LC or ^{3}ILCT nature. Most of the so far reported examples of octahedral Pt(IV) derivatives are based on heteroleptic and homoleptic systems containing phenyl-pyridine-type cyclometalating (C^N) ligands, reaching PLQY up to ca. 0.80 [109]. To date, only two examples of Pt(IV) derivatives, namely **58** and **59**, have been reported to be employed as active compounds in polymer-based OLEDs and their chemical structure is reported in Figure 24 [110]. The compounds contain a bis-cyclometalating tetradentate ligand scaffold based on phenylisoquinoline moiety decorated with hole-transporting triphenylamine groups, and two chlorine ancillary ligands in *trans* geometry. The complexes showed NIR luminescence (λ_{em} ca. 750 nm) in dilute 2-methyltetrahydrofuran solution and long-lived excited states with lifetime in the order of 0.7 μs.

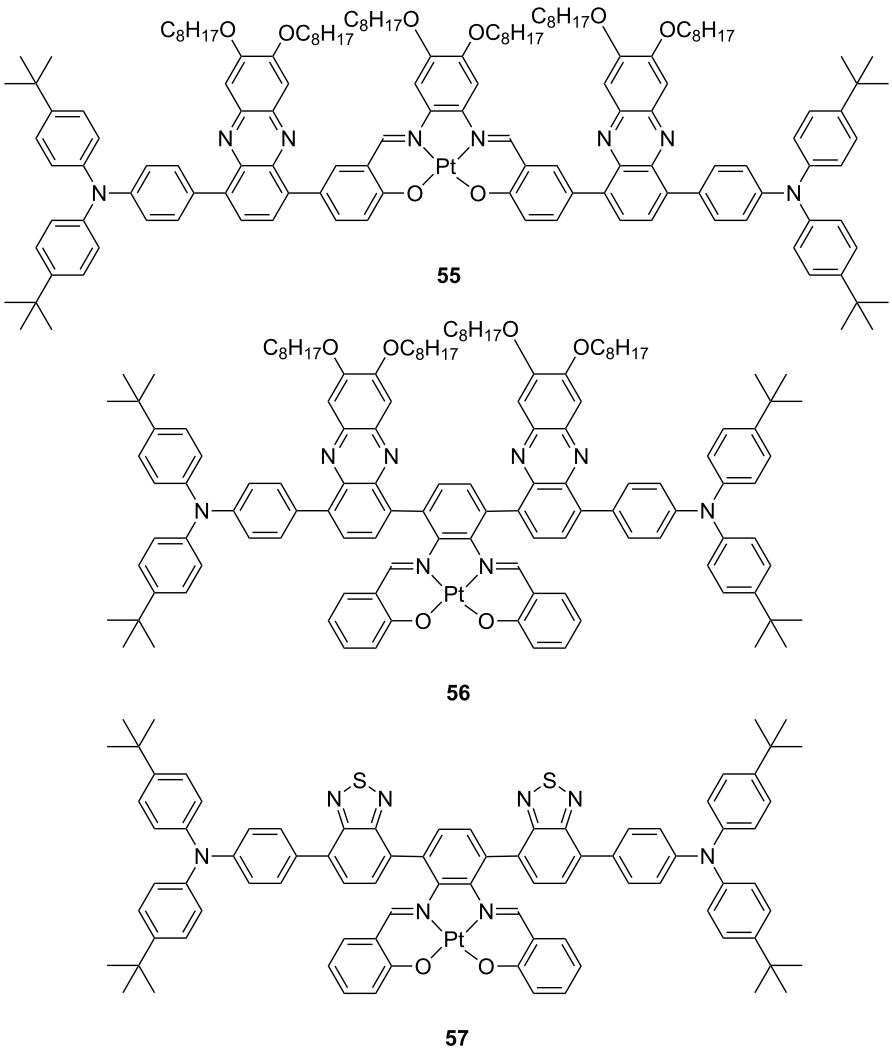


Figure 23: Chemical structure of the red-to-NIR emitting complexes **55**–**57** bearing donor–acceptor triphenylaminophenazine and triphenylaminobenzothiadiazole moieties [101,102].

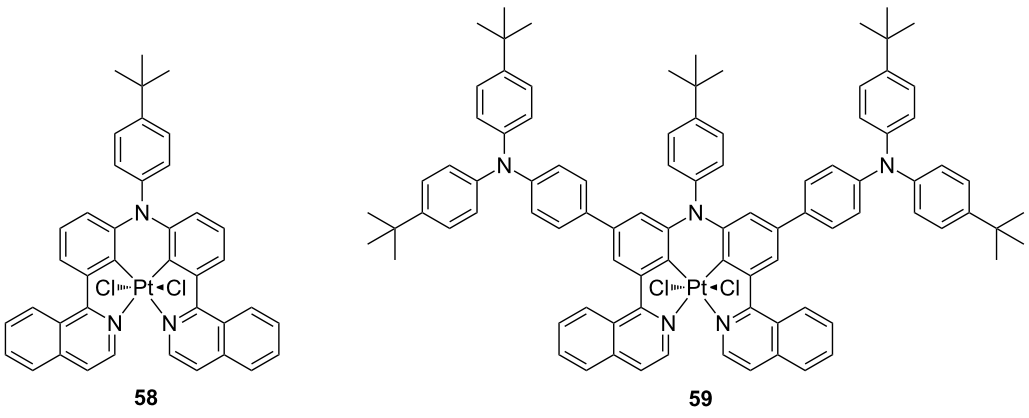


Figure 24: Molecular structures of the Pt(IV) derivatives **58** and **59** employed as triplet emitters in solution-processed OLEDs [110].

To explore the potentiality of such phosphorescent Pt(IV) compounds as active materials in electroluminescent devices, solution-processed OLEDs with the following architecture ITO/PEDOT (40 nm)/PVK:complex (50–60 nm)/TPBi (30 nm)/Ba (4 nm)/Al, where PVK is poly(9-vinylcarbazole), were fabricated with dopant concentration adjusted in the range 1–8 wt % and their EL performances investigated. The devices showed interesting NIR emission similar to the PL spectra with emission maximum at λ_{EL} of about 750 nm for both compounds. Maximum radiant intensity and EQE of 164 μW cm^{-2} and 0.85% were recorded for compound **59** with relatively low roll-off at higher current densities.

Conclusion

In conclusion, we have here reviewed the most recent trends in the field of phosphorescent platinum complexes, and their use

Table 1: EL device performances reported for selected examples of luminescent platinum(II) and platinum(IV) complexes reviewed in this manuscript.

cmpd	device architecture	EL performances[a]				Ref. #
		CE (cd A^{-1})	PE (lm W^{-1})	Brightness (cd m^{-2})	EQE (%)	
1	ITO/TAPC (30 nm)/TCTA (10 nm)/DPEPO:**1** 10 wt % (20 nm)/DPEPO (10 nm)/TPBi (30 nm)/LiF/Al	–	–	–	8	[19]
4	ITO/TAPC (40 nm)/CBP:**4** 8 wt % (30 nm)/BP4mPy (40 nm)/LiF (0.8 nm)/Al (150 nm)	23.2	22.8	10 318	11.5	[26]
8	ITO/MoO_3 (2 nm)/NPB (25 nm)/mCP (8 nm)/**8** neat (40 nm)/3TPyMB (50 nm)/LiF (1 nm)/Al	21.0	15.5	43 000	19.0	[27]
10	ITO/MoO_3 (1 nm)/TAPC (65 nm)/mCP (8 nm)/**10** neat (30 nm)/3TPYMB (50 nm)/LiF (1 nm)/Al (120 nm)	90.0[b]	–	–	25.9[b]	[34]
11a	ITO/TAPC:MoO_3 20 wt % (20 nm)/TAPC (40 nm)/26DCzppy:**11a** 8 wt % (20 nm)/TmPyPB (50 nm)/LiF (0.8 nm)/Al (150 nm)	44.0	28.0	–	12.5	[35]
13	ITO (100 nm)/TAPC (80 nm)/ TCTA (10 nm)/**13** neat (30 nm)/BMPYPB (15 nm)/BMPYPB:Rb_2CO_3 1 wt % (40 nm)/Al (100 nm)	62.0	53.8[c]	–	38.8	[13]
16	ITO (100 nm)/HATCN (10 nm)/NPB (50 nm)/mCP (15 nm)/**16** neat (20 nm)/TPBi (60 nm)/Liq (2 nm)/Al (100 nm)	–	–	–	24.0 (55)[d]	[14]
22b	ITO/TAPC (50 nm)/TCTA:**22b** 2 wt % (10 nm)/TmPyPB (50 nm)/LiF (1 nm)/Al (100 nm)	76.7	33.8	–	22.8	[53]
22c	ITO/TAPC (50 nm)/TCTA:**22c** 4 wt % (10 nm)/TmPyPB (50 nm)/LiF (1 nm)/Al (100 nm)	34.8	18.2	–	22.1	[53]
23g	ITO (120 nm)/Mo_2O_x (2 nm)/TCTA (80 nm)/**23g** (15 nm)/TPBi (25 nm)/LiF (0.5 nm)/Al (100 nm)				1.2[e]	[56]
24c	ITO/PEDOT:PSS (70 nm)/mCP:**24c** 10 wt % (60 nm)/SPPO13 (30 nm)/LiF (0.8 nm)/Al (100 nm)	37.6	11.4	–	10.4	[62]
25b	ITO/PEDOT:PSS (70 nm)/TCTA:SPPO13:**25b** 1:1:15 wt % (60 nm)/BmPyPhB 30 nm)/LiF (0.8 nm)/Al (100 nm)	57.4	–	–	16.0	[63]
28b	ITO/PEDOT:PSS (32 nm)/QUPD (10 nm)/OTPD (8 nm)/PVK:OXD-7:**28b** 13.5 wt % (30 nm)/TPBi (25 nm)/CsF (3 nm)/Al (120 nm)	15.5	16.4	–	5.6	[75]
32	ITO/HATCN (10 nm)/NPD (40 nm)/TAPC (10 nm)/TAPC:PO15:**32** 47 wt %:47 wt %:6 wt % (25 nm)/PO15 (10 nm)/BmPyPB (30 nm)/LiF/Al	–	–	–	24.8	[79]
33	ITO/HATCN(10 nm)/NPD(40 nm)/TrisPCz(10 nm)/Bebq2:**33** 2 wt %/BAlq(10 nm)/BPyTP(40 nm)/LiF (1 nm)/Al(100 nm)	–	–	3 743	21.5	[80]
35	ITO/HATCN/NPD/TrisPCz/CBP:**35** 20 wt % (10 nm)/CBP:**35** 6 wt % (20 nm)/BAlq/BPyTP/LiF/Al	–	–	5 600	15.3[c]	[82]
37	ITO/HATCN (10 nm)/NPD (40 nm)/TrisPCz (10 nm)/mCBP:**37** 10 wt % (25 nm)/mCBT (8 nm)/BPyTP (40 nm)/LiF (1 nm)/Al (100 nm)	–	–	4 929	17.8	[84]
38	ITO/HATCN (10 nm)/NPD (40 nm)/TAPC(10 nm)/26mCPy:**38** 6 wt % (25 nm)/DPPS (10 nm)/BmPyPB (40 nm)/LiF/Al	–	–	–	24.4	[85]
39	ITO/NPB (50 nm)/mCP (10 nm)/BCPO:**39** 10 wt % (20 nm)/DPEPO (10 nm)/TPBi (30 nm)/LiF (1 nm)/Al (100 nm)	11.0	10.8	10 676	9.7	[86]
41	ITO/HATCN (10 nm)/TAPC (40 nm)/TCTA (10 nm)/26mCPy:**41** 15 wt % (20 nm)/TmPyPB (45 nm)/Liq (2 nm)/Al (120 nm)	78.5	66.4	–	22.3	[88]
44	ITO/HATCN (10 nm)/TAPC (45 nm)/TCTA (10 nm)/CBP:**44** 30 wt % (20 nm)/TmPyPB (50 nm)/Liq (2 nm)/Al (110 nm)	58.0	51.6	–	16.5	[89]

Table 1: EL device performances reported for selected examples of luminescent platinum(II) and platinum(IV) complexes reviewed in this manuscript. (continued)

47	ITO/HATCN (10 nm)/TAPC (40 nm)/TCTA/mCP:**47** 10 wt %/TmPyPb (40 nm)/Liq (2 nm)/Al (120 nm)	53.0	35.9	–	16.3	[90]
50	ITO/HATCN (10 nm)/TAPC (40 nm)/TCTA (10 nm)/26mCPy:**50** 15 wt % (20 nm)/TmPyPB (45 nm)/Liq (2 nm)/Al (120 nm)	83.0	63.8	–	22.9	[96]
54b	ITO/TAPC (40 nm)/mCP:**54b** 8 wt % (17 nm)/DPEPO (3 nm)/TmPyPB (50 nm)/LiF (0.8 nm)/Al (150 nm)	36.3	38.0	4 121	15.3	[97]
57	ITO/PEDOT (40 nm)/PVK:OXD-7:**57** 2 wt % (50 nm)/TPBI (30 nm)/Ba (4 nm)/Al (100 nm)	–	–	–	0.88	[102]
59	ITO/PEDOT (40 nm)/PVK:**59** 1 wt % (50–60 nm)/TPBi (30 nm)/Ba (4 nm)/Al	–	–	–	0.85	[110]

[a]Device peak values unless differently stated; [b]recorded at 100 cd m^{-2}; [c]recorded at 1,000 cd m^{-2}; [d]device comprising light outcoupling structures; [e]recorded at a current density of 10 mA cm^{-2}.

as phosphors in light-emitting optoelectronic devices such as OLEDs. Indeed, such class of luminescent complexes still represents a fascinating research topic of enormous current interest, in particular in the case of derivatives with oxidation state +II. This is because these systems possess excellent photophysical properties that can be tuned by judicious molecular design through ligand modification. Seeking for emitters with improved features, interesting examples with great structural variety have been reported to date that are based not only on bidentate and tridentate moieties, but recently also on tetradentate scaffolds. Differently from many other transition metals, square planar platinum(II) complexes bearing π-conjugated ligands also possess a peculiar tendency to establish weak intermolecular interactions, such as metallophilic and π–π interactions. These additional features could further widen the already available chemical toolbox for designing highly efficient electrophosphorescent solid-state materials in the near future. Overall, design efforts have allowed the achievement of impressive OLED performances for devices embedding platinum-based triplet emitters with EQE above 30%. Such results have been achieved thanks to the combination of molecular and dipole moments orientation engineering in the electroactive thin film. Finally, recent reports on platinum(IV) derivatives demonstrate that this type of complexes do also possess interesting photophysics and therefore, further growing interest in their use as emitters in OLEDs could be also foreseen.

ORCID® iDs

Cristina Cebrián - https://orcid.org/0000-0002-1773-6722
Matteo Mauro - https://orcid.org/0000-0001-6393-8053

References

1. Zysman-Colman, E., Ed. *Iridium(III) in optoelectronic and photonics applications;* Wiley, 2017; Vol. 1, pp 1–686. doi:10.1002/9781119007166
2. Armaroli, N.; Bolink, H. J., Eds. *Photoluminescent, materials and electroluminescent devices;* Top. Curr. Chem.; Springer, 2016; pp 1–395. doi:10.1007/978-3-319-59304-3
3. Wallesch, M.; Volz, D.; Zink, D. M.; Schepers, U.; Nieger, M.; Baumann, T.; Bräse, S. *Chem. – Eur. J.* **2014,** *20,* 6578–6590. doi:10.1002/chem.201402060
4. Panigati, M.; Mauro, M.; Donghi, D.; Mercandelli, P.; Mussini, P.; De Cola, L.; D'Alfonso, G. *Coord. Chem. Rev.* **2012,** *256,* 1621–1643. doi:10.1016/j.ccr.2012.03.006
5. Yersin, H., Ed. *Highly efficient OLEDs with phosphorescent materials;* Wiley-VCH: Weinheim, Germany, 2008. doi:10.1002/9783527621309
6. Twilton, J.; Le, C.; Zhang, P.; Shaw, M. H.; Evans, R. W.; MacMillan, D. W. C. *Nat. Rev. Chem.* **2017,** *1,* No. 0052. doi:10.1038/s41570-017-0052
7. Mauro, M.; Aliprandi, A.; Septiadi, D.; Kehr, N. S.; De Cola, L. *Chem. Soc. Rev.* **2014,** *43,* 4144–4166. doi:10.1039/C3CS60453E
8. Zhao, Q.; Huang, C.; Li, F. *Chem. Soc. Rev.* **2011,** *40,* 2508–2524. doi:10.1039/c0cs00114g
9. Hagfeldt, A.; Boshloo, G.; Sun, L.; Kloo, L.; Pettersson, H. *Chem. Rev.* **2010,** *110,* 6595–6663. doi:10.1021/cr900356p
10. Baldo, M. A.; O'Brien, D. F.; You, Y.; Shoustikov, A.; Sibley, S.; Thompson, M. E.; Forrest, S. R. *Nature* **1998,** *395,* 151–154. doi:10.1038/25954
11. Costa, R. D., Ed. *Light-emitting electrochemical cells: concepts, advances and challenges;* Springer, 2017. doi:10.1007/978-3-319-58613-7
12. Helander, M. G.; Wang, Z. B.; Qiu, J.; Greiner, M. T.; Puzzo, D. P.; Liu, Z. W.; Lu, Z. H. *Science* **2011,** *332,* 944–947. doi:10.1126/science.1202992
13. Kim, K.-H.; Liao, J.-L.; Lee, S. W.; Sim, B.; Moon, C.-K.; Lee, G.-H.; Kim, H.-J.; Chi, Y.; Kim, J.-J. *Adv. Mater.* **2016,** *28,* 2526–2532. doi:10.1002/adma.201504451
14. Ly, K. T.; Chen-Cheng, R.-W.; Lin, H.-W.; Shiau, Y.-J.; Liu, S.-H.; Chou, P.-T.; Tsao, C.-S.; Huang, Y.-C.; Chi, Y. *Nat. Photonics* **2017,** *11,* 63–68. doi:10.1038/nphoton.2016.230
15. Huo, S.; Carroll, J.; Vezzu, D. A. K. *Asian J. Org. Chem.* **2015,** *4,* 1210–1245. doi:10.1002/ajoc.201500246
16. Lu, C.-W.; Wang, Y.; Chi, Y. *Chem. – Eur. J.* **2016,** *22,* 17892–17908. doi:10.1002/chem.201601216
17. Tang, M.-C.; Chan, A. K.-W.; Chan, M.-Y.; Yam, V. W.-W. *Top. Curr. Chem.* **2016,** 67–109. doi:10.1007/978-3-319-59304-3_3

18. Li, K.; Tong, G. S. M.; Wan, Q.; Cheng, G.; Tong, W.-Y.; Ang, W.-H.; Kwong, W.-L.; Che, C.-M. *Chem. Sci.* **2016,** *7,* 1653–1673. doi:10.1039/C5SC03766B
19. Bullock, J. D.; Salehi, A.; Zeman IV, C. J.; Abboud, K. A.; So, F.; Schanze, K. S. *ACS Appl. Mater. Interfaces* **2017,** *9,* 41111–41114. doi:10.1021/acsami.7b12107
20. Xiong, W.; Meng, F.; Tan, H.; Wang, Y.; Wang, P.; Zhang, Y.; Tao, Q.; Su, S.; Zhu, W. *J. Mater. Chem. C* **2016,** *4,* 6007–6015. doi:10.1039/C6TC00825A
21. Xu, L.-J.; Zeng, X.-C.; Wang, J.-Y.; Zhang, L.-Y.; Chi, Y.; Chen, Z.-N. *ACS Appl. Mater. Interfaces* **2016,** *8,* 20251–20257. doi:10.1021/acsami.6b06707
22. Zhang, L.-Y.; Xu, L.-J.; Wang, J.-Y.; Zeng, X.-C.; Chen, Z.-N. *Dalton Trans.* **2017,** *46,* 865–874. doi:10.1039/C6DT04249J
23. Li, Y.-P.; Fan, X.-X.; Wu, Y.; Zeng, X.-C.; Wang, J.-Y.; Wei, Q.-H.; Chen, Z.-N. *J. Mater. Chem. C* **2017,** *5,* 3072–3078. doi:10.1039/C7TC00382J
24. Shu, H.-X.; Wang, J.-Y.; Zhang, Q.-C.; Chen, Z.-N. *Inorg. Chem.* **2017,** *56,* 9461–9473. doi:10.1021/acs.inorgchem.7b00452
25. Williams, J. A. G. Photochemistry and Photophysics of Coordination Compounds: Platinum. In *Photochemistry and Photophysics of Coordination Compounds II;* Balzani, V.; Campagna, S., Eds.; Topics in Current Chemistry, Vol. 281; Springer: Berlin, Heidelberg, 2007; pp 205–268. doi:10.1007/128_2007_134
26. Ku, H.-Y.; Tong, B.; Chi, Y.; Kao, H.-C.; Yeh, C.-C.; Chang, C.-H.; Lee, G.-H. *Dalton Trans.* **2015,** *44,* 8552–8563. doi:10.1039/C4DT03028A
27. Hsu, C.-W.; Zhao, Y.; Yeh, H.-H.; Lu, C.-W.; Fan, C.; Hu, Y.; Robertson, N.; Lee, G.-H.; Sun, X. W.; Chi, Y. *J. Mater. Chem. C* **2015,** *3,* 10837–10847. doi:10.1039/C5TC02261D
28. Bourissou, D.; Guerret, O.; Gabbaï, F. P.; Bertrand, G. *Chem. Rev.* **2000,** *100,* 39–92. doi:10.1021/cr940472u
29. Peris, E.; Crabtree, R. H. *Coord. Chem. Rev.* **2004,** *248,* 2239–2246. doi:10.1016/j.ccr.2004.04.014
30. Benhamou, L.; Chardon, E.; Lavigne, G.; Bellemin-Laponnaz, S.; César, V. *Chem. Rev.* **2011,** *111,* 2705–2733. doi:10.1021/cr100328e
31. Bellemin-Laponnaz, S.; Dagorne, S. *Chem. Rev.* **2014,** *114,* 8747–8774. doi:10.1021/cr500227y
32. Andrew, R. E.; González-Sebastián, L.; Chaplin, A. B. *Dalton Trans.* **2016,** *45,* 1299–1305. doi:10.1039/C5DT04429D
33. Hameury, S.; de Frémont, P.; Braunstein, P. *Chem. Soc. Rev.* **2017,** *46,* 632–733. doi:10.1039/C6CS00499G
34. Hsu, C.-W.; Ly, K. T.; Lee, W.-K.; Wu, C.-C.; Wu, L.-C.; Lee, J.-J.; Lin, T.-C.; Liu, S.-H.; Chou, P.-T.; Lee, G.-H.; Chi, Y. *ACS Appl. Mater. Interfaces* **2016,** *8,* 33888–33898. doi:10.1021/acsami.6b12707
35. Tseng, C.-H.; Fox, M. A.; Liao, J.-L.; Ku, C.-H.; Sie, Z.-T.; Chang, C.-H.; Wang, J.-Y.; Chen, Z.-N.; Lee, G.-H.; Chi, Y. *J. Mater. Chem. C* **2017,** *5,* 1420–1435. doi:10.1039/C6TC05154E
36. Leopold, H.; Tronnier, A.; Wagenblast, G.; Münster, I.; Strassner, T. *Organometallics* **2016,** *35,* 959–971. doi:10.1021/acs.organomet.5b00991
37. Leopold, H.; Heinemeyer, U.; Wagenblast, G.; Münster, I.; Strassner, T. *Chem. – Eur. J.* **2017,** *23,* 1118–1128. doi:10.1002/chem.201604456
38. Leopold, H.; Tenne, M.; Tronnier, A.; Metz, S.; Münster, I.; Wagenblast, G.; Strassner, T. *Angew. Chem., Int. Ed.* **2016,** *55,* 15779–15782. doi:10.1002/anie.201607075
39. Chang, S.-Y.; Kavitha, J.; Li, S.-W.; Hsu, C.-S.; Chi, Y.; Yeh, Y.-S.; Chou, P.-T.; Lee, G.-H.; Carty, A. J.; Tao, Y.-T.; Chien, C.-H. *Inorg. Chem.* **2006,** *45,* 137–146. doi:10.1021/ic051393b
40. Wang, Q.; Oswald, I. W. H.; Yang, X.; Zhou, G.; Jia, H.; Qiao, Q.; Chen, Y.; Hoshikawa-Halbert, J.; Gnade, B. E. *Adv. Mater.* **2014,** *26,* 8107–8113. doi:10.1002/adma.201402947
41. Fuertes, S.; Chueca, A. J.; Perálvarez, M.; Borja, P.; Torrell, M.; Carreras, J.; Sicilia, V. *ACS Appl. Mater. Interfaces* **2016,** *8,* 16160–16169. doi:10.1021/acsami.6b03288
42. Wild, A.; Winter, A.; Schlütter, F.; Schubert, U. S. *Chem. Soc. Rev.* **2011,** *40,* 1459–1511. doi:10.1039/C0CS00074D
43. Constable, E. C. *Chem. Soc. Rev.* **2007,** *36,* 246–253. doi:10.1039/B601166G
44. McGuire, R., Jr.; McGuire, M. C.; McMillin, D. R. *Coord. Chem. Rev.* **2010,** *254,* 2574–2583. doi:10.1016/j.ccr.2010.04.013
45. Tang, M.-C.; Chan, A. K.-W.; Chan, M.-Y.; Yam, V. W.-W. *Top. Curr. Chem.* **2016,** *374,* 46. doi:10.1007/s41061-016-0046-y
46. Kalinowski, J.; Fattori, V.; Cocchi, M.; Williams, J. A. G. *Coord. Chem. Rev.* **2011,** *255,* 2401–2425. doi:10.1016/j.ccr.2011.01.049
47. Chassot, L.; Müller, E.; von Zelewsky, A. *Inorg. Chem.* **1984,** *23,* 4249–4253. doi:10.1021/ic00193a030
48. Sandrini, D.; Maestri, M.; Balzani, V.; Chassot, L.; von Zelewsky, A. *J. Am. Chem. Soc.* **1987,** *109,* 7720–7724. doi:10.1021/ja00259a021
49. Constable, E. C.; Henney, R. P. G.; Leese, T. A.; Tocher, D. A. *J. Chem. Soc., Dalton Trans.* **1990,** 443–449. doi:10.1039/DT9900000443
50. Lai, S.-W.; Chan, M. C.-W.; Cheung, T.-C.; Peng, S.-M.; Che, C.-M. *Inorg. Chem.* **1999,** *38,* 4046–4055. doi:10.1021/ic990238s
51. Kui, S. C. F.; Sham, I. H. T.; Cheung, C. C. C.; Ma, C.-W.; Yan, B.; Zhu, N.; Che, C.-M.; Fu, W.-F. *Chem. – Eur. J.* **2007,** *13,* 417–435. doi:10.1002/chem.200600686
52. Yuen, M.-Y.; Kui, S. C. F.; Low, K.-H.; Kwok, C.-C.; Chui, S. S.-Y.; Ma, C.-W.; Zhu, N.; Che, C.-M. *Chem. – Eur. J.* **2010,** *16,* 14131–14141. doi:10.1002/chem.201001570
53. Chow, P.-K.; Cheng, G.; Tong, G. S. M.; To, W.-P.; Kwong, W.-L.; Low, K.-H.; Kwok, C.-C.; Ma, C.; Che, C.-M. *Angew. Chem., Int. Ed.* **2015,** *54,* 2084–2089. doi:10.1002/anie.201408940
54. Williams, J. A. G.; Beeby, A.; Davies, E. S.; Weinstein, J. A.; Wilson, C. *Inorg. Chem.* **2003,** *42,* 8609–8611. doi:10.1021/ic035083+
55. Cocchi, M.; Virgili, D.; Fattori, V.; Rochester, D. L.; Williams, J. A. G. *Adv. Funct. Mater.* **2007,** *17,* 285–289. doi:10.1002/adfm.200600167
56. Nisic, F.; Colombo, A.; Dragonetti, C.; Roberto, D.; Valore, A.; Malicka, J. M.; Cocchi, M.; Freeman, G. R.; Williams, J. A. G. *J. Mater. Chem. C* **2014,** *2,* 1791–1800. doi:10.1039/c3tc32086c
57. Botchway, S. W.; Charnley, M.; Haycock, J. W.; Parker, A. W.; Rochester, D. L.; Weinstein, J. A.; Williams, J. A. G. *Proc. Natl. Acad. Sci. U. S. A.* **2008,** *105,* 16071–16076. doi:10.1073/pnas.0804071105
58. Baggaley, E.; Botchway, S. W.; Haycock, J. W.; Morris, H.; Sazanovich, I. V.; Williams, J. A. G.; Weinstein, J. A. *Chem. Sci.* **2014,** *5,* 879–886. doi:10.1039/C3SC51875B
59. Colombo, A.; Fiorini, F.; Septiadi, D.; Dragonetti, C.; Nisic, F.; Valore, A.; Roberto, R.; Mauro, M.; De Cola, L. *Dalton Trans.* **2015,** *44,* 8478–8487. doi:10.1039/C4DT03165B
60. Yersin, H.; Rausch, A. F.; Czerwieniec, R.; Hofbeck, T.; Fischer, T. *Coord. Chem. Rev.* **2011,** *255,* 2622–2652. doi:10.1016/j.ccr.2011.01.042
61. Hwang, S.-H.; Moorefield, C. N.; Newkome, G. R. *Chem. Soc. Rev.* **2008,** *37,* 2543–2547. doi:10.1039/b803932c

62. Kong, F. K.-W.; Tang, M.-C.; Wong, Y.-C.; Chan, M.-Y.; Yam, V. W. W. *J. Am. Chem. Soc.* **2016,** *138,* 6281–6291. doi:10.1021/jacs.6b02632
63. Kong, F. K.-W.; Tang, M.-C.; Wong, Y.-C.; Ng, M.; Chan, M.-Y.; Yam, V. W.-W. *J. Am. Chem. Soc.* **2017,** *139,* 6351–6362. doi:10.1021/jacs.7b00479
64. Giebink, N. C.; Forrest, S. R. *Phys. Rev. B* **2008,** *77,* 235215. doi:10.1103/PhysRevB.77.235215
65. Chan, A. K.-W.; Ng, M.; Wong, Y.-C.; Chan, M.-Y.; Wong, W.-T.; Yam, V. W.-W. *J. Am. Chem. Soc.* **2017,** *139,* 10750–10761. doi:10.1021/jacs.7b04952
66. Lu, W.; Chan, M. C. W.; Cheung, K.-K.; Che, C.-M. *Organometallics* **2001,** *20,* 2477–2486. doi:10.1021/om0009839
67. Berenguer, J. R.; Lalinde, E.; Torroba, J. *Inorg. Chem.* **2007,** *46,* 9919–9930. doi:10.1021/ic701298z
68. Kui, S. C. F.; Hung, F.-F.; Lai, S.-L.; Yuen, M.-Y.; Kwok, C.-C.; Low, K.-H.; Chui, S. S.-Y.; Che, C.-M. *Chem. – Eur. J.* **2012,** *18,* 96–109. doi:10.1002/chem.201101880
69. Galstyan, A.; Naziruddin, A. R.; Cebrián, C.; Iordache, A.; Daniliuc, C. G.; De Cola, L.; Strassert, C. A. *Eur. J. Inorg. Chem.* **2015,** 5822–5831. doi:10.1002/ejic.201500949
70. Septiadi, D.; Aliprandi, A.; Mauro, M.; De Cola, L. *RSC Adv.* **2014,** *4,* 25709–25718. doi:10.1039/C4RA02351J
71. Mydlak, M.; Mauro, M.; Polo, F.; Felicetti, M.; Leonhardt, J.; Diener, G.; De Cola, L.; Strassert, C. A. *Chem. Mater.* **2011,** *23,* 3659–3667. doi:10.1021/cm2010902
72. Mauro, M.; Aliprandi, A.; Cebrián, C.; Wang, D.; Kübel, C.; De Cola, L. *Chem. Commun.* **2014,** *50,* 7269–7272. doi:10.1039/C4CC01045K
73. Aliprandi, A.; Mauro, M.; De Cola, L. *Nat. Chem.* **2016,** *8,* 10–15. doi:10.1038/nchem.2383
74. Strassert, C. A.; Chien, C.-H.; Galvez Lopez, M. D.; Kourkoulos, D.; Hertel, D.; Meerholz, K.; De Cola, L. *Angew. Chem., Int. Ed.* **2010,** *50,* 946–950. doi:10.1002/anie.201003818
75. Cebrián, C.; Mauro, M.; Kourkoulos, D.; Mercandelli, P.; Hertel, D.; Meerholz, K.; Strassert, C. A.; De Cola, L. *Adv. Mater.* **2013,** *25,* 437–442. doi:10.1002/adma.201202123
76. Li, K.; Cheng, G.; Ma, C.; Guan, X.; Kwok, W.-M.; Chen, Y.; Lu, W.; Che, C.-M. *Chem. Sci.* **2013,** *4,* 2630–2644. doi:10.1039/c3sc21822h
77. Vezzu, D. A. K.; Deaton, J. C.; Jones, J. S.; Bartolotti, L.; Harris, C. F.; Marchetti, A. P.; Kondakova, M.; Pike, R. D.; Huo, S. *Inorg. Chem.* **2010,** *49,* 5107–5119. doi:10.1021/ic1002226
78. Hang, X.-C.; Fleetham, T.; Turner, E.; Brooks, J.; Li, J. *Angew. Chem., Int. Ed.* **2013,** *52,* 6753–6756. doi:10.1002/anie.201302541
79. Fleetham, T.; Li, G.; Wen, L.; Li, J. *Adv. Mater.* **2014,** *26,* 7116–7121. doi:10.1002/adma.201401759
80. Fleetham, T.; Li, G.; Li, J. *ACS Appl. Mater. Interfaces* **2015,** *7,* 16240–16246. doi:10.1021/acsami.5b01596
81. Norby, G. E.; Park, C.-D.; O'Brien, B.; Li, G.; Huang, L.; Li, J. *Org. Electron.* **2016,** *37,* 163–168. doi:10.1016/j.orgel.2016.06.007
82. Zhu, Z.-Q.; Klimes, K.; Holloway, S.; Li, J. *Adv. Mater.* **2017,** *29,* 1605002. doi:10.1002/adma.201605002
83. Li, G.; Fleetham, T.; Turner, E.; Hang, X.-C.; Li, J. *Adv. Opt. Mater.* **2015,** *3,* 390–397. doi:10.1002/adom.201400341
84. Li, G.; Klimes, K.; Fleetham, T.; Zhu, Z.-W.; Li, J. *Appl. Phys. Lett.* **2017,** *110,* 113301. doi:10.1063/1.4978674
85. Fleetham, T. B.; Huang, L.; Klimes, K.; Brooks, J.; Li, J. *Chem. Mater.* **2016,** *28,* 3276–3282. doi:10.1021/acs.chemmater.5b04957
86. Wang, X.; Peng, T.; Nguyen, C.; Lu, Z.-H.; Wang, N.; Wu, W.; Li, Q.; Wang, S. *Adv. Funct. Mater.* **2017,** *27,* 1604318. doi:10.1002/adfm.201604318
87. Liu, L.; Wang, X.; Wang, N.; Peng, T.; Wang, S. *Angew. Chem., Int. Ed.* **2017,** *56,* 9160–9164. doi:10.1002/anie.201705785
88. Li, J.; Liang, F.; Zhao, Y.; Liu, X.-Y.; Fan, J.; Liao, L.-S. *J. Mater. Chem. C* **2017,** *5,* 6202–6209. doi:10.1039/C7TC01369H
89. Zhao, D.; Tang, X.; Liu, X.-Y.; Fan, J.; Liao, L.-S. *Org. Electron.* **2017,** *50,* 473–479. doi:10.1016/j.orgel.2017.07.002
90. Zhang, X.-Q.; Xie, Y.-M.; Zheng, Y.; Liang, F.; Wang, B.; Fan, J.; Liao, L.-S. *Org. Electron.* **2016,** *32,* 120–125. doi:10.1016/j.orgel.2016.02.016
91. Vezzu, D. A. K.; Deaton, J. C.; Jones, J. S.; Bartolotti, L.; Harris, C. F.; Marchetti, A. P.; Kondakova, M.; Pike, R. D.; Huo, S. *Inorg. Chem.* **2010,** *49,* 5107–5119. doi:10.1021/ic1002226
92. Yam, V. W.-W.; Au, V. K.-M.; Leung, S. Y.-L. *Chem. Rev.* **2015,** *115,* 7589–7728. doi:10.1021/acs.chemrev.5b00074
93. Williams, E. L.; Haavisto, K.; Li, J.; Jabbour, G. E. *Adv. Mater.* **2007,** *19,* 197–202. doi:10.1002/adma.200602174
94. Murphy, L.; Brulatti, P.; Fattori, V.; Cocchi, M.; Williams, J. A. G. *Chem. Commun.* **2012,** *48,* 5817–5819. doi:10.1039/c2cc31330h
95. Cheng, G.; Kui, S. C. F.; Ang, W.-H.; Ko, M.-Y.; Chow, P.-K.; Kwong, C.-L.; Kwok, C.-C.; Ma, C.; Guang, X.; Low, K.-H.; Su, S.-J.; Che, C.-M. *Chem. Sci.* **2014,** *5,* 4819–4830. doi:10.1039/C4SC01105H
96. Liu, G.; Liang, F.; Zhao, Y.; Hu, H.; Fan, J.; Liao, L.-S. *J. Mater. Chem. C* **2017,** *5,* 1944–1951. doi:10.1039/C6TC04312G
97. Liao, K.-Y.; Hsu, C.-W.; Chi, Y.; Hsu, M.-K.; Wu, S.-W.; Chang, C.-H.; Liu, S.-H.; Lee, G.-H.; Chou, P.-T.; Hu, Y.; Robertson, N. *Inorg. Chem.* **2015,** *54,* 4029–4038. doi:10.1021/acs.inorgchem.5b00281
98. Chang, S.-H.; Chang, C.-F.; Liao, J.-L.; Chi, Y.; Zhou, D.-Y.; Liao, L.-S.; Jiang, T.-Y.; Chou, P.-T.; Li, E. Y.; Lee, G.-H.; Kuo, T.-Y.; Chou, P.-T. *Inorg. Chem.* **2013,** *52,* 5867–5876. doi:10.1021/ic302829e
99. Liu, T.-H.; Hsu, S.-F.; Ho, M.-H.; Liao, C.-H.; Wu, Y.-S.; Chen, C. H.; Tung, Y.-L.; Wu, P.-C.; Chi, Y. *Appl. Phys. Lett.* **2006,** *88,* 063508. doi:10.1063/1.2172405
100. Chen, P.; Meyer, T. J. *Chem. Rev.* **1998,** *98,* 1439–1478. doi:10.1021/cr941180w
101. Zhang, Y.; Meng, F.; You, C.; Yang, S.; Xiong, W.; Wang, Y.; Su, S.; Zhu, W. *Dyes Pigm.* **2017,** *138,* 100–106. doi:10.1016/j.dyepig.2016.11.034
102. Zhang, Y.; Yin, Z.; Meng, F.; Yu, J.; You, C.; Yang, S.; Tan, H.; Zhu, W.; Su, S. *Org. Electron.* **2017,** *50,* 317–324. doi:10.1016/j.orgel.2017.08.006
103. Chassot, L.; von Zelewski, A.; Sandrini, D.; Maestri, M.; Balzani, V. *J. Am. Chem. Soc.* **1986,** *108,* 6084–6085. doi:10.1021/ja00279a092
104. Johnstone, T. C.; Suntharalingam, K.; Lippard, S. J. *Chem. Rev.* **2016,** *116,* 3426–3486. doi:10.1021/acs.chemrev.5b00597
105. Johnstone, T. C.; Wilson, J. J.; Lippard, S. J.; Link, C. *Inorg. Chem.* **2013,** *52,* 12234–12249. doi:10.1021/ic400538c
106. Bouché, M.; Dahm, G.; Wantz, M.; Fournel, S.; Achard, T.; Bellemin-Laponnaz, S. *Dalton Trans.* **2016,** *45,* 11362–11368. doi:10.1039/C6DT01846G
107. Juliá, F.; Bautista, D.; Fernández-Hernández, J. M.; González-Herrero, P. *Chem. Sci.* **2014,** *5,* 1875–1880. doi:10.1039/C3SC53187B
108. Jenkins, D. M.; Bernhard, S. *Inorg. Chem.* **2010,** *49,* 11297–11308. doi:10.1021/ic100761f

109. Juliá, F.; Bautista, D.; González-Herrero, P. *Chem. Commun.* **2016,** *52,* 1657–1660. doi:10.1039/C5CC09566B
110. Zhang, Y.; Meng, F.; You, C.; Yang, S.; Xiong, L.; Xiong, W.; Zhu, W.; Wang, Y.; Pei, Y.; Su, S. *Dyes Pigm.* **2017,** *142,* 457–464. doi:10.1016/j.dyepig.2017.04.002

License and Terms

This is an Open Access article under the terms of the Creative Commons Attribution License (http://creativecommons.org/licenses/by/4.0), which permits unrestricted use, distribution, and reproduction in any medium, provided the original work is properly cited.

The license is subject to the *Beilstein Journal of Organic Chemistry* terms and conditions: (https://www.beilstein-journals.org/bjoc)

The definitive version of this article is the electronic one which can be found at: doi:10.3762/bjoc.14.124